Airborne Gravity Gradiometry as an Exploration Tool

by

Tim Dohey, B. Sc., P.Geo.

A thesis submitted to the School of Graduate Studies in partial fulfillment of the requirements for the degree of Master of Science

Department of Geography and Earth Sciences

McMaster University

MASTER OF SCIENCE (2010) McMaster University

(Earth and Environmental Science) Hamilton, Ontario

TITLE: Airborne Gravity Gradiometry as an Exploration Tool

AUTHOR: Tim Dohey, B.Sc., P.GEO.

SUPERVISOR: Professor W. A. Morris

NUMBER OF PAGES: xiii, 171

Abstract

Airborne gravity gradiometry (AGG) is a relatively new technology to the mineral exploration industry which has been increasingly used over the past decade. AGG systems are capable of separating linear accelerations due to aircraft movement from the accelerations related that represent the gravity signal, resulting in a much higher resolution measurement than airborne gravity. The rapid and cost-effective deployment of an AGG survey gives it an advantage when compared to traditional ground gravity survey. With the momentum of existing AGG technology in the exploration industry and the multitude of next-generation AGG sensors currently in development the technique promises to be a valuable exploration tool for the foreseeable future. This thesis focuses on the capabilities of the AGG technology as an exploration tool, its niche within the exploration process, and how AGG compares to other gravity methods. An overview of the AGG method provides context for the aim of the study. A history of airborne gravimetry is presented, as well as a detailed technical description of AGG measurements and units. A summary of all existing airborne gravity and airborne gravity gradiometry technology is provided, along with the major research initiatives aimed at making more sensitive AGG sensors in the future. A discussion of the potential sources of error and uncertainty when working with AGG data highlights many of the technique's obstacles that we will be closely examining within this study. The AGG case study which is examined includes an AGG dataset collected as part of a nickel exploration program to image prospective troctolite chambers in Northern Labrador, by Vale. The study focuses on the portion of the survey over the Voisey's Bay main block that contains several economic nickel deposits, including the world-class Ovoid deposit. This area has been characterized both geologically and geophysically in the past, and contains multiple datasets, including ground gravity. Forward modeling is completed using Voisey's Bay physical rock properties to calculate the response that could be expected over a nickel-bearing troctolite chamber. The methodology and considerations of AGG data acquisition are reviewed in the context of this survey and the dataset is then taken through a terrain correction involving the determination of the best possible background density choice. The limitations and potential pitfalls of the terrain correction are examined in relation to the digital elevation model being used. The problem of thick, variable overburden in portions of the survey is also examined. Several filtering techniques are completed on the data, including vertical integration and the removal of the regional signal. The AGG resolution is then quantitatively compared to the historical ground gravity data and an upward continued version of the ground gravity (representing the response of an airborne gravity survey) by using 2D power spectra and radially averaged power spectra plots. Although the ground gravity is found to contain better resolution in some areas due to its proximity to the ground, the more regular spatial sampling of the AGG survey provided resolution advantages in other areas. The much higher sensitivity of the AGG sensor resulted in a strong resolution advantage over the upward

continued gravity. This comparison is extended to include the differences in interpretive products produced from each dataset, in the form of 3D gravity inversions. Inversions were completed on all three datasets and the results are compared. Although the resolution of an individual ground gravity measurement is greater than that of an AGG measurement, the uniformity of the AGG survey provides superior coverage and leads to a more detailed inversion model, particularly for features greater than ~200-400m, such as the prospective nickel bearing troctolite chambers.

Acknowledgements

I would like to thank my supervisor, Bill Morris, for his supervision and support of this thesis over the many years of its completion. I would like to thank Vale for supporting my efforts to complete this study. In particular, I would like to offer special thanks to Alan King and Brian Bengert who initially encouraged my pursuit of a Master's degree and continued to support me throughout my program. Special thanks to the Voisey's Bay exploration team for the support and encouragement I received, as well as the insights into nickel exploration. Finally, I would like to thank my mother, father, sister, girlfriend Iris, and my many friends who have constantly supported, prodded, and pushed me to finally complete this program.

Table of Contents

List of Figures

Chapter 2:

Chapter 3

Chapter 4

Chapter 5

Chapter 6

Chapter 1: Introduction

A major development within mineral exploration over the past decade has been the introduction and increased use of airborne gravity gradiometry (AGG). This technology has been adapted enthusiastically throughout the industry as an exploration tool for a variety of commodities, across both green-fields and brown-fields projects. However there are still often questions commonly asked about the exact niche that an AGG survey should occupy within an exploration program, what are reasonable expectations from the technology, and how it technically compares to the more traditional method of ground gravity. These questions will be addressed throughout the course of this study by examining the role of AGG in the context of a 2007 nickel exploration program in Northern Labrador, by Vale.

In Chapter 2 an overview of the airborne gravimetry method is provided, including both airborne gravity and airborne gravity gradiometry. A description of the technique and measured units is given, along with a review of the history and development of the technology. The current state of airborne gravimetry system technology is presented, as well as a summary of several major R&D initiatives around the world to develop better future AGG systems. Finally, the practical uncertainties and sources of error in airborne gravimetry are considered.

In Chapter 3 we examine the gravity response of the Voisey's Bay nickel system, and how this is significant to an exploration strategy aimed at finding massive Ni-sulphides in other areas of Labrador. A geological description of the Voisey's Bay regional geology and specific deposits is first given. In order to appreciate the niche of the gravity method in Ni exploration amongst other available techniques, a geophysical characterization of the Voisey's Bay

mineralized system is presented. The role of airborne gravity gradiometry technology in the collection of gravity and identification of other major nickel-hosting systems is described, and a forward modeling exercise using the physical properties of Voisey's Bay geology is completed and discussed.

Chapter 4 summarizes the collection and treatment of the airborne gravity gradiometry data in the Voisey's Bay study. Issues and details around field data acquisition of the data are reviewed. A through discussion of the terrain correction applied to the dataset is presented, as well as other digital elevation model (DEM) considerations. Finally, a summary of filtering completed on the final AGG data in order to produce interpretive maps is given.

In order to examine the technical differences in data content, a spectral analysis of both the AGG, the ground gravity data, and an upward-continued version of the ground gravity (meant to represent the sensitivity of an airborne gravity survey) over the Voisey's Bay mineralized system is completed in Chapter 5. This begins with a discussion of the spatial sampling of both data sets and the qualitative features contained in both. The methodology behind the analysis is reviewed, and both datasets are subjected to a 2D power and radially averaged spectral analysis.

In Chapter 6 the AGG, ground gravity, and upward-continued ground gravity datasets are compared in the context of their final interpretive results. The interpretation technique of choice in this case is geophysical inversion using software from the University of British Columbia's Geophysical Inversion Facility (UBC-GIF). Inversion theory and methodology is discussed in terms of the components of the model objective function, the optimization of the

inversion solution, and the discretization of the Earth. Final inversion results for all three datasets are shown and discussed.

Chapter 7 provides a summary of the observations made over the course of this study. A consideration of the results and the capabilities of airborne gravity, particularly in terms of how it compares to ground gravity is given. Also, and overview of what the study results mean to the use of AGG as a tool in the exploration industry will be concluded.

Chapter 2: Airborne Gravimetry

2.1: Introduction

In this chapter, an overview of the AGG method is given in order to provide the context for the examination of AGG as an exploration tool. A history of airborne gravimetry will be presented, as well as a technical description of AGG measurements and units. A summary of all existing commercially available airborne gravity and airborne gravity gradiometry technology is provided, along with several of the major research initiatives from around the world aimed at making more sensitive AGG sensors in the future. A discussion of the potential sources of error and uncertainty when working with AGG data highlights many of the technique's obstacles that we will be closely examining within this study.

2.2: Introduction to Airborne Gravimetry

Gravity prospecting involves measuring variations in the Earth's gravitational field in order to locate local masses of greater or lesser density within the subsurface geology. Traditional gravimetry measures gravitational acceleration, for which the unit is meter per second squared (m/s^2). In most geophysical applications, however, we are dealing with very small variations in the Earth's gravitational acceleration that is better represented by micrometer per second squared ($\mu m/s^2$). The industry standard for reporting gravity measurements is the mGal, which is a CGS unit for acceleration that is equivalent to 10

micrometers per second squared (1mGal=10μm/s^2). The method has been very effective in a range of exploration uses including helping constrain seismic interpretations of sedimentary packages in oil exploration, mapping regional lithology, and even discovering economic mineral deposits in some cases.

The modern gravimeter was originally developed in the 1930's by Lucien LaCoste and Arnold Romberg. This invention provided the framework for all gravimeter developments up until today, and consisted basically of a mass on a spring that is deflected due to minute variations present in the earth's gravity field. This type of system measures relative gravity which must be calibrated to an absolute value either by extending the survey to a location with a known gravitational acceleration or by using an absolute gravimeter. Absolute gravimeters are based on measuring the acceleration of free fall for a given mass, and provide an absolute value of the Earth's gravitational acceleration at a given location. These are generally much more bulky, and are not practical for field use (Telford, 1990).

Due to the versatility and usefulness of the gravity method, it was quickly recognized as a primary means of geophysical prospecting. As with any type of geophysical method, there is a trade-off in an increased resolution from performing a survey on the ground in comparison to an increased production rate and cheaper survey cost from performing a survey from the air. However while other passive geophysical methods, such as magnetics, benefited from adaption into airborne acquisition system decades ago the advent of airborne gravimetry has become commercially available relatively recently. The reasons behind this extended development

delay lie in the fundamental difficulties associated with the collection of gravity data in comparison to many other types of geophysical datasets.

One such difficulty is that the range of physical properties affecting gravity data is relatively smaller, resulting in much smaller anomalous signal relative to the Earth's field. Another factor is that topography variations have a much greater effect on gravity data than on other geophysical datasets (Lane et al, 2010). However while both of these issues effectively impede the signal to noise ratio of gravity data, the chief difficulty within the context of acquiring airborne gravity measurements is the sensitivity of gravity measurements to the motion of a moving (accelerating) survey platform. In order to collect meaningful measurements of gravitational acceleration in such a highly dynamic environment, great effort must be taken to distinguish the inertial accelerations of the vehicle from the accelerations due to gravity, and measure these small changes in gravity accurately . In order to separate the two, an independent measure of inertial acceleration is required.

Over the course of the past 75 years, the basic design and principles behind the gravimeter have remained very similar, and much of the effort for the development of airborne gravimetry involved trying to tackle the problem of how to best separate the 'geologic' signal within the gravity data from the inertial noise. Advancements focused on improving the original design of a stabilization platform that allows for the gravimeter to measure only in the vertical direction, and more accurately measuring the location of a surveying aircraft in space. This work has seen airborne gravimetry come from the original methods of using Doppler radar to measure its northing and easting position and an altimeter which relied on measuring the

varying boiling point of a liquid, to much more accurate methods using dual frequency carrier phase GPS and radar altimeter. Independent measurement of the motion of the aircraft via GPS navigation information allows inertial acceleration to be calculated and subtracted from the total acceleration, leaving the component of acceleration due to gravity (Lane, 2004). However even with the advantage of advanced and highly precise methods the best measures are limited by the uncertainty in GPS and the resultant signal is of limited bandwidth (Brunton, 2000).

More recently, a second method of taking gravity measurements from an aircraft has been developed in the form of airborne gravity gradiometry (AGG). The AGG systems which are currently in use are composed of groups of four acceleration sensors mounted on rotating disks (Lee, 2001). The inertial acceleration of the disk is common to all sensors, and the combinations of the sensor outputs can be used to estimate gradients of the acceleration due to gravity in the plane of the disk. Multiple components of the gravity gradient tensor are measured and subsequently transformed into vertical gravity (Lane, 2004). By measuring the gradient of the gravity it is possible to ignore linear contributions to the gravity signal from aircraft movement noise, although there is still sensitivity to angular noise. Although AGG data is limited at short wavelengths by inertial acceleration due to turbulence and at long wavelengths by the survey size and associated truncation errors from the integration of gradient signals over a finite area, it typically contains much more resolution and bandwidth than traditional airborne gravity.

While airborne gravity measures the same quantity as previously described for traditional gravity, airborne gravity gradiometry measures the gradient of acceleration. The unit of measurement for this quantity is acceleration divided by distance unit, thus "per second square" ($1/s^2$) is the appropriate unit in the SI system. Due to the diminutive nature of gravity gradient variations, the units most commonly dealt with are "per nanosecond squared" (ns^{-2}), which is commonly known as an Eotvos within the geophysical community (1 ns^{-2} = Eo). In considering resolution and noise within a dynamic gravity gradiometry survey, data is generally considered in the units of Eotvos at 1 sample per second (Eo/√Hz) (Lane et al., 2004).

2.3: Airborne Gravity and Gravity Gradiometry Technology

The amount of research and investment in airborne gravimetry has seen a steady increase over the course of the past decade, with 10 companies now providing surveying services worldwide, and an estimated 45 different systems in use as of 2010 (Difrancesco, 2010). One such system is the turnkey gravity system (TAGS) developed by Micro-G Lacoste Inc. through upgrading their existing AirSea II gravimeter to be optimized for airborne purposes. This system includes a magnetic damping system to reduce the effects of large signals caused by aircraft turbulence, an enhanced stability platform, and improved data acquisition and control electronics to minimal signal filtering. Another major feature is a rubidium oscillator for greater timing precision, and an integrated GPS system for UTC time-synchronization and differential positioning (Brady, 2010).

Another prominent system is the Sander Airborne Inertially Referenced Gravimeter (AIRGrav) system. Sander Geophysics began using a 3-axis inertially stabilized platform in the early 90's for use in its airborne gravity surveys, before most other companies, but choose a gravimeter that is not spring based. The AIRGrav system instead consists of three orthogonal accelerometers that possess a wide dynamic range. This allows the system to avoid saturation sometimes experienced by spring-based systems in the presence of strong vertical motion of the aircraft (Sander, 2004).

A third noteworthy system is Canadian Micro Gravity Ltd.'s GT-2A airborne gravimetry system uses a spring-based gravimeter developed in Russia for military purposes, along with a similar 3-axis inertially stabilized platform. The specialized platform make use of horizontal accelerometers, dynamically tuned gyros, and fiber optic gyros (for azimuthal control), which all interact in order to try and prevent inertial acceleration noise from entering the dataset by keeping the gravimeter vertical despite maneuvers of the aircraft. These are, in turn, placed upon shock mounts and an arrangement of springs and dampers (Olson, 2010).

In addition to these more novel systems, there are several other systems commercially available which use traditional LaCoste & Romberg dynamic gravimeters. In general, typical airborne gravity surveys cost between $40 and $70 per line-km (Difrancesco, 2010) and tend to have noise standard deviations in the range of 0.15-0.6 mGal for wavelengths of 2-4km (Sander, 2004; Gabell et al., 2004).

Airborne gravity gradiometry providers, although more limited in number, have also seen a large growth in the past decade, including three companies who are currently offering

commercial AGG surveying services, and a number of other groups who are actively developing systems. All gravity gradiometers currently being used in commercial airborne surveys are making use of the same sensor design: the rotating accelerometer gravity-gradiometer developed by Lockheed Martin. This technology had originally been developed by Lockheed Martin for submarine detection on behalf of the US military, and incorporates high-precision, room-temperature accelerometers as the primary component. The basic function of the system involves taking the accelerometer outputs and combining these measurements to measure 2 tensor components of the gravity signal while continuously balancing scale factors of each sensor (Difrancesco et al, 2009). The first gravity gradiometer system was developed by BHP, who gained access to this technology for the purpose of mineral exploration, and in 2001 flew the first airborne gravity gradiometry survey with a system called Falcon (Dransfield et al., 2001). The Falcon system consists of a GGI (gravity gradient instrument) made up of four low-noise inertial-grade accelerometers mounted orthogonally on a rotating block. The summed output of these accelerometers provides the gravity gradient signal in the vertical axis. This system has since been sold and is now operated by Fugro Airborne Surveys.

Bell Geospace was the next group to develop an airborne gravity gradiometer system, with the full tensor gravity (FTG) system. What separated their sensor from the Falcon sensor was that it measured all 9 components of the gradiometry signal (five of which are independent vectors). This is done using three GGIs, each consisting of two opposing pairs of accelerometers arranged on a disc. The gradient of the gravity field is measured as the difference in readings between the opposing pairs of accelerometers on each disc. The GGIs are mounted so that their axes are perpendicular to one another, and all are the same angle to the vertical axis. This

entire setup is rotated about the vertical so as to eliminate linear noise contributions from aircraft movement. The advantage of measuring all 9 components of the gravity gradiometry signal is apparent not only in the additional data which can be useful in interpretation, but also in QA/QC processing of the data. False anomalies from system noise can be eliminated in this way by checking between different components for validation (Murphy, 2004; Mims et al., 2012). The third company currently offering commercial AGG surveys is ARKeX, whose system shares similarities to the Bell Geospace FTG system in recording the full tensor gravity gradient by using the same sensor set up (3 angled GGIs rotating about a vertical axis).

All three listed systems are primarily flown in fixed-wing aircraft; however Fugro has recently begun offering Falcon surveys using a Eurocopter AS350 helicopter. Helicopter surveys benefit from slower survey speeds and being able to drape the topography closer than a fixed-wing aircraft, but generally suffer from more high-frequency vibrational noise in the data. A notable exception in typical aircraft platforms for AGG surveys was the historic deployment of an FTG system on a Zeppelin airship in South Africa as joint effort by Bell Geospace and DeBeers. The airship proved to be a radically more stable platform for AGG data collection and provided the most accurate AGG data published to date, demonstrating a noise level of 1.7 Eotvos RMS (Hatch et al., 2007). The airship also suffered numerous operational issues, especially downtime and safety concerns surrounding high winds (Hatch and Pitts, 2010). In general, however, AGG surveys using the more traditional fixed-wing platform commonly have noise levels of 4-7 Eotvos for wavelengths of 300-600m (Murphy, 2004, Dransfield and Lee, 2004).

In addition to the rotating accelerometer-based gravity gradiometer sensors that are currently available for commercial use, there are also a number of different new sensors being developed. The amount and variety of AGG sensors currently being developed is evidence of the momentum of this technique throughout the geophysical community. One of the more notable sensor development projects includes ARKeX's Exploration Gravity Gradiometer (EGG), which uses a superconducting gradiometer sensor, is reported to be in the advanced stages of testing. This system would theoretically have no moving parts, and use superconductivity and low temperatures to achieve low noise and negligible scale factor or drift. The two key principles of superconductivity that the EGG takes advantage of are the 'Meissner effect', which provides levitation of the proof masses, and 'flux quantization', which gives the system inherent stability. All this relies on sets of superconducting circuits that are balanced such that their responses are largely indifferent to linear and angular accelerations associated with plane motion (DiFrancesco, 2009).

Another interesting development project is underway by GEDEX, who is working to develop a high performance gravity gradiometer integrated with an active six-degree-of-freedom isolation system to minimize vehicle dynamic inputs, potentially resulting in a very sensitive and robust system for exploration. The sensor being used is the Orthogonal Quadrupole Responder (OQR), which is based on micro-flexures supporting pairs of balance beams, which directly measure gravity gradients. The gradiometer design also uses superconducting components to achieve low instrumental quiescent noise (DiFrancesco, 2009). Another similar sensor development project is collaboration between Rio Tinto and the

University of Western Australia (UWA) to develop a OQR gravity gradiometer with the goal of a 1 Eotvos noise level or better (Anstie et al, 2010).

A ribbon sensor has been developed by Gravitec Instruments Ltd. in order to measure gravity gradients. The sensor is comprised of a single sensing ribbon that responds to gravity gradient forces. External electronics provide control, measurement and modulation functions (Veryaskin, 2000). This could potentially be adapted in the future for applications on ground, in the air, or in boreholes.

Stanford University has developed an Atomic Interferometer (AI) gravity gradiometer that uses the traditional approach of measuring free-falling objects, with the unique aspect of having atomic particles to serve as the measured test masses. Atom trajectories are monitored by coherent laser pulses to derive inertial information. Combining two such sensors provides the basis for a gravity gradient measurement. This process is enabled by laser cooling techniques to achieve the required velocity (wavelength) control for the atom source and by the production of bright, coherent atomic sources (DiFrancesco, 2009).

2.4: Uncertainties and Sources of Error

As previously mentioned, exploration gravimetry tends to require more corrections than most other geophysical methods in order to reduce the observed data to an image which reflects the desired residual gravity signature. Traditional gravity readings tend to be affected by five primary factors: latitude, elevation, topography of the surrounding terrain, earth tides,

and density variations in the subsurface. In gravity exploration, of course, we are concerned with the latter-most of these features, which tends to be smaller in magnitude than gravity responses caused by elevation and latitude and smaller in magnitude than those responses cause by tides and, usually, topography (Telford et al., 1990). The process of gravity data reduction traditionally involves steps to account for each of these factors, including 1) a latitude correction, to account for the Earth's equatorial bulge, 2)a free-air correction, to account for the elevation of the survey readings above the geoid, 3)the Bouguer correction, which accounts for the material between the survey elevation and the geoid, 4)the terrain correction, which accounts for irregularities in topography in the vicinity of the survey, and 5)an Earth-tide correction, that corrects for changes caused by the movement of the Sun and moon (Telford et al., 1990). Resolution of ground gravity surveys tend to be limited primarily by spatial sampling, which in turn is usually limited by logistical factors. A gravity program using multiple crews and gravimeters can be expensive, and if access to the survey area is an issue, which is very common in many parts of the world, then the survey will often rely on very expensive helicopter support to move from one area to another. For local, highly detailed surveys ground gravity tends to provide the highest resolution possible, but if the scope of a survey requires coverage of a regional area then resolution is quickly reduced as the survey design involves very large station spacing (5-15km) in order to make the work cost-effective. In addition, and accurate GPS signal is a requirement for the collection of accurate gravity data, and for areas in which this may be problematic (under a thick canopy, or next to steep hills at higher latitudes) highly accurate ground gravity may be impossible to collect.

Airborne gravity offers a solution to fast and effective regional surveys, and while some signal resolution is lost by taking survey measurements from a higher elevation, there are other resolution benefits realized through denser spatial sampling. An added source of uncertainty in airborne gravity is the inertial acceleration of the aircraft, which has the potential to impact the measurement of the Earth's gravitational acceleration. Airborne gravity systems require an independent measurement of aircraft motion, which is gained through the use of inertial navigation along information along with GPS measurements. Inertial acceleration is calculated and subtracted from the total acceleration, leaving the component of acceleration due to gravity. Due to its dependency on GPS navigation, the controlling factor on airborne gravity resolution is directly related to GPS uncertainties, which rise in magnitude as wavelength decreases (**Figure 2.1**) (Brunton, 2000). This noise is suppressed by low-pass filtering of the

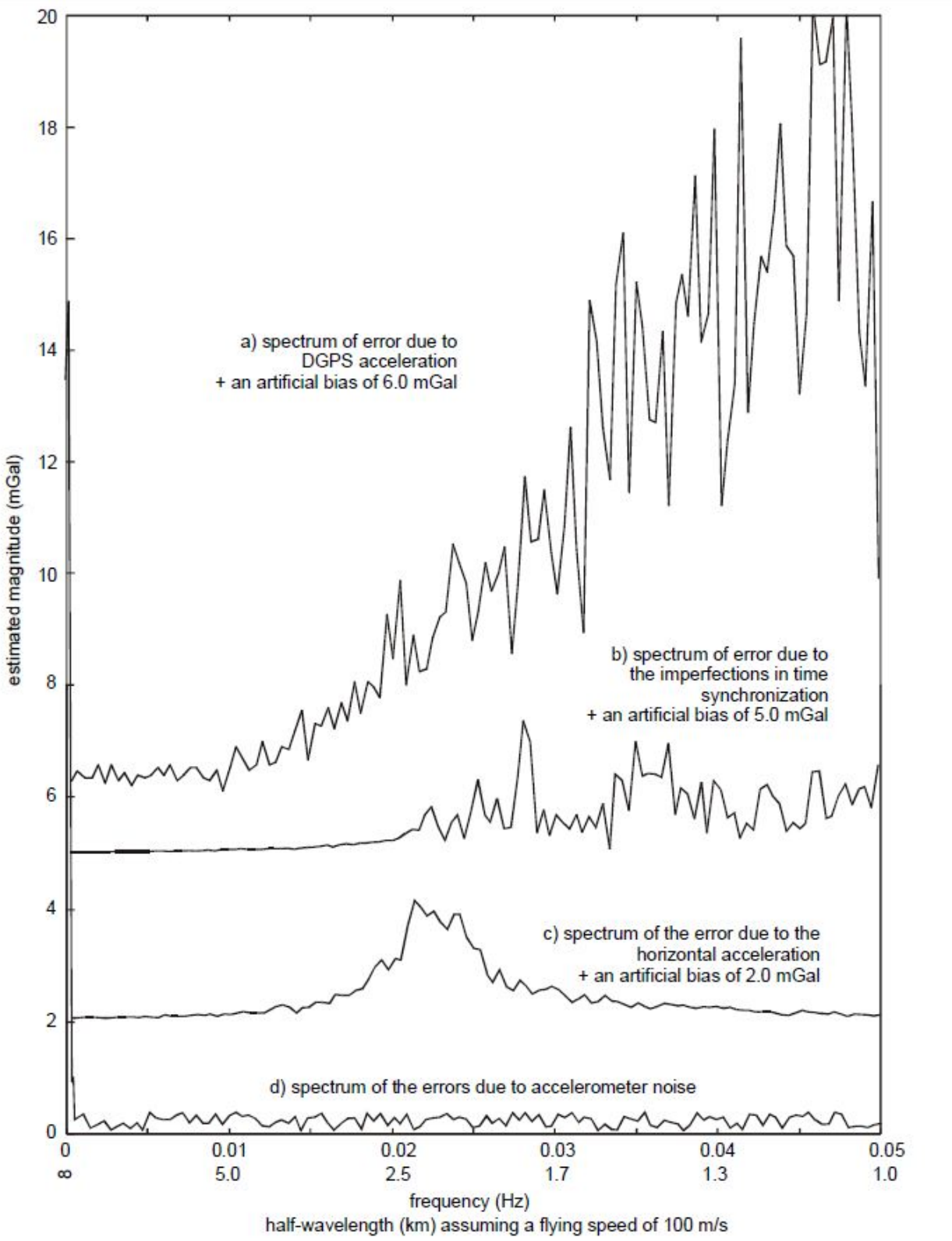

Figure 2.1: Spectra of samples of the errors affecting scalar gravimetry, after (Brunton, 2000)

GPS data. In order for airborne gravity to be useful for detailed mapping and direct detection of economic mineral deposits with a distinct density contrast, an improvement of at least an order of magnitude in GPS accuracy would be required. Such an improvement is not expected to be achievable in the foreseeable future, and therefore the high-resolution capabilities of airborne gravimetry are not expected to soon improve (Kann, 2004).

The current noise floor and future prospects for improvement of AGG systems are much better. A common theme in the consideration of noise in airborne gravity gradiometry systems is that although this technology offers great advantages in sensitivity over previous sensors, the challenges of noise from many sources are also much greater. The challenges of noise for any given AGG sensor include both intrinsic and external sources. Noise may be encountered within the design of the sensor itself via electronic noise, sensitivity to molecular motion or Eddy currents (DiFrancesco, 2009). Potential system noise challenges external to the sensor include changes in temperature and pressure, and, most importantly of all, the dynamic input from the aircraft. If the linear and angular motion associated with the aircraft is not removed then the gradient signal quickly becomes overwhelmed.

The primary sources of noise associated with an AGG survey include not only instrumental and system noise, but terrain and elevation noise as well. Although these factors have been noted as challenges in traditional gravimetry, their influence is magnified in the case of AGG surveys due to the fact that the gradient of the gravity falls off more rapidly as a function of distance from the source ($\frac{1}{r^3}$ as opposed to $\frac{1}{r^2}$), and tends to contain a much higher frequency content (Kass and Li, 2008). As a result, the influence of elevation and terrain are

vital pieces of information, and are very capable of limiting the accuracy of any AGG survey beyond the point of being able to benefit from advances in sensor technology.

Knowledge of the terrain in a survey area is often a limiting factor in how close gravity data may come to detecting features of interest in the subsurface. The detailed variation of hills or valleys which may go unaccounted for may add very significant artifacts to the data, overwhelming smaller gradient signals of interest. The most accurate current method for terrain control is the deployment of a Light Detection and Ranging (LiDAR) system, which measures distances by illuminating a target with a laser and then analyzing the resulting reflection. LiDAR surveys are commonly flown separately from airborne gravimetry surveys because they are commonly flown at a greater height and to sample a greater swatch of ground. By surveying many such overlapping swaths of topography in the survey area a LiDAR survey creates the necessarily high level of statistical repeatability and reliability required to build and accurate DEM. Geophysical surveys, such as AGG, on the other hand are primarily concerned with signal strength and resolution, and are flown as close to the ground as safely possible. LiDAR methods commonly provide vertical resolution to within 5-10 cm (DiFrancesco, 2009). This data is used to create a digital elevation model (DEM) surface. This surface is assigned with assumed density information to represent the host rock geology, and is used in processing for the terrain correction. There are many additional nuances in the terrain correction of an AGG dataset, which will be considered in Chapter 4.

As discussed, the strength of the gravity gradient decreases rapidly as a function of the distance from the source, and therefore uncertainty of the survey measurement height may

also introduce large errors to an AGG dataset. The survey height measurement is derived using GPS data. The most significant advances in the accuracy of GPS data in the past decade has come from the area of processing. Modern GPS methods may currently provide a vertical resolution of +/- 5cm. (DiFrancesco, 2009) shows that a combined gravity gradient error of +/- 75cm can produce a 1 Eotvos error, overwhelming the potential benefit of improved future AGG sensors. Through this example we can see that a continued improvement in the correction of terrain and elevation effects is a key factor in future research in order to get the most out of potentially improved sensor developments (DiFrancesco, 2009).

The standard noise level attainable by most commercially available AGG systems today is approximately 10 Eo/√Hz, which is a great deal more sensitive than even the most modern airborne gravity surveys. A target resolution of 1 Eo/√Hz has been set within the geophysical community for future AGG systems to reliably permit the direct detection of ore bodies in the presence of variable host rock (Kann, 2004).

Chapter 3: Voisey's Bay Gravity

3.1: Introduction

This chapter introduces the AGG case study which will be examined throughout the remainder of the thesis. The case study includes an AGG dataset collected as part of a nickel exploration program to image prospective troctolite chambers in Northern Labrador, by Vale, during 2007. More specifically, we will examine the portion of the survey over the Voisey's Bay main block that contains several economic nickel deposits, including the world-class Ovoid deposit. This area has been characterized both geologically and geophysically in the past, and contains multiple datasets, including ground gravity, which will be very useful for comparison. A geological and geophysical description of the Voisey's Bay environment will be reviewed, and a forward modeling exercise is completed using Voisey's Bay physical rock properties to calculate the response that could be expected over a nickel-bearing troctolite chamber.

3.2: Geology of Voisey's Bay

Voisey's Bay is located 45 km west-southwest of the community of Nain, Labrador (**Figure 3.1).** It was discovered during a grass-roots diamond exploration program by Archean Resources in 1993. Although the focus of the program was on diamonds, the recognition of a gossan led to subsequent sampling and discovery of disseminated Ni-Cu-Co mineralization at Discovery Hill (**Figure 3.2**) (Evans-Lamswood et al., 2000). Follow up work in the following months included an extensive field mapping and horizontal-loop electro-magnetics (HLEM)

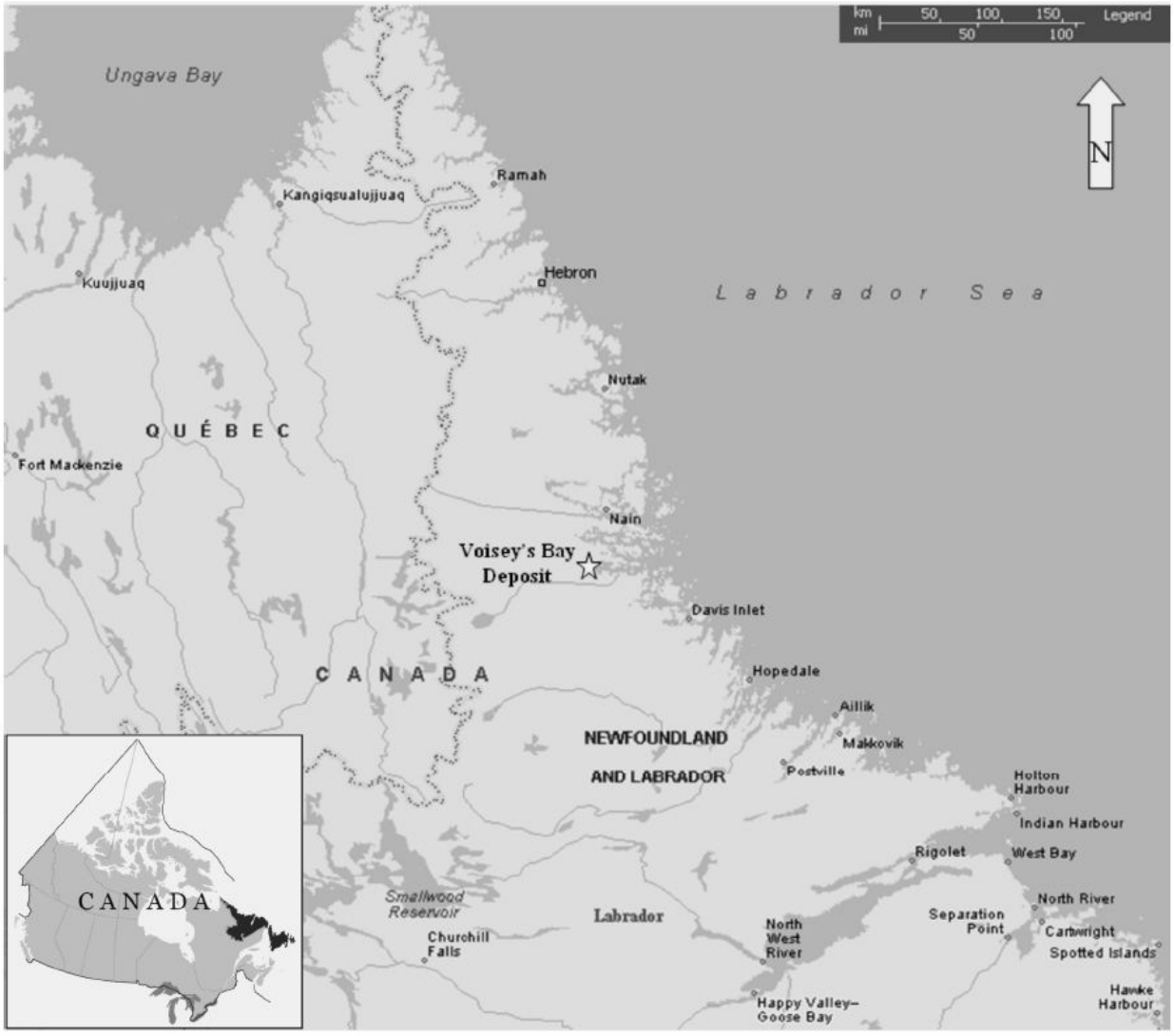

Figure 3.1: Location map for Voisey's Bay, Labrador, Canada.

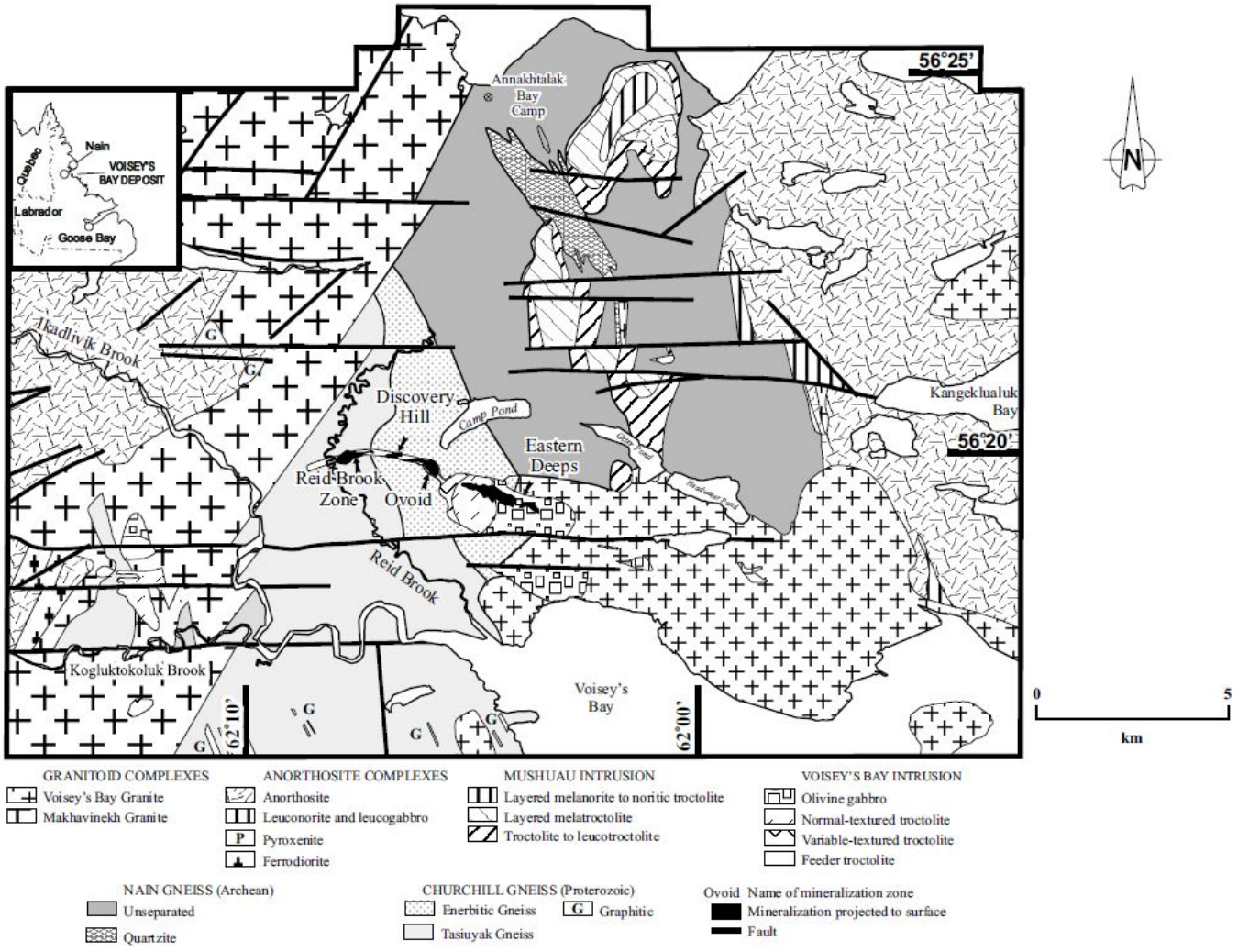

Figure 3.2: Geologic map of the Voisey's Bay area (after Evans-Lamswood, 2000)

program, the latter of which discovered an excellent east-west trending 1200m long conductor. The ensuing drill testing of this conductive trend found 41.2m of semi-massive to massive sulphide grading 2.98% Ni, 1.89% Cu, and 0.12% Co, and marked the discovery of the world-class, 31.7 million ton, nickel deposit known as the Ovoid.

The Voisey's Bay Ni-Cu-Co deposits are associated within the 1.334 Ga Voisey's Bay Intrusion (VBI), which is a troctolite-gabbro intrusion and dike complex located proximal to the 1.85 Ga collisional suture of the Proterozoic Churchill Province to the west and Archean Nain Province to the east (Ryan et al., 1995) **(Figure 3.3).** The VBI intrudes Archean quartz feldspar-biotite gneiss of the Nain province as well as Proterozoic sulfidic garnetiferous paragneiss of the Churchill province (Ryan et al., 1995), and is a member of the Nain Plutonic Suite (1.34-1.29 Ga) (Ryan, 1996). The Nain Plutonic Suite includes granitic, anorthositic, ferrodioritic, and troctolitic-gabbro intrusions that straddle the boundary between the Proterozoic Churchill province to the west and the Archean Nain province to the east. The Churchill Province, on the other hand, consists of the reworked Archean rocks and inter-banded sulphide and graphite bearing paragneiss, known as the "Tasiuyak gneiss", which is commonly believed to be the sulfur source for the Voisey's mineralization (Naldrett and Li, 2007). What was initially interpreted to be one large troctolitic intrusion, within the Nain province, was later found, through detailed mapping and geochronology, to be two separate Ni-sulphide bearing intrusions: The Voisey's Bay Intrusion (VBI) and the Mushua Intrusion (Evans et al., 2000).

The VBI consists of an upper chamber of olivine gabbro and normal to variably-textured troctolite, the Eastern Deeps, which is fed by a gabbroic/troctolitic feeder sheet. This feeder

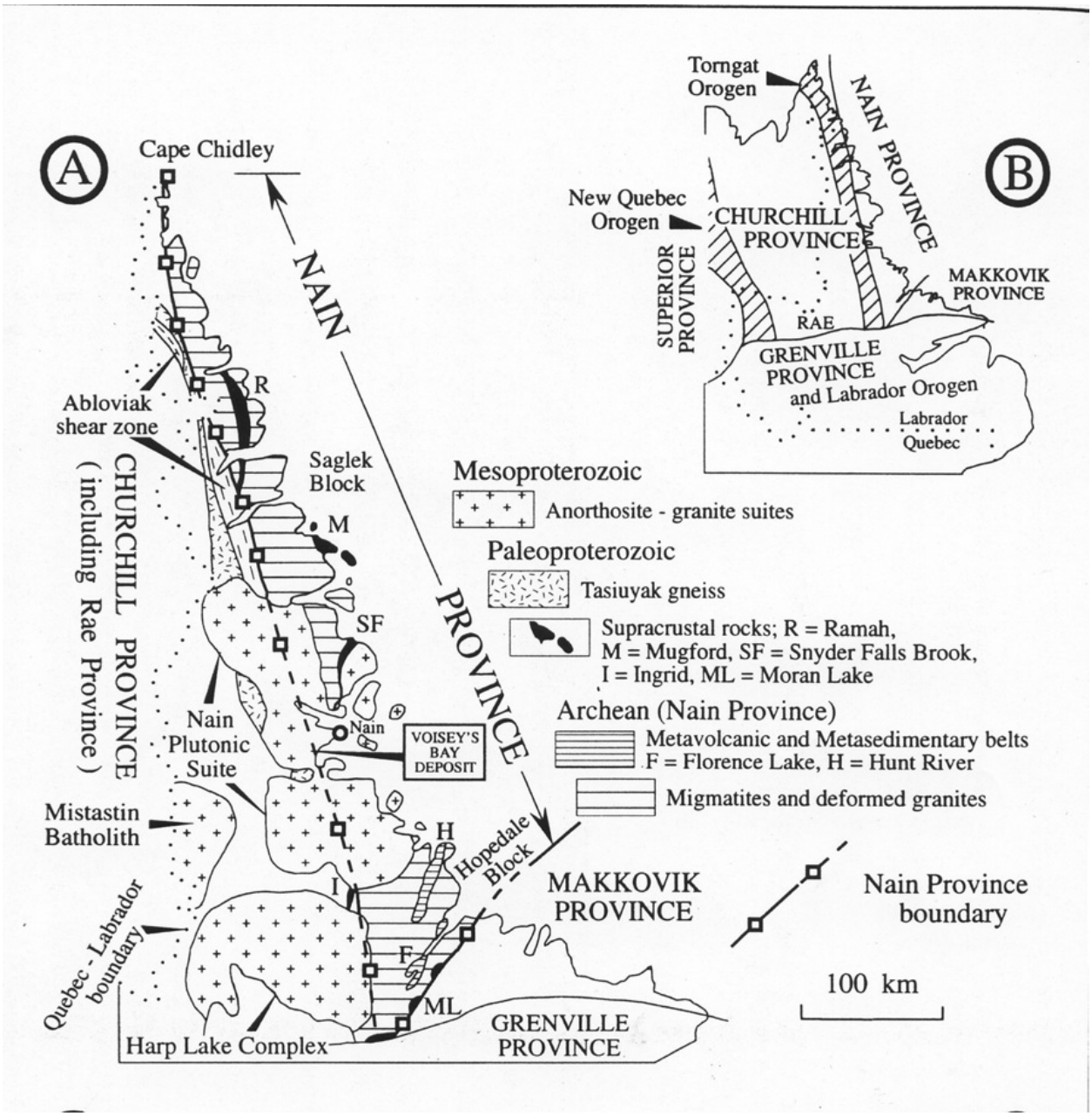

Figure 3.3: Regional Geology of Northern Labrador A: regional frame-work ; B: major litho-tectonic units (after Naldrett *et al.*,1996).

sheet is the conduit through which magma pulses were transported upward to the VBI, and contains the Ovoid, Mini-Ovoid, Discovery Hill, and Reid Brook mineralized zones. The feeder sheet comes to surface towards the west at the Discovery Hill zone, and eventually dips steeply south, widening out into a lower troctolite chamber, the Western Deeps (Naldrett and Li, 2007) (**Figure 3.2).** The Mushua intrusion is located to the northeast of the VBI, and shares many spatial and structural similarities. This intrusion has only been found to contain sub-economic amounts of Ni-sulphides to date. The lesser amount of Ni-sulphides in the Mushua intrusion is thought to be due to the lack of sulfur contamination in comparison to the VBI. As a result, this troctolite intrusion has been the subject of much less study than the VBI.

The economic deposits at Voisey's Bay are all contained within either the troctolite magma chambers or conduits connected to these chambers. There are five mineralized zones within the VBI: Eastern Deeps, Ovoid, Mini-Ovoid, Discovery Hill, and the Reid Brook (**Figure 3.4)**. Throughout these zones, mineralization exists as magmatic textured sulfide associated with fragment-bearing troctolites and olivine gabbros. The mineralization at Voisey's Bay does not follow the typical model of gravity settling within a large magma chamber subsequent to sulfide saturation due to the assimilation of local country rock. Instead, there is evidence that sulfur saturation happened at great depth and the sulfide distribution and texture within the VBI is controlled by the interaction of the geometry of the conduit and the fluid dynamics in the fragment-bearing magma within the conduit system (Evans-Lamswood et al., 2000). Although the Ovoid, Mini-Ovoid, Discovery Hill, and Reid Brook occur within, or immediately adjacent to, irregularities or embayments in the conduit (examples shown in **Figures 3.5 and 3.6)**, the Eastern Deeps mineralization occurs at the base of the Eastern Deeps chamber (**Figure 3.7)**.

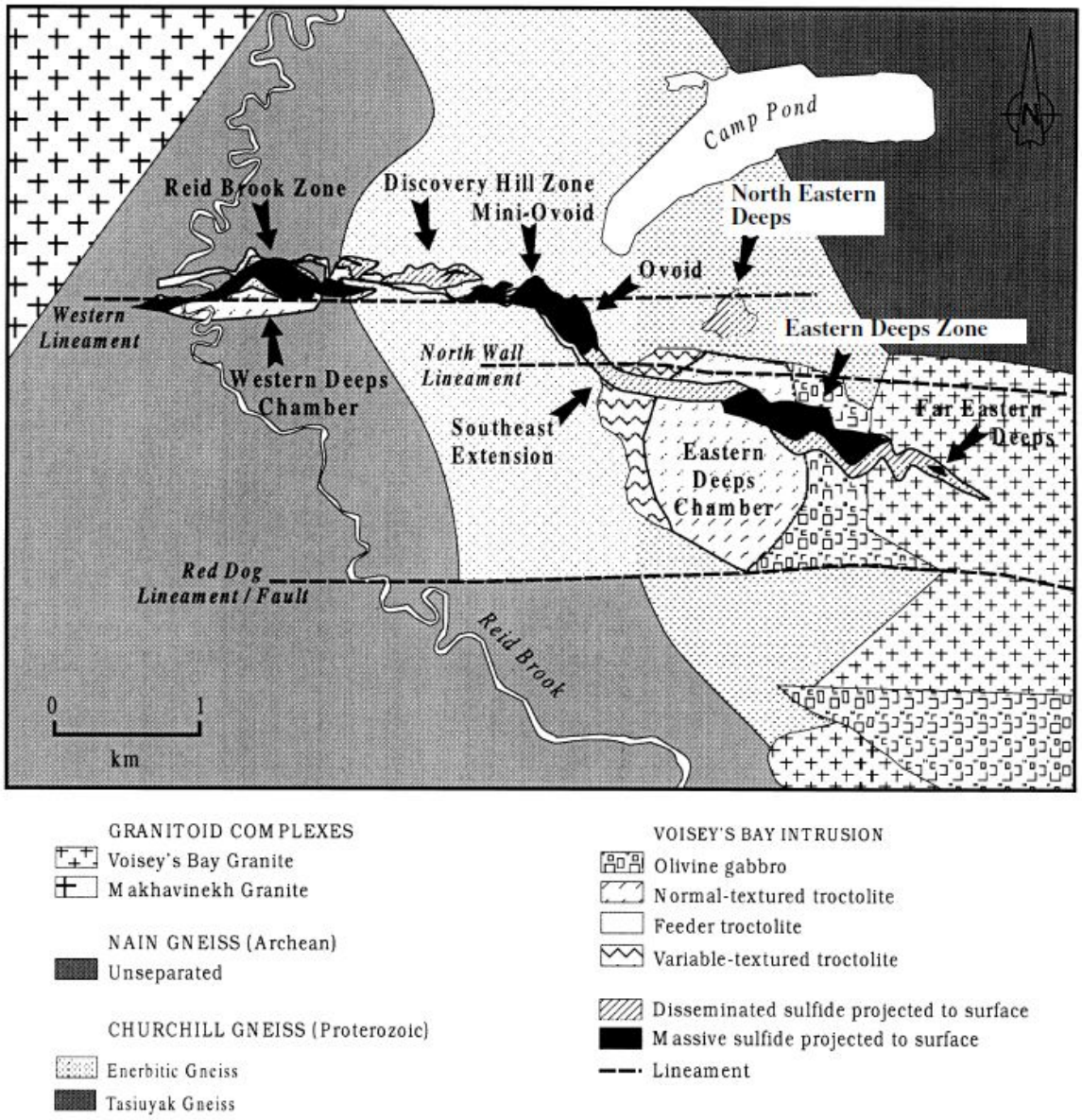

Figure 3.4: Surface projection of the Voisey's Bay troctolite, massive sulphide deposits, and major structures (after Evans-Lamswood, 2000)

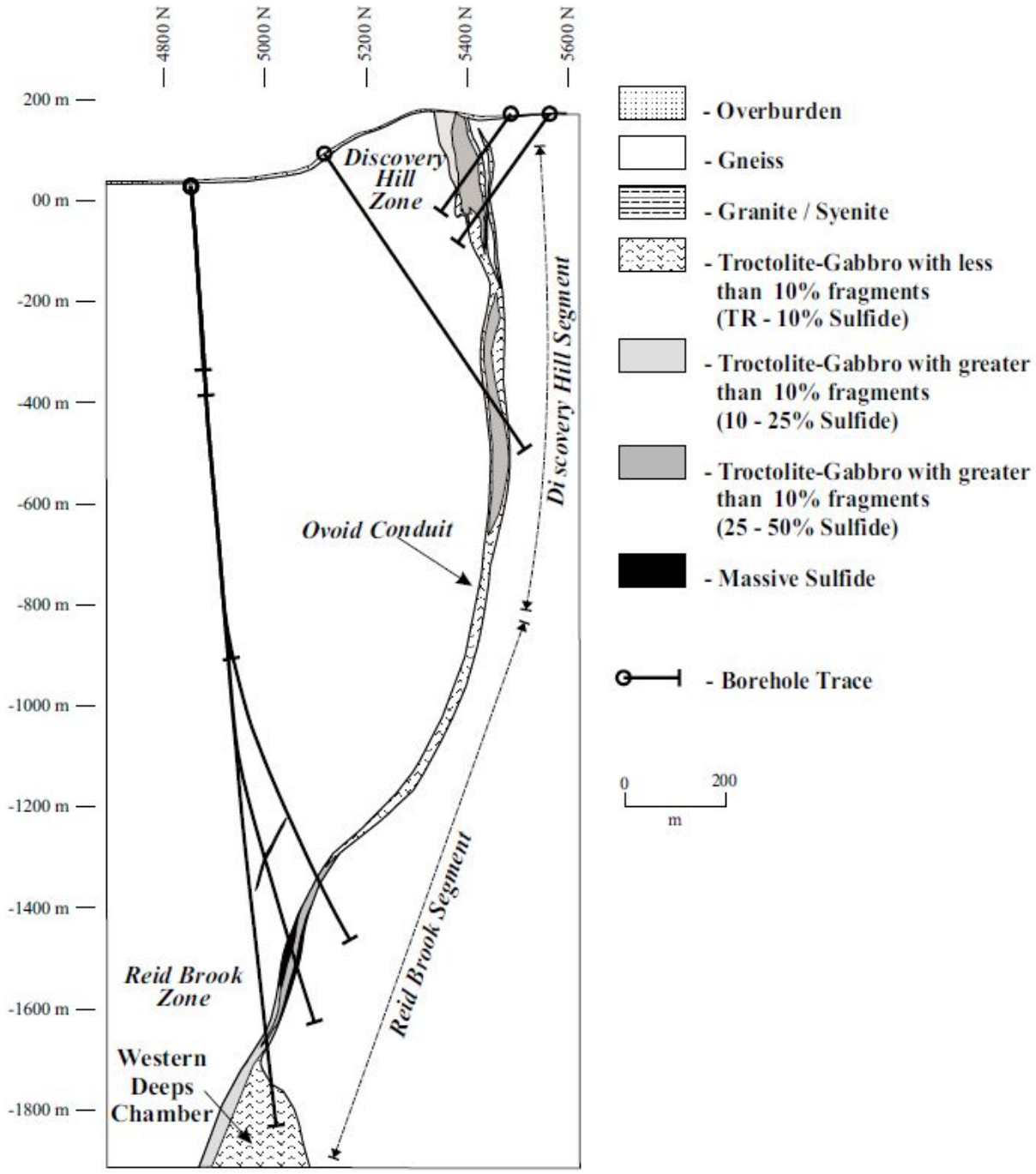

Figure 3.5: West-facing geological section showing both the Reid Brook and Discovery Hill zones occurring within the same dyke section but at different stratigraphic levels (after Evans-Lamswood, 2000)

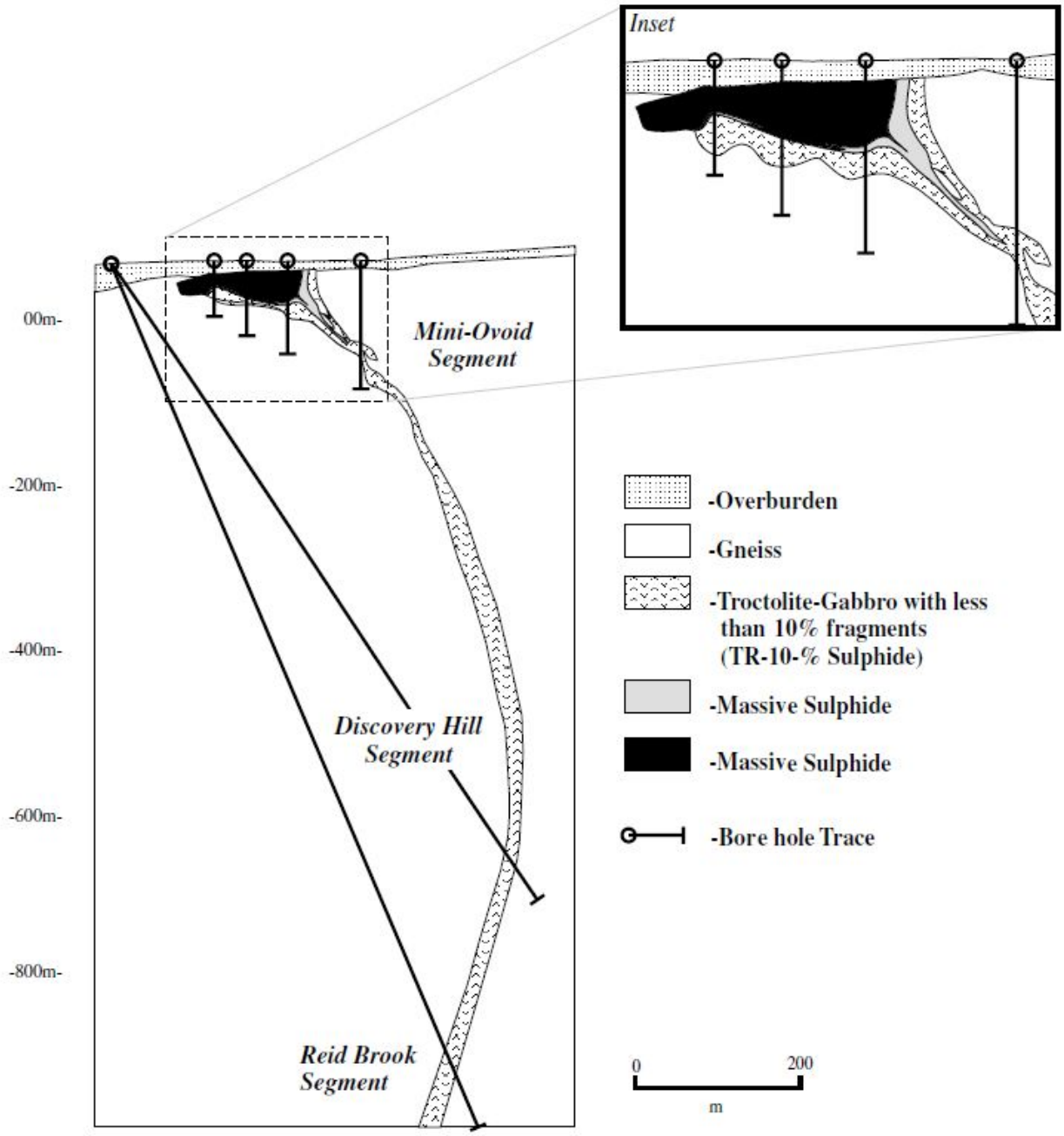

Figure 3.6: West-facing geological section through the Ovoid deposit. The deposit is interpreted to have formed within a localized major expansion of the conduit (after Evans-Lamswood, 2000)

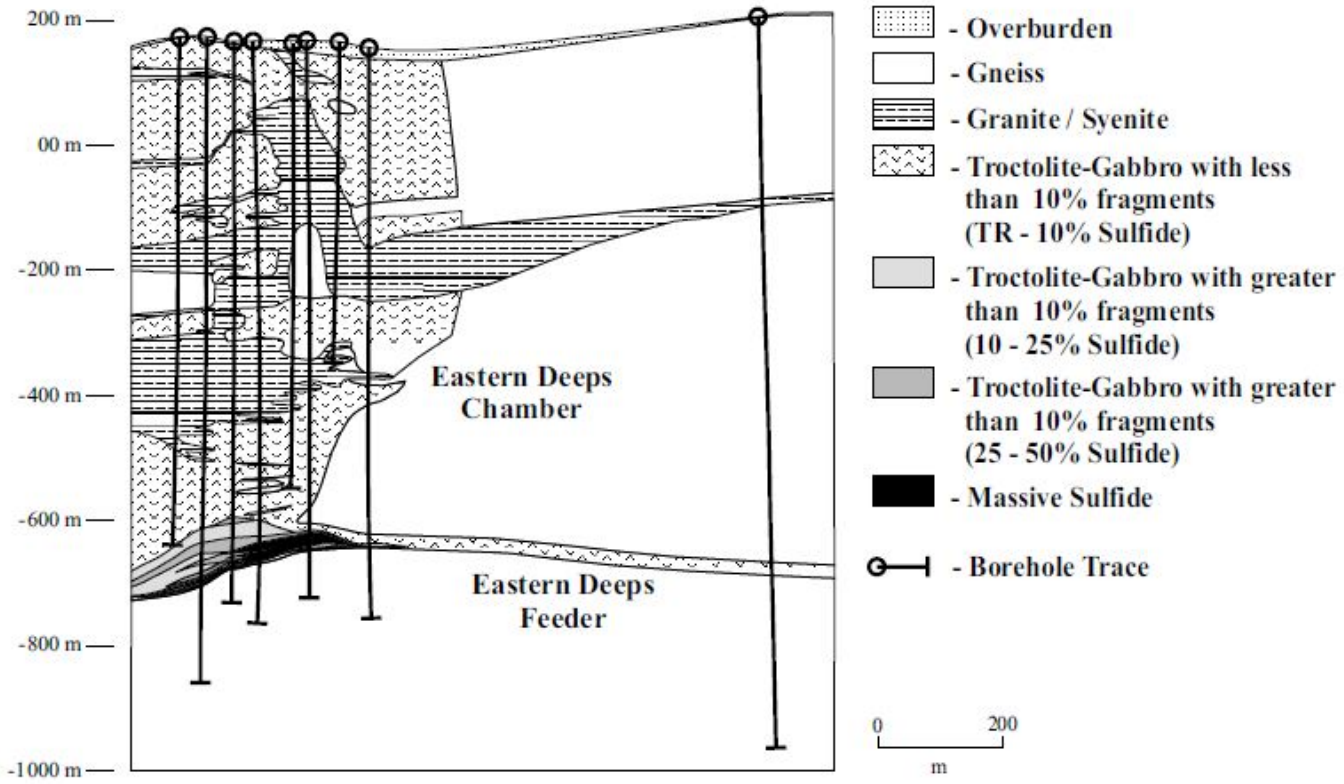

Figure 3.7: West-facing geological section showing the Eastern Deeps chamber, feeder, and deposit. The Eastern Deeps feeder occurs as a sub horizontal structure in the vicinity of the chamber, and then dips steeply into a sub vertical structure further to the North. Horizontal granite sheets intrude the chamber along a structure of similar orientation (after Evans-Lamswood, 2000)

The Ovoid deposit and Reid Brook deposits have depths of 20m and 300m, respectively, while the Eastern Deeps is significantly deeper at 700m.

For the purposes of this study, we will take a more detailed consideration of the Eastern Deeps deposit. As previously mentioned the Voisey's Bay deposits appear to have formed at depth and ascended within the system of conduits (Evans-Lamswood et al., 2000). The Eastern Deeps deposit is located at the base of the Eastern Deeps chamber and is spatially associated with the line of entry for the feeder conduit to a structural low at the base of the Eastern Deeps chamber (Evans-Lamswood et al., 2000). Mineralization consists of thick sequences of disseminated sulfides and mineralized breccia, with significant accumulations of massive sulfides. The breccia sequence is spatially associated with the ores, and a domain of troctolite with variable gneissic inclusion content forms a halo around the deposit (Lightfoot and Naldrett, 1999). Likewise, a very large envelope of troctolite containing variable amounts of disseminated sulphide surrounds the massive sulphide deposit (**Figure 3.7)**. Another common feature within the Eastern Deeps is horizontal sheets of granite that intrude themselves into the troctolite chamber, seeming to take advantage of the same types of structures as the feeder conduits. Horizontal granite sheets play a major role in the surficial expression of the Eastern Deeps chamber, as they cover it almost entirely to the east and to the south, and also intrude the troctolite chamber underlying the Reid Brook zone at multiple locations.

3.3: Geophysical Characterization of Voisey's Bay

Since its discovery in 1994, there has been a rich history of the use of geophysics in the discovery and delineation of the Voisey's Bay nickel deposits. One factor in the lead role of geophysics in Voisey's Bay early history is that although the host troctolite outcrops and strikes for several hundred meters on Discovery hill only two small gossans with low amounts of sulphide were originally visible at surface. The Eastern Deeps chamber is also exposed at surface, but is barren of sulphides down to a depth of 400m. Due to this lack of surficial expression, the initial exploration program quickly turned to geophysical methods for aid in delineation in the form of HLEM, as previously mentioned. After the incredibly successful follow-up results of the Ovoid deposit discovery, a large geophysical prospecting program was launched that included HLEM, ground magnetics, and very low frequency EM (VLF). A year later, a helicopter mag and frequency-domain EM survey using the Dighem system led to a major reconnaissance program over the Voisey's Bay area. Results from this survey and the subsequent drilling led to the discovery of the Reid Brook deposit. In the following years a large-loop time-domain EM survey mapped the Eastern Deeps zone, and borehole EM methods grew to be regularly used on every hole drilled in order to trace mineralization at depth (Balch et al., 1998).

Through the years of exploration at Voisey's Bay many types of geophysical methods have been used and/or tested over the property, including airborne and ground gravity and magnetics, airborne ground, and borehole EM, audio-magneto tellurics, induced polarization and resistivity surveys, mise-a-la-masse, seismic refraction, GPR, and cross-hole seismic

tomography (King, 2007). In the consideration of future exploration for Voisey's Bay-style deposits, it is important to consider its geophysical signature across a number of methods, especially those which might be rapidly employed in green-fields reconnaissance surveys. In this context the character of the Voisey's Bay deposits as represented in magnetics, gravity, and EM will be discussed.

One of the most common geophysical datasets used in mineral exploration is airborne magnetics. This survey is often flown in the early stages of a project, either alone or as a component of an EM survey. Magnetics also generally play a particularly prominent role in nickel exploration due to the fact that the usual host rocks, mafic/ultramafics, are highly magnetic while the sulphides associated with the Ni-Cu-S ores often have moderately magnetic components (pyrrhotite) (King, 2007). The airborne magnetics map of Voisey's Bay is shown in **Figure 3.8**, after (Balch, 1999), which was collected as a part of the Dighem airborne EM survey. Upon examination of this map, it can easily be seen that the historic method of using magnetics to explore for Ni-Cu massive sulphides does not work well at Voisey's Bay. The troctolites and ultramafic rocks here have variable levels of susceptibility according to the degree of serpentinization, but are generally low (King, 2007). Another factor in this problem is that the surrounding enderbitic orthogneiss and Nain gneiss units are very strongly magnetic (Balch, 1999), but very variably so. Yet another complication in the VB magnetics is that the sulphides related to the ore are primarily hexagonal pyrrhotite, and are non-magnetic (King, 2007). A local magnetic high exists over the core of the Ovoid deposit, but only due to a significant local concentration of coarse grained magnetite. The resulting signature of the Voisey's Bay deposit,

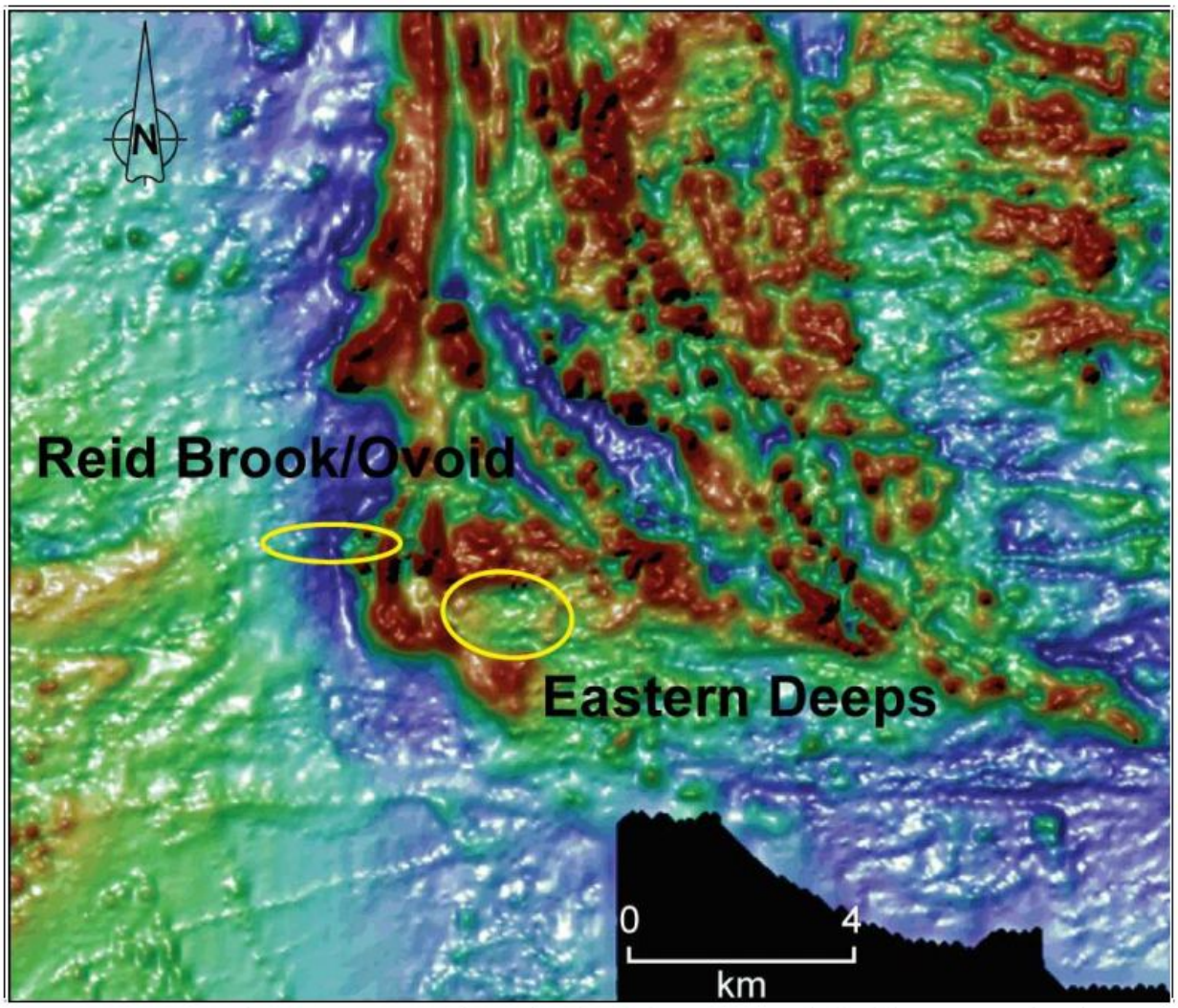

Figure 3.8: Airborne Magnetics over Voisey's Bay main block (after Balch, 1999). The non-magnetic troctolites of the VBI show little to no magnetic signature against the very magnetic and strongly variable background of the surrounding paragneissic units.

which contains both host rock and ore that is non-magnetic, is a magnetic suppression of a wildly variable background signal, and is not a characteristic easily explored for in other regions.

The ground gravity survey was collected during 1996 and 1997 by a contractor using a Lacoste and Romberg model G gravimeter and a Leica SR 299 GPS lead to the map of the Voisey's Bay main block shown in **Figure 3.9**. Gravity was found to clearly locate the main mafic intrusives and often delineate structure. The higher densities of the troctolite in the Voisey's Bay area is controlled by the iron content, and provide a sharp gravity contrast to the surrounding gneissic units. The massive sulphide ore is significantly denser than any other rock type in the area, which results in a strong local high located over the Ovoid deposit, which was located under just 20m of overburden at the time of this survey. The response of the ~800m deep Eastern Deeps massive sulphide, however, was completely lost within a broad gravity high caused by the large troctolite magma chamber hosting the mineralization (Balch, 1998). Overall, gravity was found to be an extremely accurate mapper of the troctolite host rock, but not a reliable direct detector of the economic mineralization.

The most dominant geophysical method in nickel exploration, and the type of geophysical prospective most widely and frequently used at Voisey's Bay is electro-magnetics (EM). EM methods have been used in multiple airborne, ground, and borehole configurations, using multiple systems for each survey method. Due to the extremely high conductivity of Ni-Cu sulfides and the commonly resistive nature of their crystalline host rocks, a contrast on the order of 8-9 orders of magnitude is common in nickel exploration. The conductive response of Ni-Cu sulphides are typically dominated by pyrrhotite, which is one of the most conductive

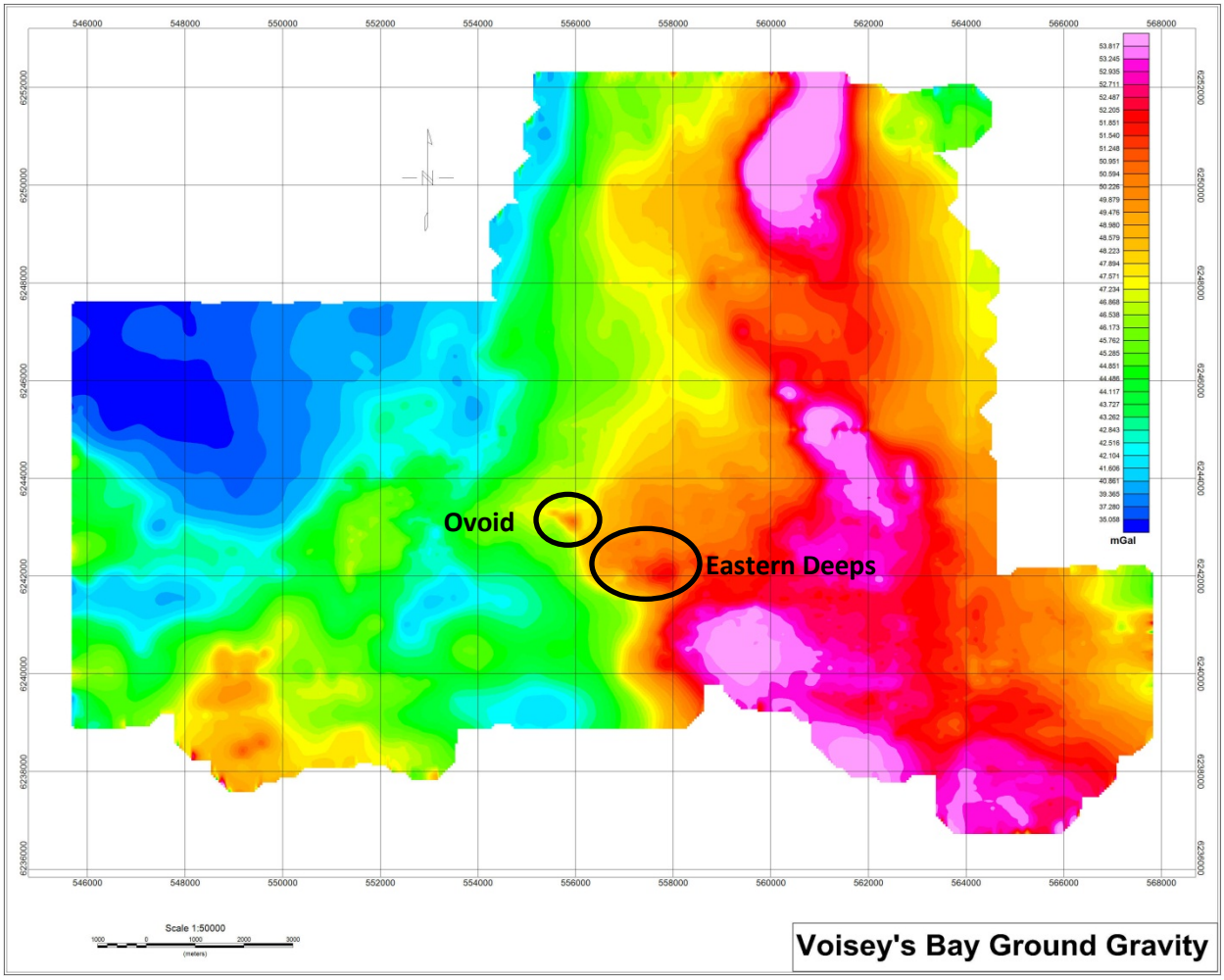

Figure 3.9: Ground gravity map over Voisey's Bay main block.

minerals on Earth (~3x10^-6 S/m) (King, 2007). As a result, massive sulphide bodies can regularly generate EM responses of over 100,000S, making nickel an extremely attractive EM target. This has driven the development of many EM systems in the direction of several key aspects: 1) detection, 2) discrimination, and 3) depth penetration.

The Ovoid deposit, as a ~40m thick flat massive sulphide body lying almost at surface, represents the ultimate EM target, but also proved to highlight some weaknesses common in EM systems **(Figure 3.10)**. Although the detection of such a strong conductor intuitively should not pose a challenge for many modern systems, those systems which rely on off-time or decay measurements (most time-domain systems of the time) actually had trouble detecting the Ovoid because the sulphide mineralization acted as a perfect conductor within the range of time-gates/frequencies being measured. Essentially the signal did not decay. In most of these cases, however, the systems did detect signal decay but this was related to the semi-massive sulphides surrounding the deposit, which were still the most conductive feature in the survey area. Frequency domain systems, on the other hand, have no upper-limit in conductance detection due to measuring the in-phase component of the signal. However because these systems were limited to higher frequencies (>900 Hz for airborne and >220 Hz for ground) very little discrimination was achieved in measuring the exact conductance, meaning that 500S conductors would usually have the same signature as 100,000S conductors.

The third major issue of EM methods for Ni exploration in general, and at Voisey's Bay, is the depth-limited nature of the technique. Due to the fact that an EM field is being imposed on the Earth in order to measure the secondary response of any conductor, the depth of

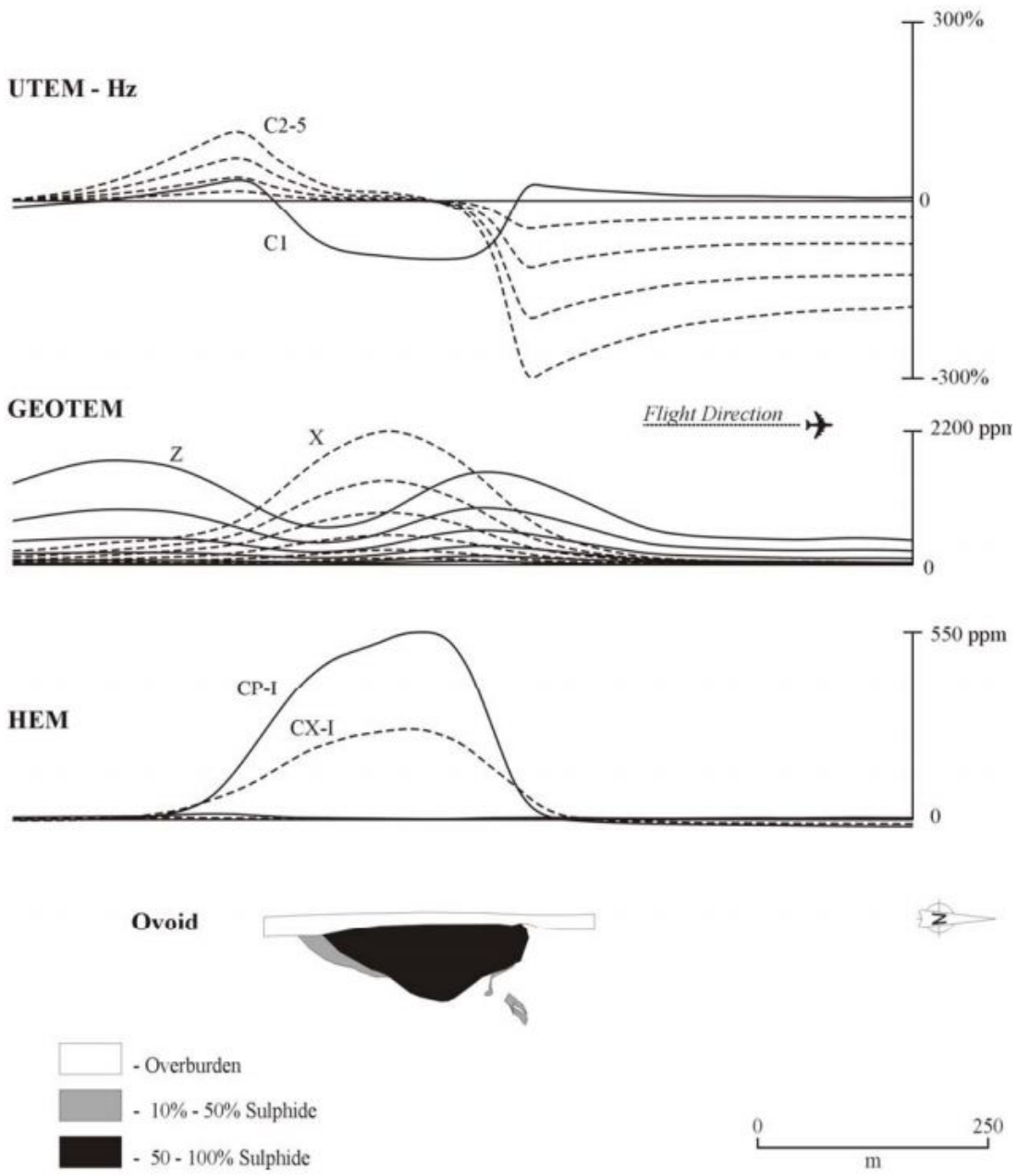

Figure 3.10: EM profiles over the Voisey's Bay Ovoid deposit (after Balch, 1999). The extreme conductance associated with this body of massive sulphides makes it difficult to directly detect by time-domain airborne EM systems which measure a 'decaying' signal (such as the GEOTEM, which is measuring the strongly decaying field from the semi-massive sulphides surrounding the deposit). Frequency-domain airborne EM systems have no problem measuring identifying the massive sulphides, but have almost no quadrature response, and thus no discrimination ability to gauge the conductance. Low-frequency ground EM methods which measured both EM decay and the primary field are most successful in identifying and qualifying the Ovoid. (after Balch 1999)

investigation is inherently limited by the depth of the inducing field. A commonly used criterion for the penetration of electromagnetic waves is the skin depth,

$$z_s \approx 500\,(\rho/f)^{\frac{1}{2}} \qquad \textbf{(Telford, 1990)}$$

where z_s is the skin depth of an EM field, ρ is the resistivity of the rock, and f is the frequency of the EM signal (Telford, 1990). From this equation we can see that if the resistivity of a rock is low, or the frequency of the inducing EM field is high, then depth penetration will be limited.

In the context of a reconnaissance airborne EM survey, this depth of investigation often varies from ~100m for older frequency domain systems to realistic depths of up to 300m for powerful, modern, time-domain systems. Another major challenge for the EM technique in the Voisey's Bay environment is the presence of other conductive material. Although the massive sulphides are the most conductive feature present, complications arose from the conductive response associated with localized sheets of graphite, lake-bottom clays, surrounding seawater, and portions of the overburden that contain related salt-brines (**Figure 3.11)**.

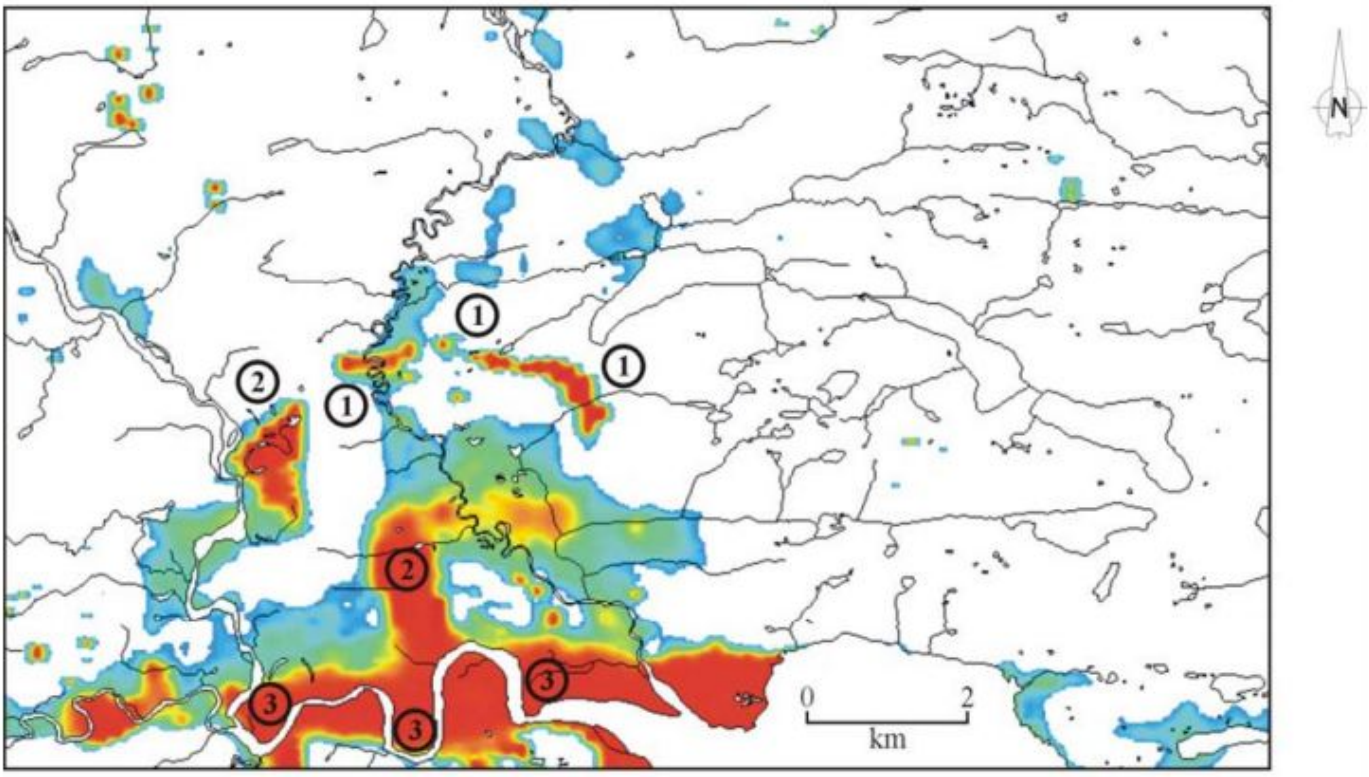

Figure 3.11: A qualitative 900Hz apparent resistivity image from the frequency-domain helicopter-borne EM DIGHEM survey (after Balch 1999). The conductivity response of the Voisey's Bay area includes responses from (1) the massive sulphide mineralization, (2) large regional graphite conductors, and (3) conductive sediment associated with salt water influence from Voisey's Bay.

3.4: AGG Nickel Exploration

Although 18 years have passed since the initial discovery of Voisey's Bay, exploration for additional nickel deposits in Northern Labrador continues. In the path forward for potential future discoveries it is important to take into consideration the lessons that have been learned during the exploration and characterization of Voisey's Bay, as well as the dominant trends in regional exploration which have thus far been unsuccessful in finding an economic nickel deposit. In the years following the Voisey's Bay discovery, exploration expenditures in Northern Labrador rose to historical levels. Regional exploration by junior mining companies demonstrated that sulphide mineralization is relatively common in a variety of rock types and geological environments, but usually does not include economic levels of nickel content. Most of these prospects were initially located by airborne EM and magnetic methods, and followed up with helicopter-supported geological surface mapping (Kerr, 2003). Due to the large amount of airborne EM and magnetic coverage in the region surrounding Voisey's much of this area is now commonly considered "sterilized" for the potential discovery of economic nickel deposits, however the lessons learned at Voisey's Bay give evidence for both the limitations of previously used exploration methods as well as the potential for hidden deposits in areas previously deemed as non-prospective.

The first important lesson to note is the limitation of airborne EM which has been observed at Voisey's Bay. As discussed, numerous "nuisance conductors" complicate EM interpretation on the Voisey's Bay main block (**Figure 3.11)**. The same features which cause these additional conductive signatures at Voisey's Bay are also frequently found throughout

northern Labrador as well. The rivers and lakes in northern Labrador often host conductive sediments, and the prominent east-west structures throughout the region often create valleys which host rivers and excess sediment. Also as discussed, the Atlantic Ocean is located merely 5km from the Voisey's Bay deposits and causes much of the nearby sediment to be contaminated with salt water brines. The many inlets and bays throughout Northern Labrador result in this often being the case elsewhere. The prominent strike of the Voisey's Bay mineralized trend is also east-west because it exploits the same structures. This means there is a large risk in dismissing any east-west conductors which may appear to have explainable origins on the surface but may in fact originate from a sulphide system at shallow depth. EM systems without the ability to discriminate between moderate and excellent conductors (frequency-domain AEM) would be unable to provide a compelling EM signature in such a situation. And finally, the paragneissic host rock at Voisey's Bay contains an abundance of sedimentary sulphides and laterally extensive graphitic sheets. Similar graphitic features are particularly common throughout Labrador and have been a very common source of EM anomalies in various exploration programs (Kerr, 2003).

Another lesson learned from exploration in Voisey's Bay pertains to the limited depth of investigation of airborne EM methods, and the AEM signatures of different mineralized deposits present at Voisey's. Nuisance conductors aside, most of the deposits would easily be detected by airborne EM methods. The ~20m deep Ovoid is a prominent feature in all AEM surveys, even those surveys which can only detect its semi-massive components. The Reid Brook mineralization is deeper (~300m) and therefore a more challenging target. Some of the more powerful modern airborne EM systems may be able to detect such a deposit; however

the vast majority of airborne EM flown in Northern Labrador was during the years immediately after the discovery of Voisey's Bay, and used the prominent frequency domain AEM technology of that time which commonly only investigated to a depth of ~100m. The Eastern Deeps deposit, at a depth of 700m, is well beyond the depth of investigation of even the most modern systems. As a result, we can see that much of the area thought to be "sterilized" for Voisey's Bay type deposit by historic AEM have really only been explored for conductors to superficial depths.

Finally, another critically strategic piece of information gleaned from exploration experience at Voisey's Bay is the prominent presence of horizontal granite sheets. These granitic bodies commonly cut the VBI to the west of the mineralized trend and throughout the Eastern Deeps Chamber. The entire southern and eastern extents of the Eastern Deeps chamber do not form outcrops at surface due to being hidden by a thin sheet of younger granite. The implication of this is that many other areas in the region that have been previously mapped at surface as granitic domains could potentially be underlain troctolitic and gabbroic intrusive chambers capable of hosting Ni-sulphides.

The observations of historical difficulties experienced in regional nickel exploration programs in the Labrador region and observations from the exploration programs performed at Voisey's Bay reflect a need for another prospective strategy. The traditional reconnaissance method of airborne EM/magnetic surveys had been met with difficulties due to AEM methods being inherently depth limited along with facing a number of other difficulties and magnetics failing to identify the Voisey's Bay troctolite. Based on the geophysical response of Voisey's

Bay, gravity surveying was known to provide a robust response identifying the dense troctolitic host rocks hosting Voisey's Bay mineralization, but to perform a ground gravity survey with similar resolution over a large region would have been extremely cost prohibitive, and would have taken an excessive amount of time.

About a decade after the Voisey's Bay discovery, the technology of airborne gravity gradiometry first became commonly commercially available. The advent of this technology represented a way to deploy a fast reconnaissance airborne technique that could map density anomalies to a level of accuracy that would reliably detect a hidden troctolite chamber with dimensions larger than 300-500m in the x, y, and z directions. By using AGG as a fast and effective reconnaissance tool to map all potentially hidden troctolite intrusions, it would be possible to test prospective anomalies by following up with exploration drilling and/or alternative geophysical methods which could detect sulphides directly, such as EM (**Figure 3.12)**.

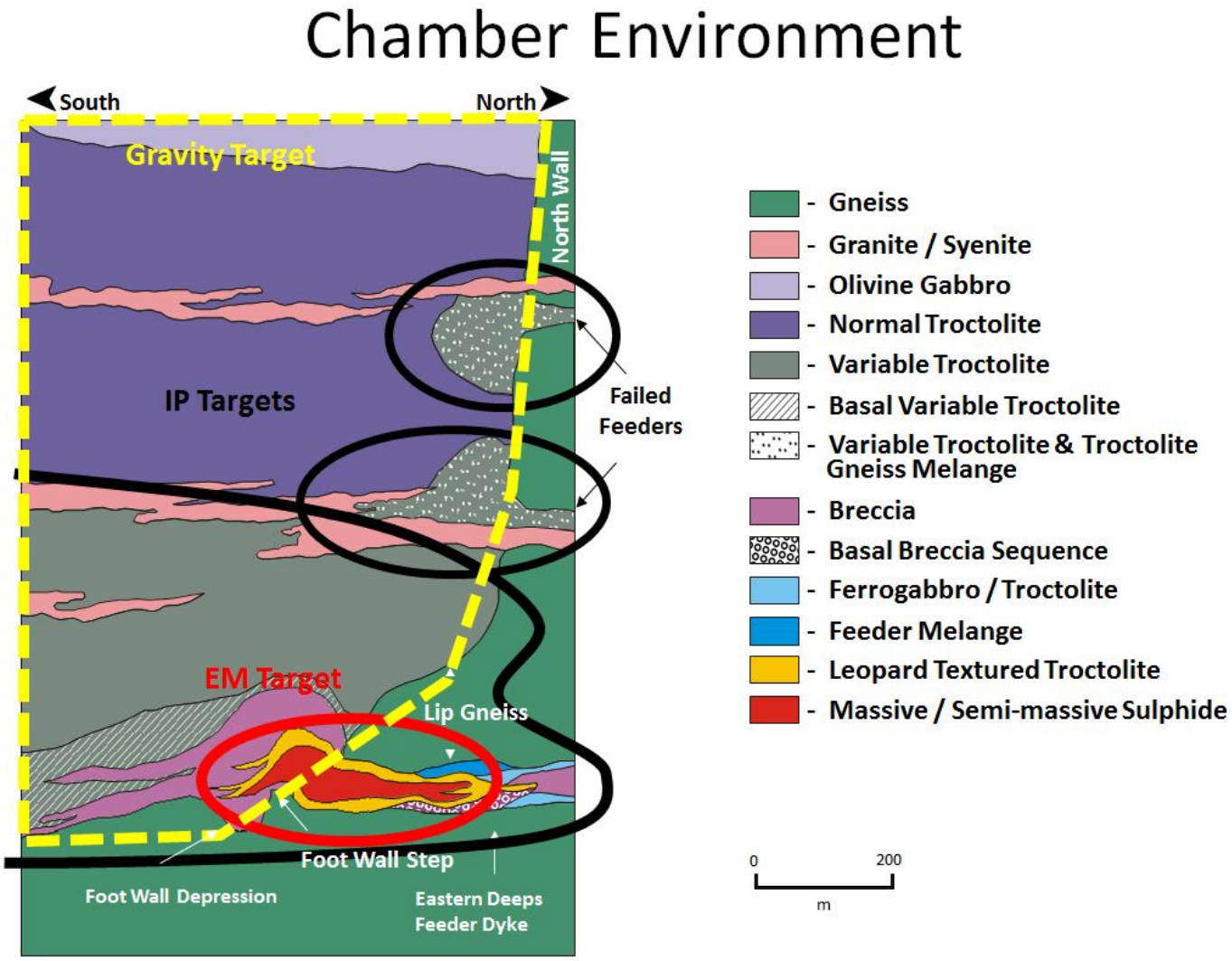

Figure 3.12: Geophysical responses expected from a chamber environment similar to the Eastern Deeps. The massive sulphide deposit is an extremely strong EM target, but would not be identified from airborne EM surveys due to its 700m depth. The halo of disseminated sulphides surrounding the deposit and the entry points of other feeders are a strong IP target. The entire troctolite chamber is significantly more dense than the surrounding country rock, and makes for a strong gravity target. (modified after Evans-Lamswood, 2000)

3.5: Forward Modeling

A crucial step in planning any geophysical survey is to first test its merit by calculating the theoretical response of the target geology. This process necessitates identifying the physical properties of the local geology that are applicable to the geophysical method being used, in this case density, and using this data to build a simplified synthetic model approximating the geological bodies of interest. Once a synthetic model that best reflects our understanding of the physical property distribution in the Earth has been created, we can use forward modeling software to calculate the geophysical response we can expect to see from this model, as well as other possible variations of the model.

There are several commonly used methods to derive density measurements of a particular rock type. One such method is the use of a gamma-gamma tool to attempt direct measurements of density either on drill core samples or in situ as a borehole logging tool. A gamma-gamma sensor includes a radioactive source with a known energy output and two or more detectors at a fixed distance away. When measurements are taken against a rock sample or within a borehole, observations can be made about the rock's density based on the attenuation of the radioactive energy. Although this has been done in the past at Voisey's Bay, problems with the calibration and reliability of historical gamma-gamma datasets prevent this from being the method of choice. Another method of density calculation is the regression analysis of assay data collected from drill core. This is completed through the following three empirical equations:

If **Fe** (%) < 20 then SG = 2.6079 + 0.0373 x **Fe** (%) - 0.011 x **S** (%)

If **Fe** (%) ≥ 20 and < 51 then SG = 2.493 + 0.0125 x **Cu** (%) + 0.0340 x **Fe** (%)

If **Fe** (%) ≥ 51 then SG = 3.0282 + 0.009 x **Cu** (%) + 0.0332 * **Ni** (%) + 0.0286 x **Fe** (%) - 0.0037 x **S** (%)

where Fe (%), S (%), and C(%) are the assayed percent values of iron, sulphur, and copper, respectively. Although this method is certainly the most complicated and cost-intensive option, it is also a by-product of the regular assaying that was routinely completed on a very large swath of the Voisey's Bay drill core. Due to the huge amount of data derived via this method over the years at Voisey's Bay, it is relied upon as a primary source of density characterization. Finally, a third method for traditional density measurement of any rock sample is through the use of Archimedes' principle, which states that the upward buoyant force exerted on a body immersed in a fluid is equal to the weight of the fluid that the body displaces. This simple procedure involves suspending a rock sample from a string attached to a scale, measuring its weight, immersing the sample in a volume of water, and measuring its weight again. Samples are often soaked in water beforehand in order to counter the effect of varying porosity, and the ratio of these measurements are used to determine the specific gravity density of a substance.

This represents a cheap and effective procedure to measure density, and was used in this case to check the accuracy of the density values derived from the assaying methodology.

The density variation amongst the major Voisey's Bay rock types has been discussed qualitatively and quantitatively by authors in the past (King, 2007; Ash, 2006; Duff, 2011). The troctolite-gabbro rocks of the VBI are abundant in olivine, which results in an abundance of iron content throughout the unit and an average density value of ~2.9g/cc. This presents a density contrast with the surrounding paragneissic country rock (average density value of ~2.78g/cc) and the local granites (which have a density ~2.7g/cc). The density of the massive sulphides bodies represent a much greater density of 4.5g/cc, but because these bodies are limited in size with respect to the other units their gravity signature is often unidentifiable amongst the responses of larger bodies. As much of the prospective troctolite chambers contain varying amounts of sulphides, from disseminated to semi-massive, the density of the troctolite may vary between the values of 2.9-3.5g/cc according to its sulphide content. The most recent publication including measurements of these densities and ranges can be seen in **Figure 3.13**, after (Duff, 2011).

With knowledge of the density distribution amongst major Voisey's Bay rock types, it is possible to proceed with the creation of a synthetic geological model, and a calculation of its geophysical response. A 2D potential fields modeling software package called GM-SYS was used for this work. This allows for the rapid construction of a 2D geological cross-section, and the calculation of its gravitational response for both Gz (vertical gravity) and Gzz (vertical gravity gradient). The geological model chosen for this exercise was a troctolite chamber that

Rock Type	Number of Samples	Density (g/cc)	Velocity (m/s)	Acoustic Impedance E+05 ($kg*m^{-2}*s^{-1}$)
Granite	12	2.69 ± 0.0194	5964 ± 230	162 ± 5.35
Gneiss	26	2.79 ± 0.0395	6133 ± 82	171 ± 3.47
Breccia (Tr-5%)	16	2.98 ± 0.0773	6142 ± 210	183 ± 6.39
Breccia (5-15%)	15	3.14 ± 0.0725	6163 ± 188	193 ± 7.23
Breccia (15-40%)	74	3.30 ± 0.122	5975 ± 240	197 ± 9.95
Breccia (40-75%)	6	3.25 ± 0.112	5746 ± 265	187 ± 11.5
Troctolite (Tr-5%)	162	2.91 ± 0.0994	6564 ± 330	191 ± 10.4
Troctolite (5-15%)	57	3.02 ± 0.103	6430 ± 275	194 ± 7.38
Troctolite (15-40%)	85	3.31 ± 0.196	6043 ± 355	200 ± 12.7
Troctolite (40-75%)	12	3.44 ± 0.198	5950 ± 211	205 ± 11.5
Massive Sulphide	217	4.62 ± 0.122	4372 ± 370	202 ± 17.0

Figure 3.13: Average values of density, velocity, and acoustic impedance for drill core from the Eastern Deeps Zone. Ranges are given in standard deviations (Duff, 2011)

was 1km deep and 1.5km wide, surrounded by paragneissic country rock, and covered by a 300m thick sheet of granite (**Figure 3.14).** This model accurately represents a prospective chamber similar to the Eastern Deeps, if it was concealed from surficial exploration by a sheet of granite. As a test of the AGG method's capability to directly detect potentially economic massive sulphide bodies, a 100x150m body of 4.5g/cc density is also included at various depths in the forward modeling exercise.

In **Figure 3.14** and **Figure 3.15**, the gravity and gravity vertical gradient responses over a buried troctolite chamber can be seen. The gravity response over the chamber includes a broad anomaly of approximately 2mGal, which is quite significant and would be easily detected in a survey. The vertical gravity gradient response (Gzz) of the buried chamber is even more distinct, with a sharper anomaly centered over the troctolite body and a large amplitude of approximately 18 Eotvos. **Figures 3.16** and **3.17** feature the same buried troctolite chamber, but with a massive sulphide body located at the top of the chamber (300m depth). The Gzz response is very distinct, with an amplitude of ~33 Eotvos and a distinctly shorter wavelength superimposed upon that of the troctolite chamber anomaly. This response would likely lead to a successful interpretation of a buried sulphide body. The gravity response, although distinct from the previous model in amplitude (almost 3mGal), is less distinctly indicative of a separate high density body, and might be explained by variations within the depth extent and geometry of the troctolite chamber itself.

The models shown in **Figure 3.18** and **Figure 3.19** depict the Gz and Gzz gravity responses to the buried troctolite chamber model with a massive sulphide body at 600m, and

those in **Figure 3.20** and **Figure 3.21** show the responses to the body at a depth of 900m. Both sets of model responses depict a very low level of distinct response of the sulphide body within the Gz data, and a quickly decreasing response in the Gzz data. The Gzz response from the massive sulphide body when it is buried at 600m is present as an obvious anomaly within the modeled data, however it is somewhat ambiguous and has the potential to be interpreted as either a massive sulphide body or a variation in chamber geometry. Detection of the massive sulphide is extremely doubtful in any of the other three models discussed.

Through the use of forward modeling, it is possible to say that an airborne gravity gradiometry survey can confidently and accurately detect a troctolite body with dimensions similar to the Eastern Deeps chamber, when buried by and contained within significantly less dense rock types which are common throughout this region of Labrador. It was also observed that even when the increased sensitivity of this technology, AGG has limited capabilities to directly detect massive sulphide bodies at depth when hosted in this type of geological environment. Despite this limitation, however, the technique still fills a vitally important exploration niche in the ability to locate the prospective environments of troctolite chambers which were previously undetectable by other airborne geophysical techniques.

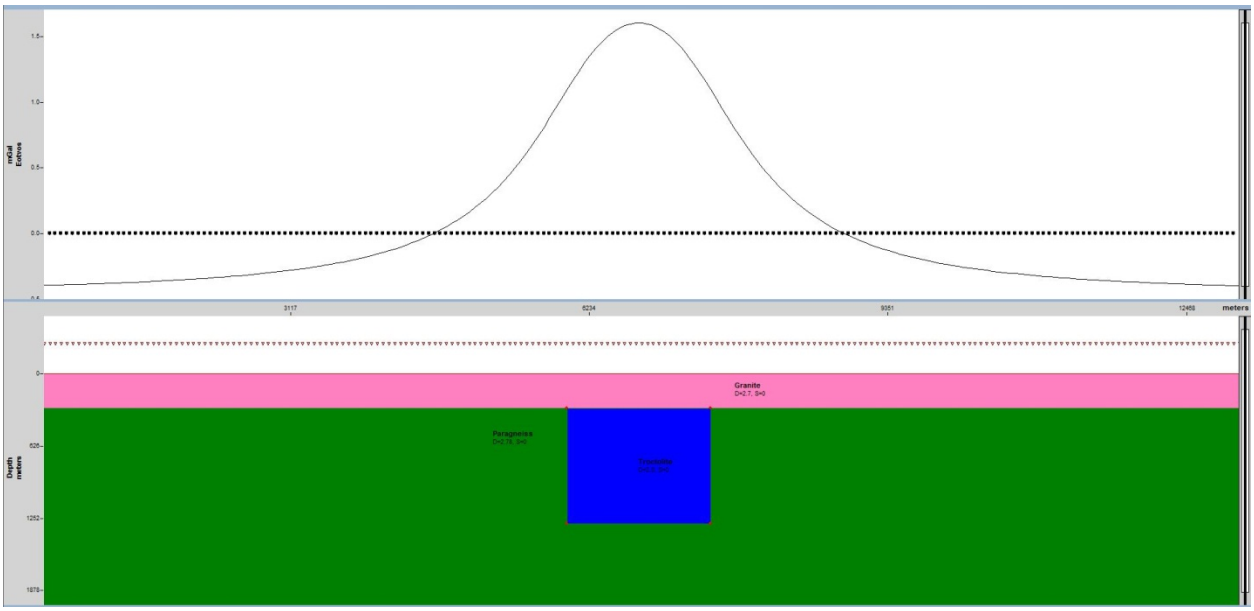

Figure 3.14: Forward modeled Gz response of a troctolite chamber with dimensions similar to the Eastern deeps under 300m of granite and contained within a paragneissic country rock.

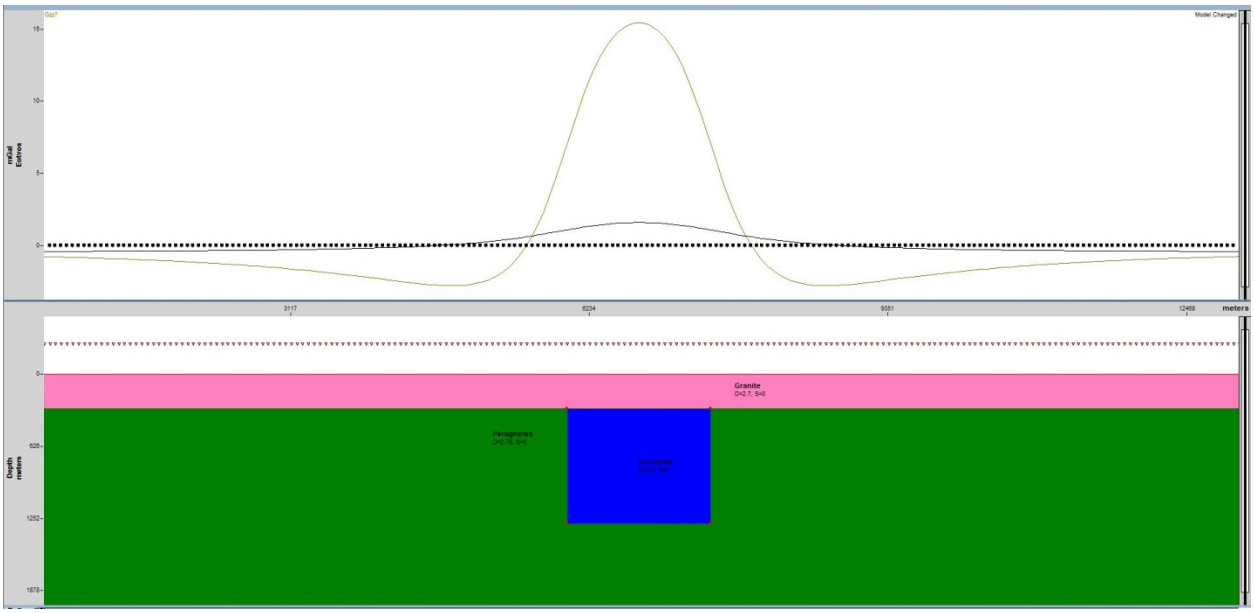

Figure 3.15: Forward modeled Gzz response of a troctolite chamber with dimensions similar to the Eastern deeps under 300m of granite and contained within a paragneissic country rock.

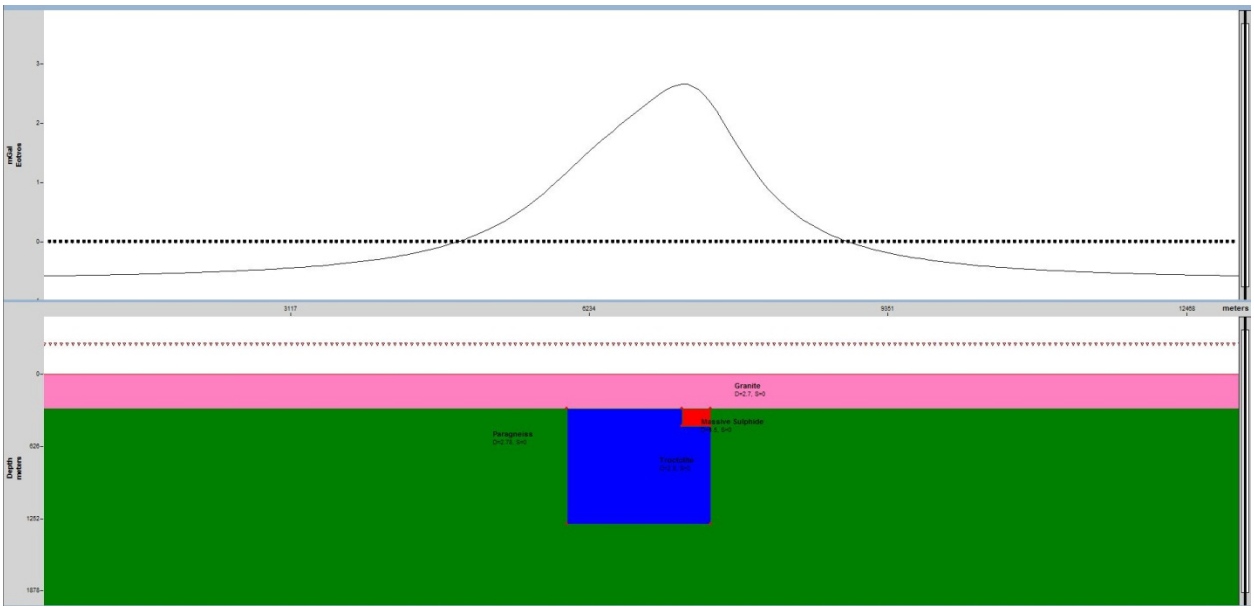

Figure 3.16: Forward modeled Gz response of a troctolite chamber with dimensions similar to the Eastern deeps under 300m of granite and contained within a paragneissic country rock. A 100x150m massive sulphide body is included at a depth of 300m

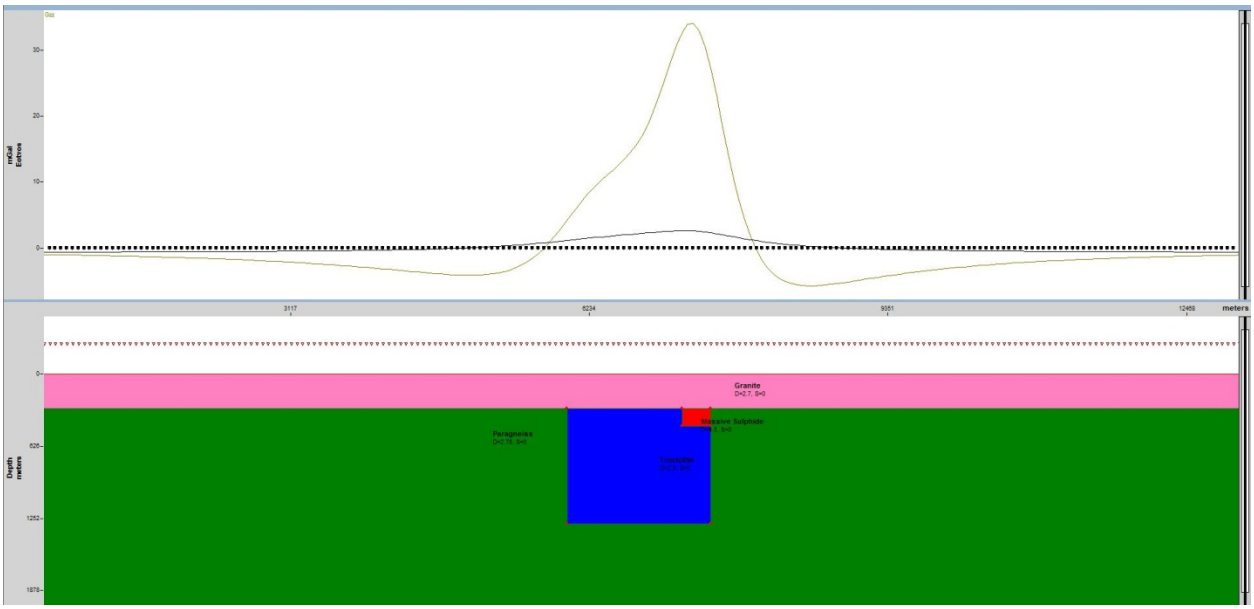

Figure 3.17: Forward modeled Gzz response of a troctolite chamber with dimensions similar to the Eastern deeps under 300m of granite and contained within a paragneissic country rock. A 100x150m massive sulphide body is included at a depth of 300m

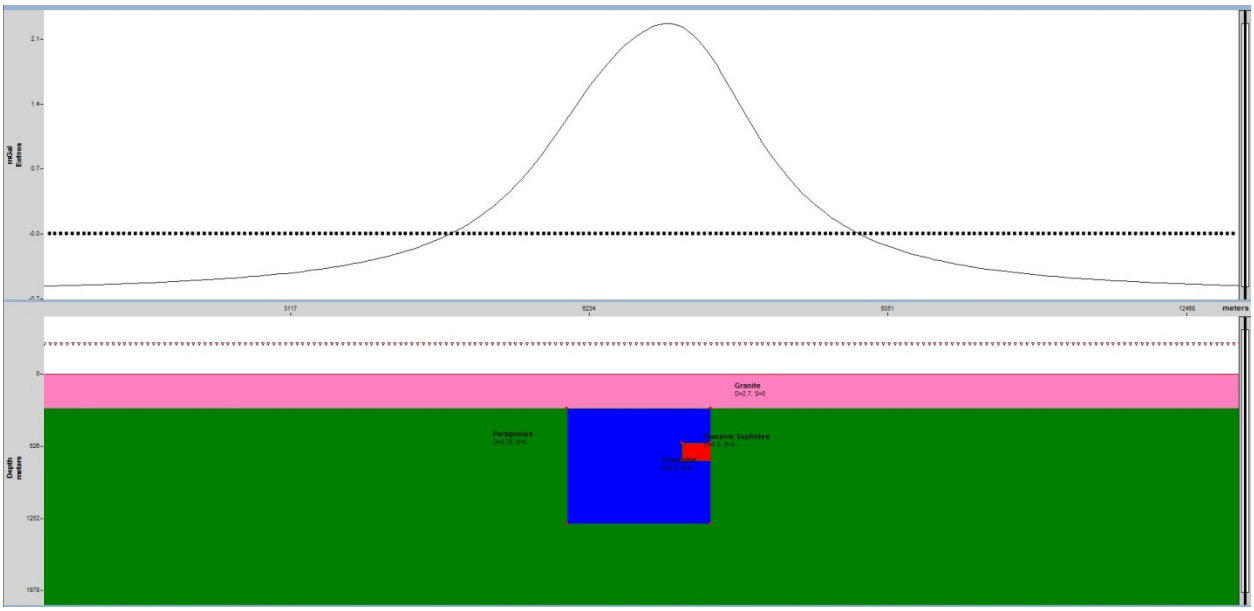

Figure3.18: Forward modeled Gz response of a troctolite chamber with dimensions similar to the Eastern deeps under 300m of granite and contained within a paragneissic country rock. A 100x150m massive sulphide body is included at a depth of 600m

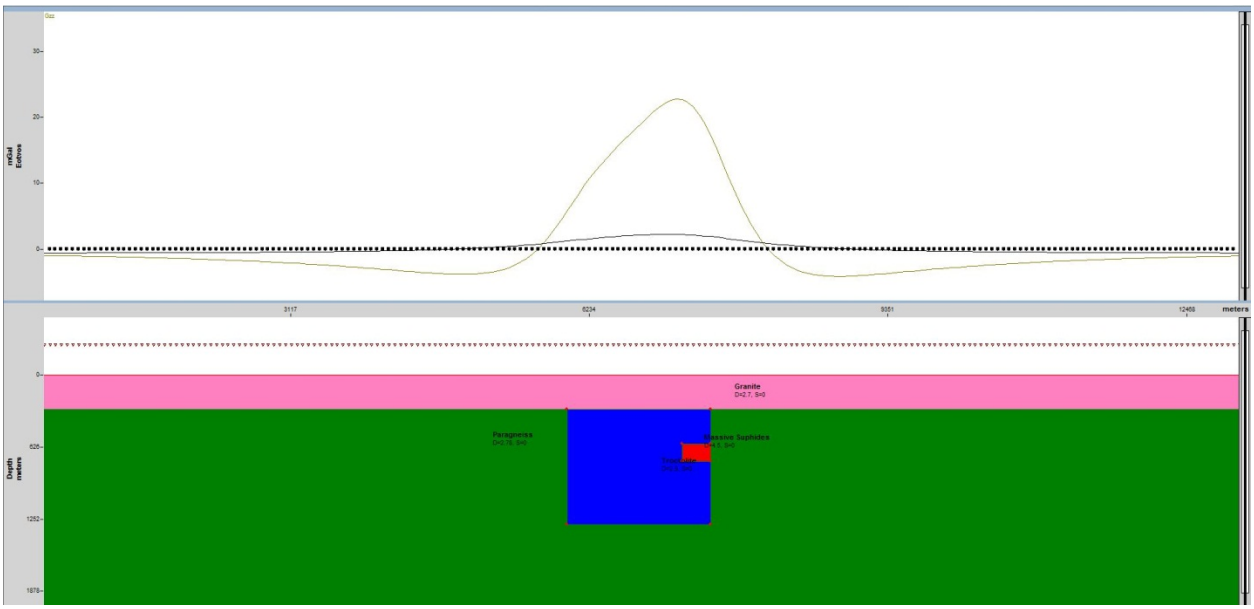

Figure 3.19: Forward modeled Gzz response of a troctolite chamber with dimensions similar to the Eastern deeps under 300m of granite and contained within a paragneissic country rock. A 100x150m massive sulphide body is included at a depth of 600m

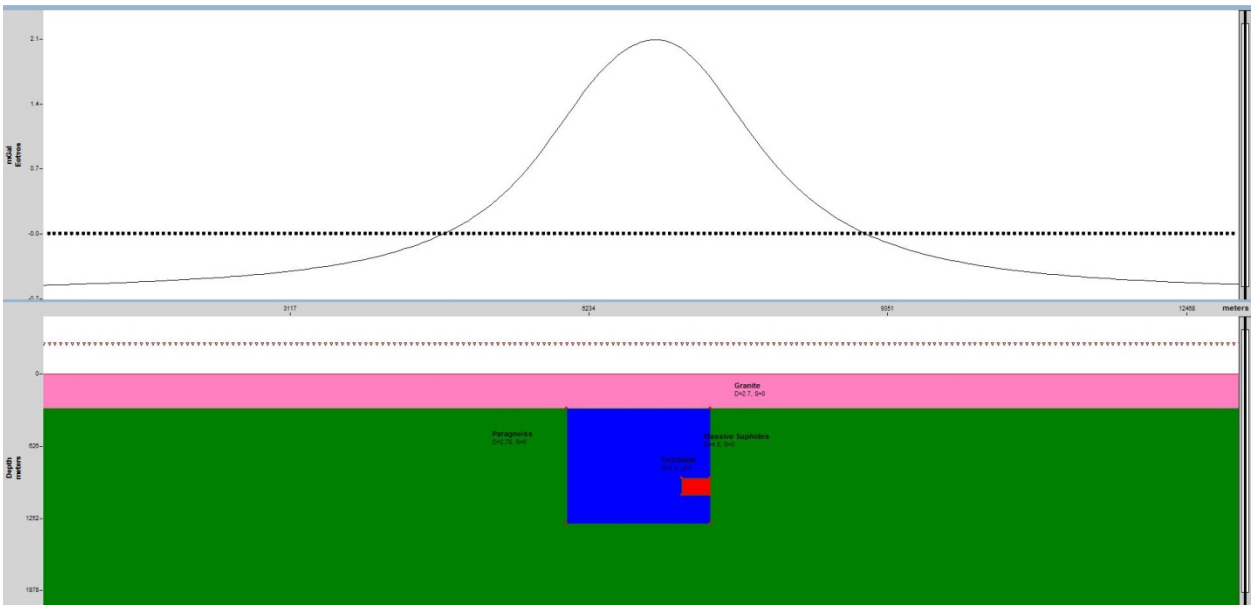

Figure 3.20: Forward modeled Gz response of a troctolite chamber with dimensions similar to the Eastern deeps under 300m of granite and contained within a paragneissic country rock. A 100x150m massive sulphide body is included at a depth of 900m

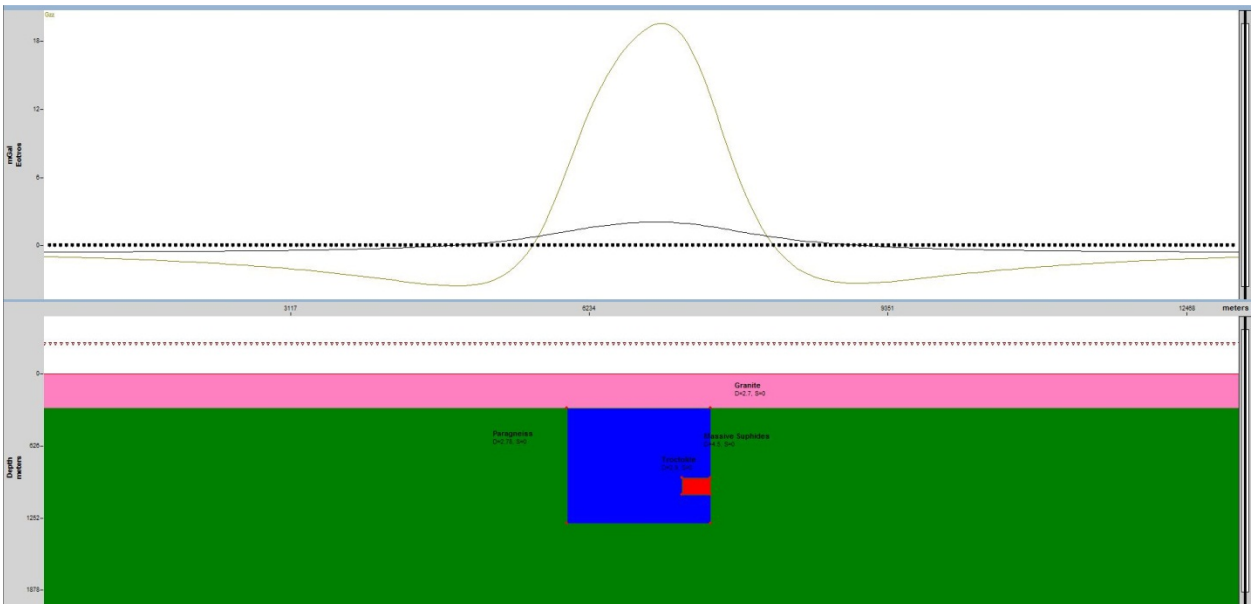

Figure 3.21: Forward modeled Gzz response of a troctolite chamber with dimensions similar to the Eastern deeps under 300m of granite and contained within a paragneissic country rock. A 100x150m massive sulphide body is included at a depth of 900m

Chapter 4: Acquisition and Processing

4.1: Introduction

In Chapter 4 we will review the methodology and considerations of AGG data acquisition in the context of this survey. A description of the standard AGG processing commonly performed by contractors will be detailed. The Voisey's Bay AGG dataset will then be terrain-corrected using a digital elevation model. A special focus will be given to the process of determining of the best possible background density choice. The limitations and potential pitfalls of the terrain correction will be examined in relation to the digital elevation model being used, and the problem of thick, variable overburden in portions of the survey is also discussed. Several filtering techniques are completed on the data in order to produce maps which are more easily interpreted, including vertical integration and the removal of the regional signal.

4.2: Data Acquisition

The Airborne Gravity Gradiometry survey at Voisey's Bay was flown simultaneously with another survey to the south of the main block. This second survey area was chosen for the purposes of greenfields exploration, and due to its propriety nature will not be considered within this study. The Voisey's Bay AGG survey block was designed with North-South lines spaced 200m apart and East-West tie lines flown 1km apart. The total number of lines was 304 all together, resulting in 3084.93 line-km of AGG data.

The survey was flown under contract by Bell Geospace, a company that specializes in FTG AGG surveying. The Bell Geospace crew arrived in Nain, Labrador, which was the base of operations for the survey, on June 16th. Survey operations began on June 24, 2006, and continued through July 28th, 2006. The aircraft used for data collection was a Cessna Grand Caravan C-GSKT. Although the survey was designed as a constant elevation drape of 80m, the extreme topography in the Voisey's Bay area made it impossible to maintain constant clearance when the terrain relief increased or decreased rapidly. As a result, the average height of clearance was approximately 250m. The weather during data acquisition varied from clear sky to low ceiling clouds to rain and thunderstorms. In many cases data collection was prevented or delayed in the presence of adverse weather, as gradient data quality is adversely affected by excessive turbulence. Data acquisition was halted when vertical accelerations were sustained above the 60 mill-g range, with most of the final collected data set being acquired in the range of 20-40 mill-g.

The acquired FTG survey data is typically treated by a series of proprietary processing steps before being presented to the client. The raw data recorded by the AGG system consists of two signals from each of the three Gravity Gradient Instruments (GGIs). One of these signals is the in-line component and the other is the cross-line component. The three sets of raw data are first processed to compensate for most of the physical conditions during signal acquisition, including the gradients relating to the aircraft motion and the rotation of the instrument itself. Next, the data undergoes an averaging and reformatting process which results in the data being effectively low-pass filtered to eliminate noise. All contractors consider this processing to be proprietary, including Bell Geospace, which limits the client's knowledge of the nature of the

filtering that has been completed on the data and can cause a problem in subsequent processing by the client, which will be discussed later. It is also during the averaging procedure that navigation and aircraft altitude data are merged with the gradient data. Next a series of line corrections in which the tensor components are calculated from the measured inline and cross-line data sets, and the bulk low-frequency errors are removed through time based line leveling and correlated GGI output. After this step, the data should be free of any DC shifts due to instrumental noise.

A key aspect in noise reduction of FTG data is provided by the nature of recording independent measures of the gravity signal: a tensor set of measurements. All measurements taken are related through the measurement of the same source, and therefore any signal in one tensor must be supported in another. If signals are unsupported in other tensors then they are flagged as erroneous noise, and are removed. This procedure is a key advantage to improving the signal to noise ratio when compared to AGG systems that measure a single tensor, and is commonly performed in one of two ways. The first method is completed through the use of equivalent source methods and approaching the problem as a linear inversion. A continuous surface mass distribution below the observation datum is parameterized, and by solving for the optimum mass distribution that best explains the response of all tensor channel outputs simultaneously model tensor fields can be produced which must be associated with geological bodies (Jorgensen et al, 2001). The second method of full tensor noise removal relies on the solution of Laplace's equation outside of the source region. This method also sets the problem up as a linear inversion, but the only signals that are preserved through this technique are those that satisfy Laplace's equation for all tensor channels simultaneously

(Jorgensen et al, 2001). This latter method is model independent and much faster than the first, and is more commonly used.

4.3: Terrain Correction

The terrain correction is a processing step in any gravity dataset that holds incredible importance, and has the potential to define the accuracy of a dataset as much as the survey parameters. This step accounts for the gravitational influence of all surrounding topographic variance, such as hills and valleys. Although this is key in the reduction of any gravity dataset, it holds even greater importance in the processing of Airborne Gravity Gradiometry, as the gradient field strength falls off as a function of $1/r^3$, and is therefore more sensitive to the relatively closer effects of local topography (Kass and Li, 2008). Since topography may reflect geology to a varying degree, these topographic effects are not always totally unrelated to the geological signals which we want to measure.

For the initial terrain correction of the Voisey's Bay dataset, the Canadian Digital Elevation Data (CDED) was used (**Figure 4.1**). This data was extracted from the hypsographic and hydrographic elements of the National Topography Data Base (NTDB) at a cell size of 90m. This topographic data was collected before the removal of the overburden over the Ovoid, the excavation of the open pit, and the creation of several waste rock piles in the vicinity of the mine. As a result, local artifacts from these inaccuracies were expected, however the CDED topographic data was the most accurate option available at the time and was used in the terrain correction despite this.

The topographic data were then used to create a digital elevation model (DEM) with a 3D prism base modeling package. The program then calculates the gravity effect of each defined prism assuming a density of 1.0 gm/cc and also calculates the gravity response of a model that represents the mass of the Earth between the terrain surface and the ellipsoid (Bell Geospace Acquisition & Processing Report, 2007). This results in the computation of a terrain correction for each tensor component that can be subtracted from the measured data, and scaled to any desired background density by the processer.

The choice of background density is an issue as old as the concept of a terrain correction itself. Conventional practice is to calculate the effect of the topography assigned with a homogeneous density value. The suitability of a homogeneous background density varies, of course, with the density variance in regional lithologies that the survey area is spread across. As a result, larger surveys may often have more trouble with a homogeneous terrain correction. If the background density value assigned to the DEM is too low then the effect of the local topography will not be sufficiently accounted for, and artificial positive anomalies will be correlated with topographic highs. Similarly, negative anomalies will be correlated with topographic lows. In the case of the background density choice being too high the

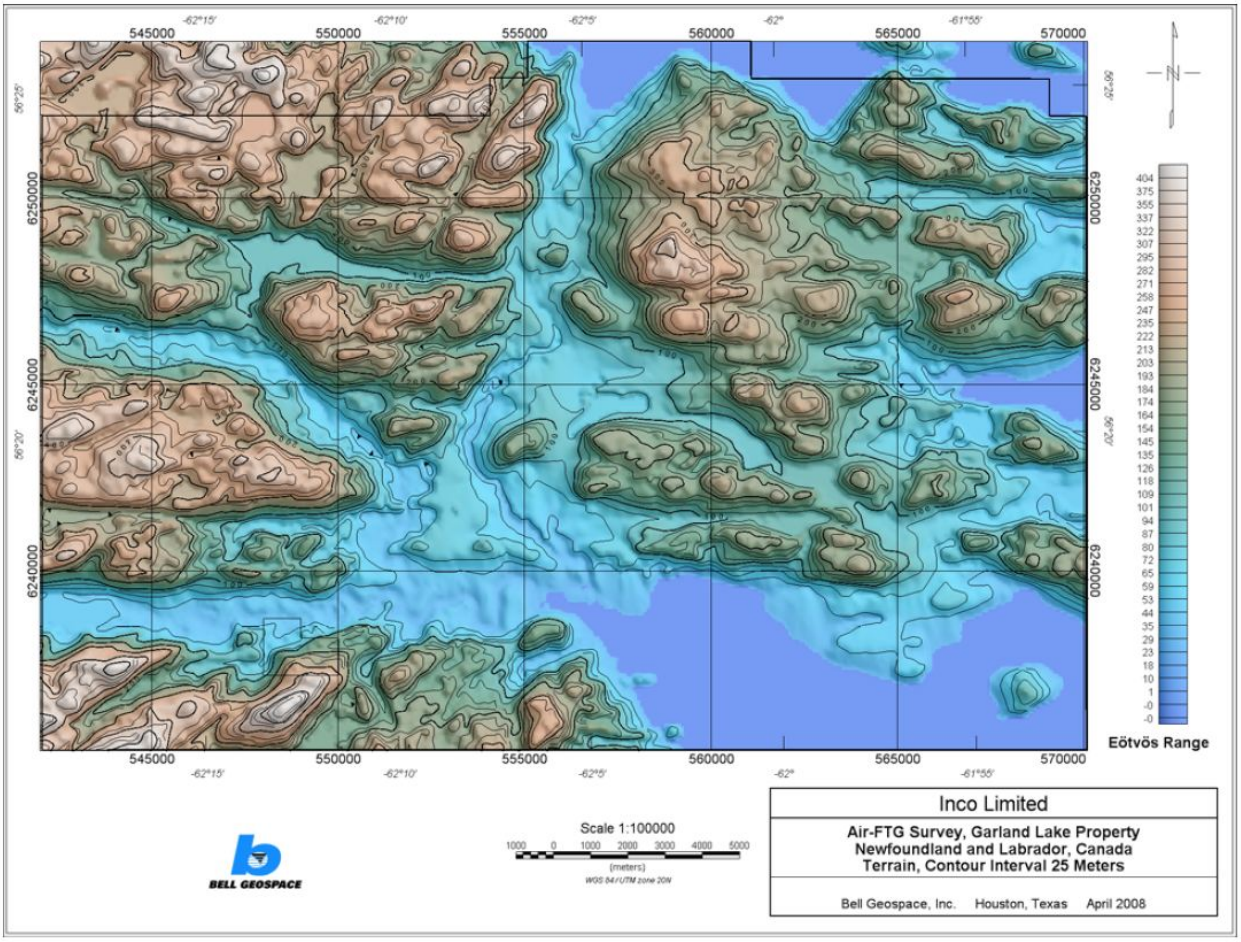

Figure 4.1: Canadian Digital Elevation Data topography used in the terrain correction of the Voisey's Bay AGG survey.

topographic effects in the gravity data will be overcompensated for. This situation results in false negative gradient anomalies being correlated with topographic highs and false positive gradient anomalies being correlated with topographic lows. Obviously, the improper application of the terrain correction runs the risk of artifacts such as those discussed being produced in the final gravity map, and being subsequently interpreted as geological signals. In the case of surveys covering multiple regional lithologies whose density varies greatly and a homogeneous background density is very troublesome, laterally variable density values may be used for the terrain correction (Vajk, 1956).

The application of a terrain correction is often a qualitative trial-and-error process, even with prior knowledge of the physical properties of the regional geology. The process of deciding on a background density value in the case of the Voisey's Bay AGG dataset was completed by calculating the terrain correction over an array of different background densities and comparing the correlation or anti-correlation of gravity responses with the local topography, while keeping in mind that some topography may be related to preferential geological weathering. The array of background densities used for terrain corrections in this case ranged from 2.20g/cc to 3.6g/cc, increasing by 0.1g/cc. For the sake of brevity, only the even values of this range are shown as examples in **Figure 4.3 A-H**. Also, for ease of qualitative comparison, these are all colored with the same linear color stretch, shown in **Figure 4.2**. Full tensor gravity datasets require terrain correction for each tensor map produced, but for the purpose of this study only the Gzz terrain correction is discussed here.

In **Figure 4.3 A**, we see the terrain correction to the vertical gravity gradient Gzz applied with a homogeneous background density value of 2.2 g/cc. With our prior knowledge of the physical rock properties in this area, it is unsurprising to see the typical signs of a background density that is too low. Most topographic peaks in the survey area are well correlated with topographic peaks, and gravity lows are commonly located in the areas of topographic lows. Observing **Figures 4.3 B and C**, we see these data artifacts drastically reduced, and in **Figures 4.3 D and E** they are almost non-existent. This latter point is to be expected, given that much of the regional geology in Voisey's Bay is made up of troctolite, granite, and paragneiss units (**Figure 3.2**), which have average densities of about 2.9 g/cc, 2.7 g/cc, and 2.78 g/cc, respectively (**Figure 3.13**). Naturally, background density values in the range of 2.8 g/cc and 3.0 g/cc provide the best possible terrain correction. As the Terrain background density values increase in **Figures 4.3 F, G,** and **H** to 3.2 g/cc, 3.4 g/cc, and 3.6 g/cc, respectively, a trend of anti-correlation between gradient response and topography can be seen to emerge and then dominate the overall character of the grid. In the latter of these figures, with a background density of 3.6 g/cc, topographic highs correspond with very pronounced gradient lows, while areas of low elevation have a generally strong gravity gradient response.

Although many more additional background densities were considered and analyzed, a final homogeneous background density value of 2.8 g/cc was chosen as the most applicable for this dataset. This value does an excellent job of minimizing the effect of terrain, particularly in the regions of paragneiss and granite. Although a choice of 2.9 g/cc may have done a better job at negating topographic effects in areas which are predominantly troctolite, the main purpose

of the AGG program is imaging of the troctolitic chambers and in a green-field environment we expect this to be the target lithology rather than the dominant background.

One issue which the final terrain correction was unable to account for, unfortunately, was the presence of variable overburden in the area known as the flood plain. The flood plain is immediately south of the Reid Brook zone and north of the Kogluktokoluk Brook (**Figure 3.2**). The overburden here is extremely variable, as a result of rough glaciation processes having carved out troughs in the paragneiss here, which were later filled in by sediment. By using the surface of this overburden in the terrain correction DEM, all the sand in this area is being assigned a uniform density of 2.8g/cc, instead of the approximate 2.0g/cc density which is what it has in reality. This functionally introduces a false negative anomaly over the entire overburden area, potentially masking interesting density features which could exist in the highly prospective rocks below. If the overburden here was uniform in thickness, the local density contrasts would at least be preserved, but unfortunately this is not the case.

With as much as 80m change in depth to bedrock over a horizontal distance of 150m, it is impossible to accurately predict the overburden thickness given the current drilling data. In the immediate vicinity of the Reid Brook area we have enough drilling to be able to construct a reliable overburden-bedrock interface, however as we move away from this our control points are very few and far between. The drilling in the Flood Plain area is extremely sparse, effectively providing 2-3 points of control over the highly variable 8x5km area. It would be possible to make an extremely rough estimate of this contact throughout the area and factor this into the terrain correction in order to attempt to correct the false low. The uncertainty

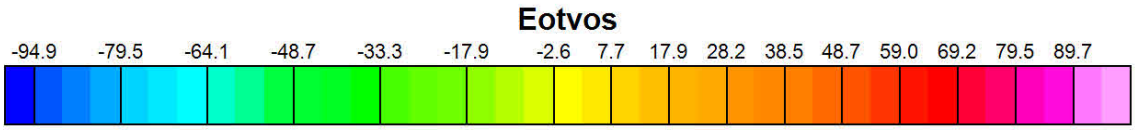

Figure 4.2: Common color scale used in all terrain corrected grids in Figure 4.3.

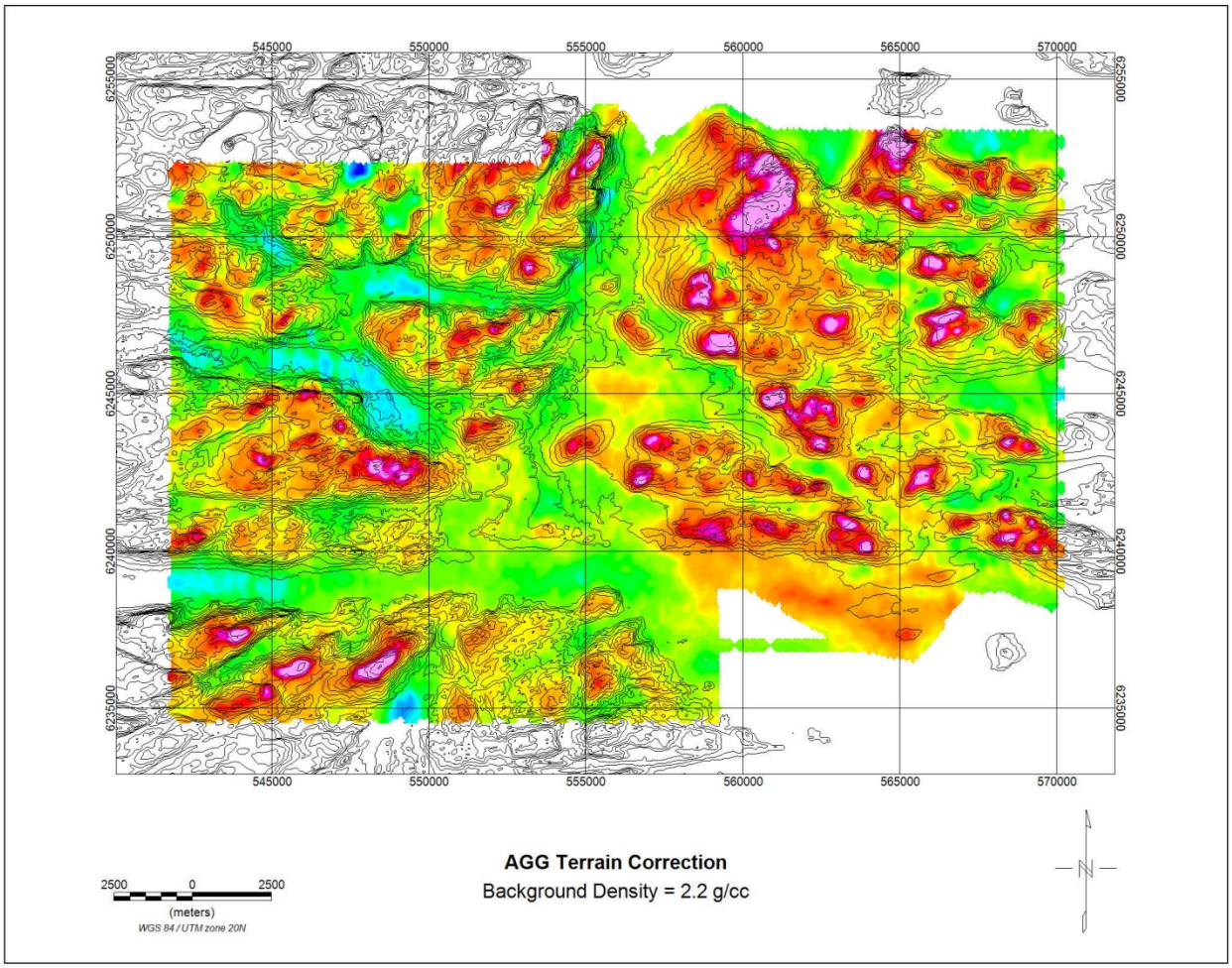

Figure 4.3 A: Terrain Correction of the AGG Gzz component using a background density of 2.2 g/cc, superimposed by CDED topographic contours.

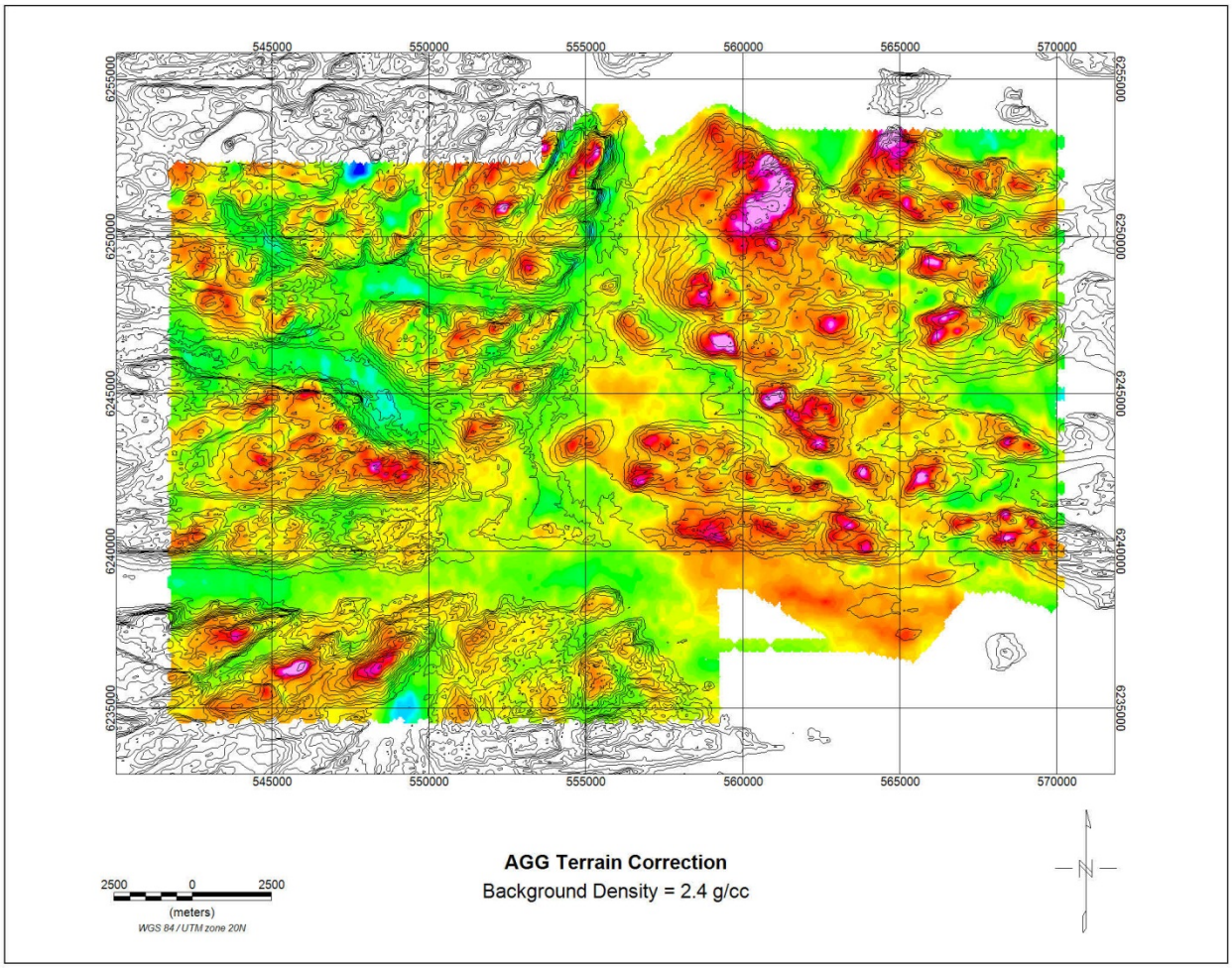

Figure 4.3 B: Terrain Correction of the AGG Gzz component using a background density of 2.4 g/cc, superimposed by CDED topographic contours.

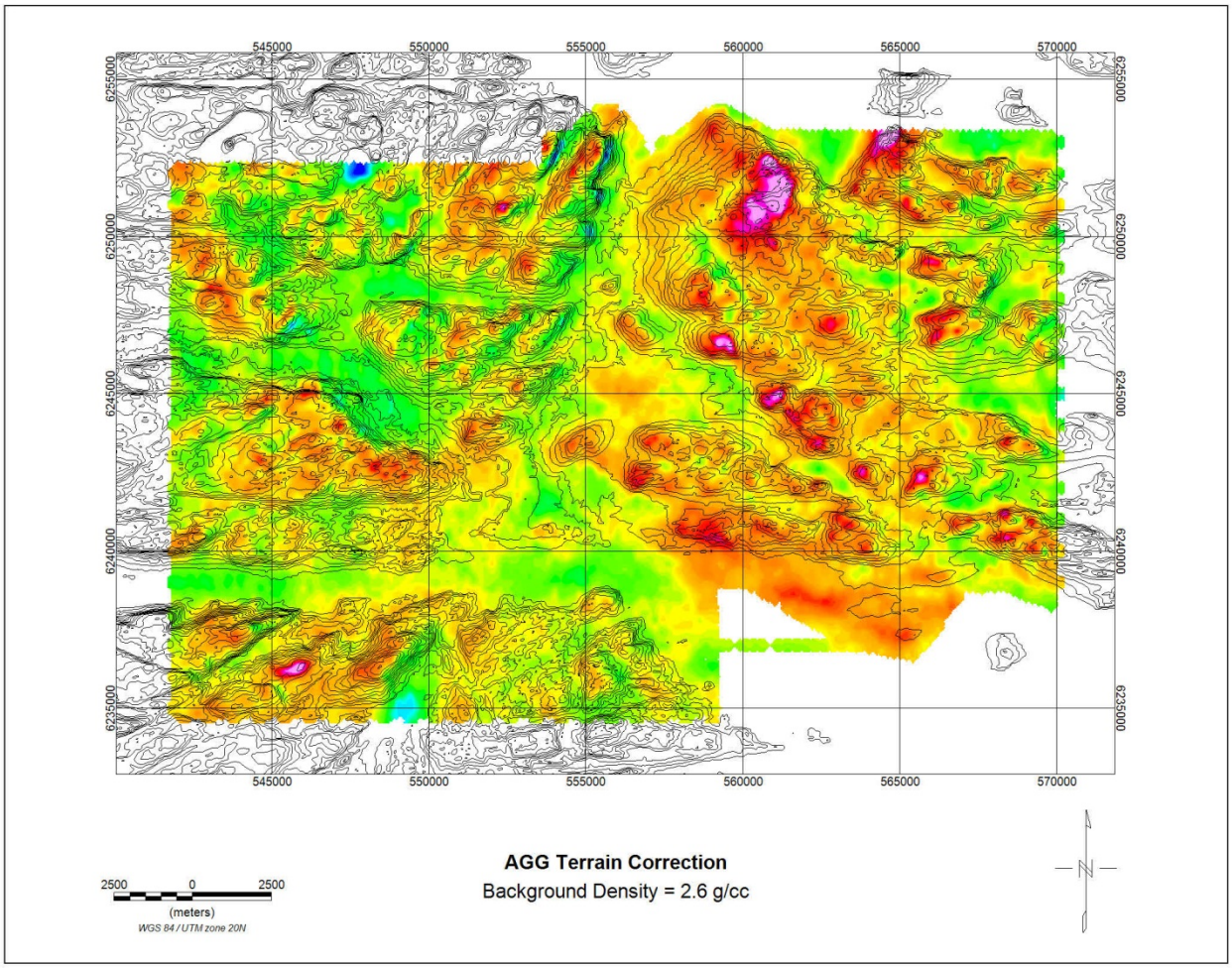

Figure 4.3 C: Terrain Correction of the AGG Gzz component using a background density of 2.6 g/cc, superimposed by CDED topographic contours.

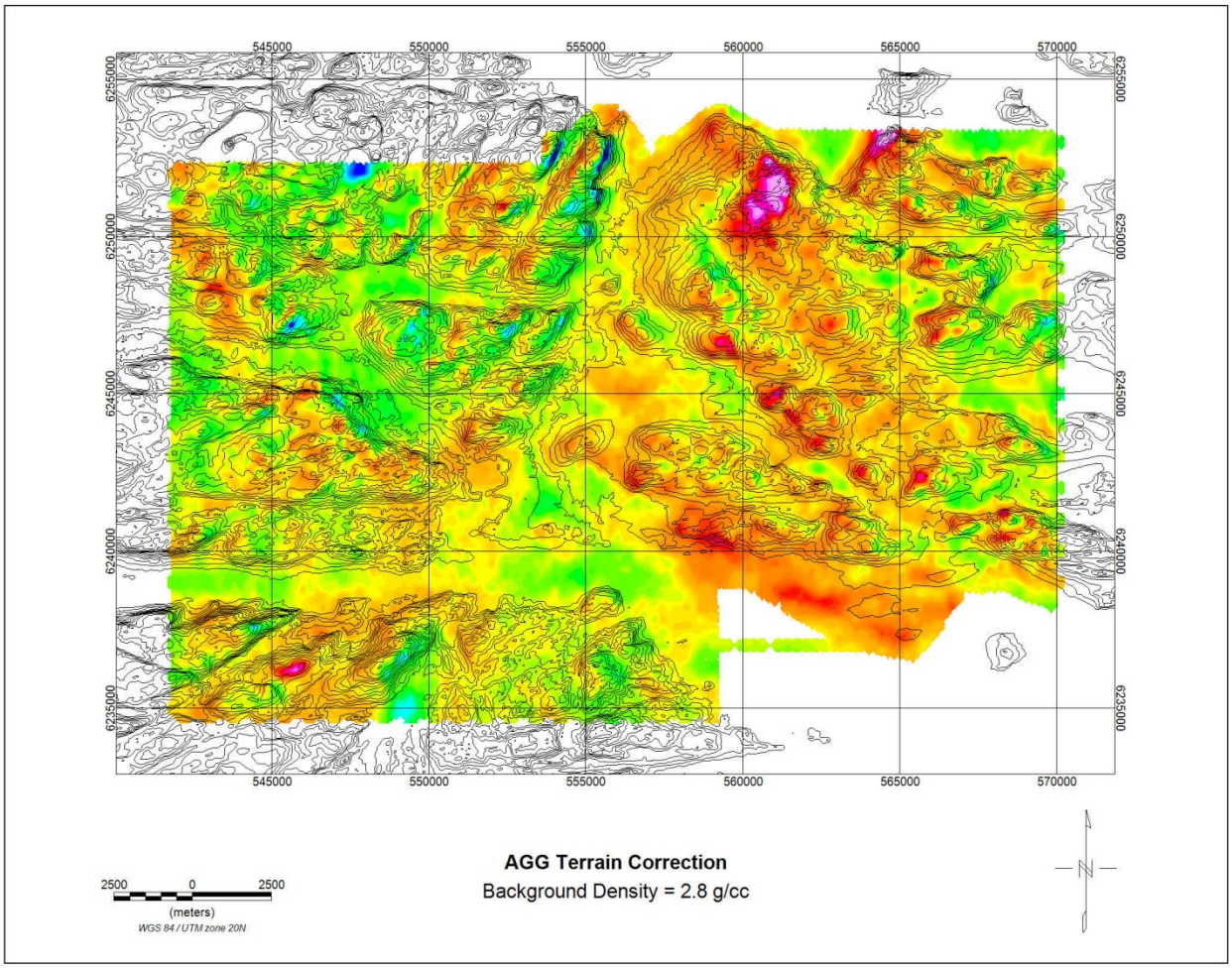

Figure 4.3 D: Terrain Correction of the AGG Gzz component using a background density of 2.8 g/cc, superimposed by CDED topographic contours.

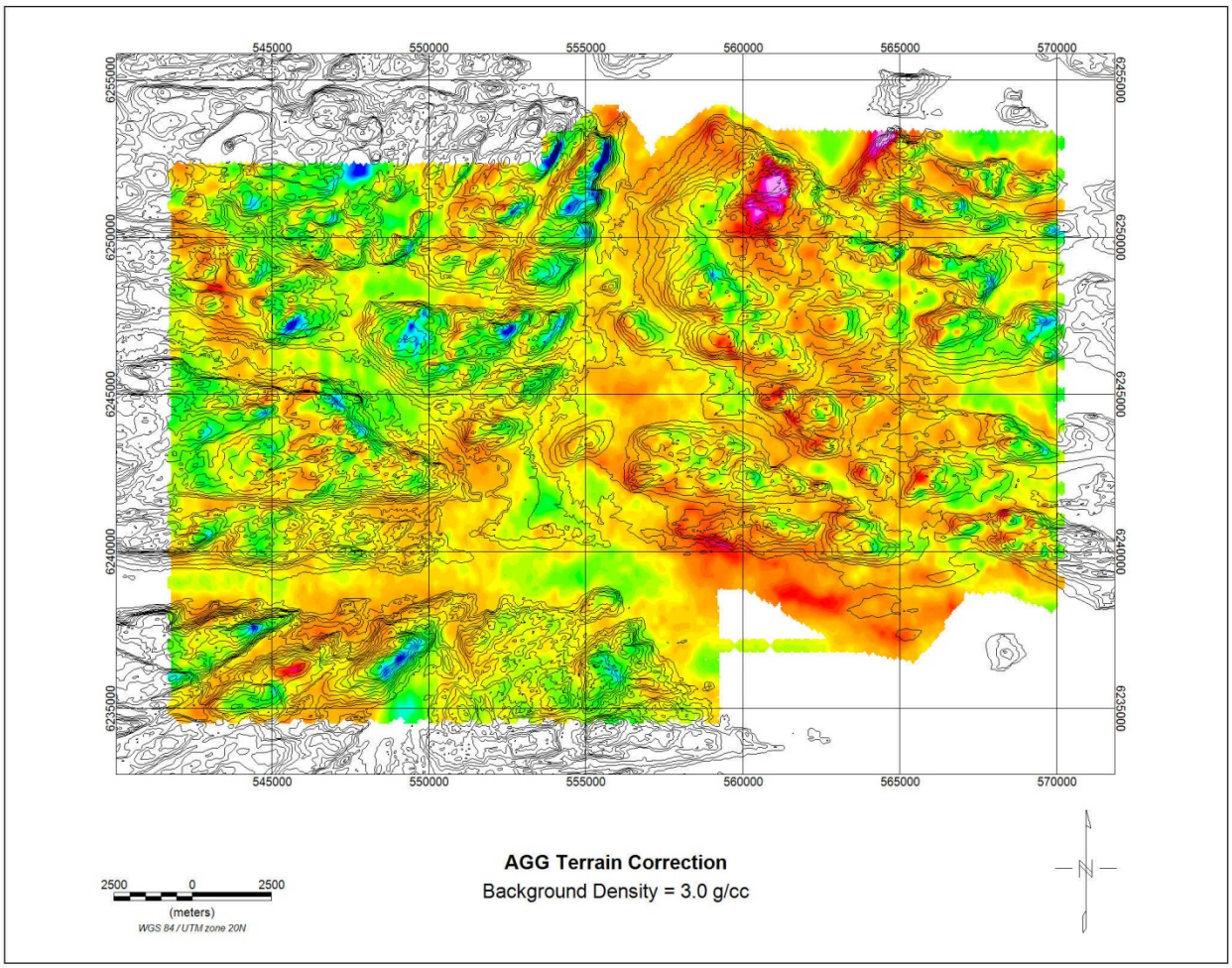

Figure 4.3 E: Terrain Correction of the AGG Gzz component using a background density of 3.0 g/cc, superimposed by CDED topographic contours.

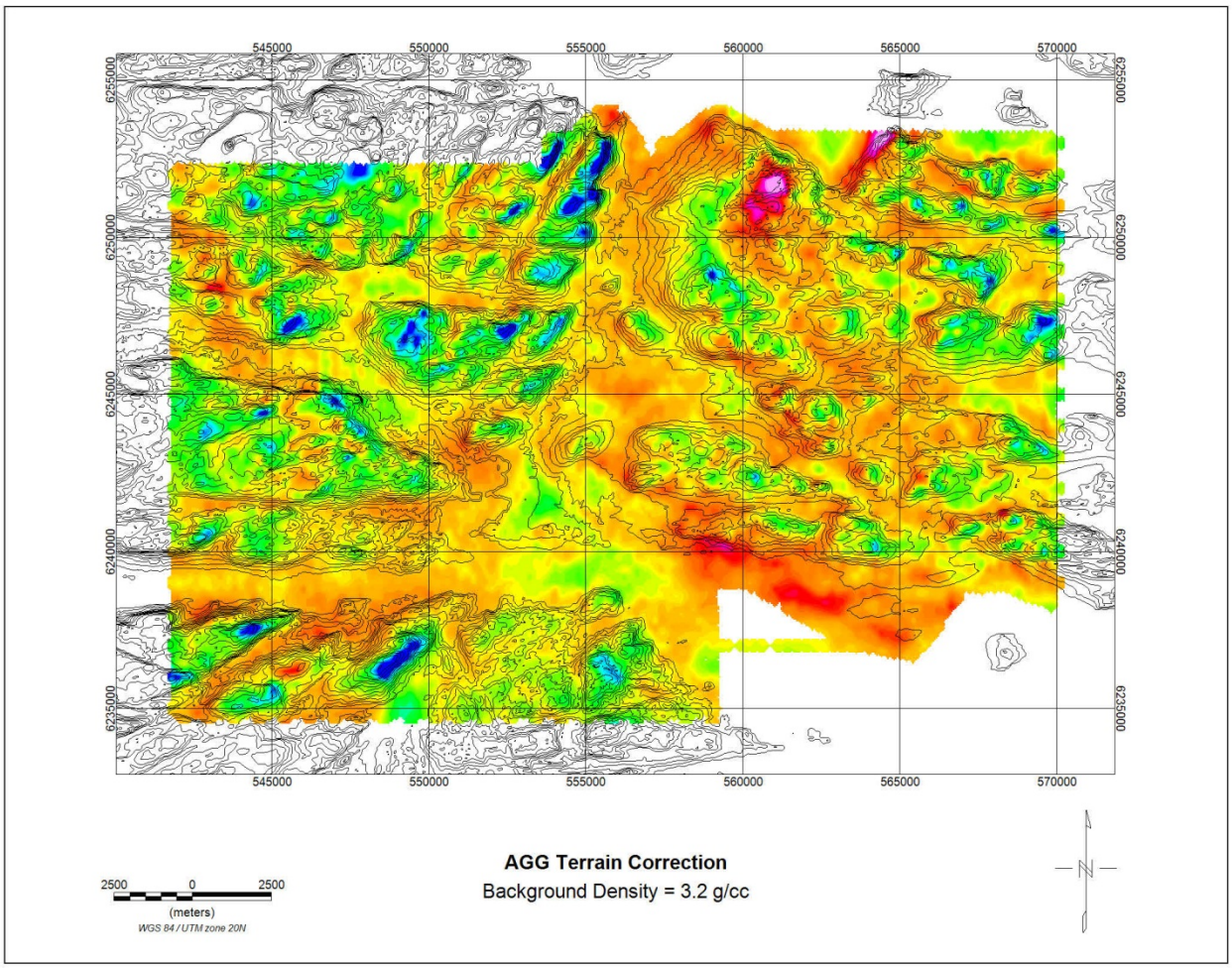

Figure 4.3 F: Terrain Correction of the AGG Gzz component using a background density of 3.2 g/cc, superimposed by CDED topographic contours.

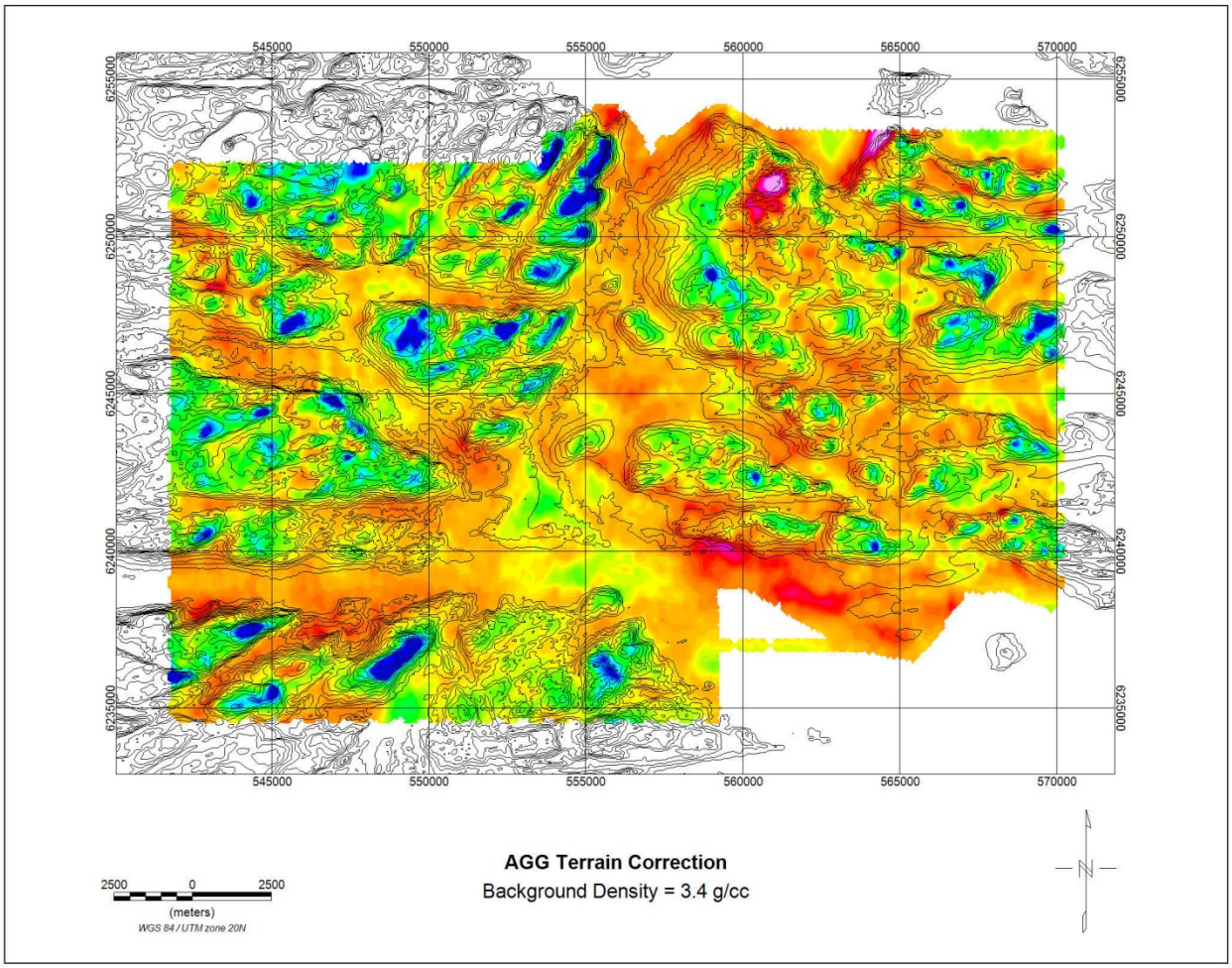

Figure 4.3 G: Terrain Correction of the AGG Gzz component using a background density of 3.4 g/cc, superimposed by CDED topographic contours.

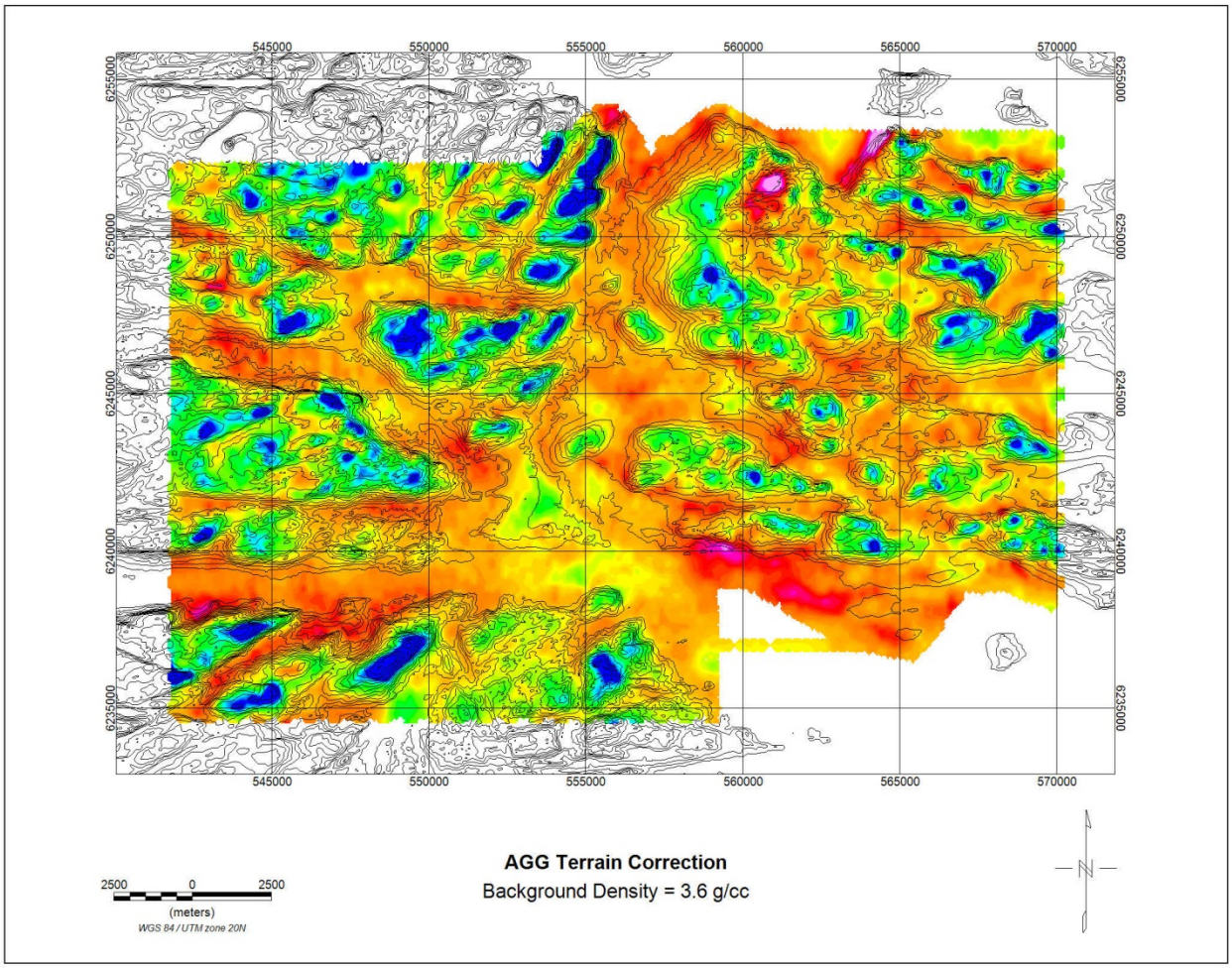

Figure 4.3 H: Terrain Correction of the AGG Gzz component using a background density of 3.6 g/cc, superimposed by CDED topographic contours.

involved in such an estimate, however, would likely mean we would introduce further artifacts into the data by using an incorrect overburden boundary. For this reason, the analysis and interpretation of all data in this study is restricted to the main portion of the Voisey's Bay mineralized trend, and does not include the flood plain region.

If more accurate information were gained in the future about the overburden-bedrock interface in this area, a variable density terrain correction could remove the effect of the variable overburden with little risk of introducing artifacts to the data. One common method in geophysically estimating overburden thicknesses is to use EM, however in this case the EM signature over this area is entirely dominated by the conductive response of the salt water brines and graphite (**Figure 3.11**). The two additional ways of mapping the bedrock interface in the future could include a surface refraction seismic program or further regularly spaced shallow drilling in the area. Unfortunately neither of these options are cheap, and even a simple seismic refraction survey in wet overburden over 120m deep would require explosives, which add environment and safety complications.

4.4: DEM Considerations

As previously noted, the terrain correction is a vitally important step in gravity processing. In section 4.3 we considered how an estimate of the background density could potentially create artifacts in the terrain-corrected gravity data by either under or over

correcting for surrounding terrain features, and how these false-anomalies could potentially mask or be mistaken for anomalous density contrasts related to geological sources. An equally, or perhaps greater, concern exists in the accuracy and frequency content of the Digital Elevation Model (DEM) to which the background density estimate is assigned. Of all density contrasts present in any given survey, the greatest contrast will be between the air and the surface of the Earth. Nearby topographic features are capable of producing gravity signals equal to or significantly greater than many of the sub-surface geological features that we are attempting to image. As a result, a DEM which is inaccurate can also easily result in an over or under compensation of the surrounding terrain's gravity field, and therefore produce false positive or negative gravity anomalies. These challenges are amplified when measuring the gravity gradient because the sensitivity of this measurement decreases with inverse distance cubed, and therefore the relative strength of the terrain effect is much higher (Kass and Li, 2008).

The cause of a DEM introducing errors to a terrain correction are primarily either topography data that includes large errors or that contains significantly different frequency content than the dataset it is being applied to. In the latter case, a common example is a low resolution DEM being applied to a much higher resolution AGG survey, and therefore being unable account for higher frequency topographic features (steeper slopes or valleys). Another possible issue is when a high resolution topographic dataset is applied to compute corrections for a lower resolution gravity dataset. In this case the calculated terrain response will have more detail and higher frequency content than the initial dataset, resulting in a terrain-corrected product that will also have a significantly different spectral character than the free-air

dataset. As a result of this over-correction, the terrain corrected data tends to invert over terrain peaks due to the greater amplitude of the correction, but exhibits positive anomalies on the flanks of terrain related anomalies due to the sharper nature of the computed correction. The terrain related anomalies in the tensor data are generally lower amplitude and smoother features than the corresponding computed terrain correction. Commonly in AGG datasets a low-pass filter is applied to remove high frequency noise caused by non-linear accelerations of the observation platform (Lane 2004), however details of the filtering are usually considered proprietary and are not passed on to clients. If a high-resolution DEM is used to terrain correct the AGG data after the fact this can lead to a mismatching of frequency content between the two. This is the case for the terrain correction of the Voisey's Bay AGG dataset when using the topographic data from a subsequently flown LiDAR survey to construct the DEM.

The LiDAR survey was flown over the Voisey's Bay property by Terrapoint Canada Ltd. in July of 2008 using a 100 kHz fixed wing LiDAR system mounted on a P-31 Navajo plane. The survey covered approximately 500 square km over the Voisey's Bay main block, and took 11 days to complete. The data collection took place at an optimum height of 1550m above ground and a speed of approximately 150 knots. The deliverable products from the LiDAR survey included both bare-earth and full-features datasets. The Bare-earth data had been stripped of everything but ground points whereas the full-feature included all vegetation and cultural features detected in the LiDAR survey. The DEM produced from the LiDAR survey contained a great deal more detail than the CDED DEM. Whereas the CDED DEM captured major terrain features, the LiDAR data imaged individual trees and trucks, before the bare-earth stripping process.

When the under-filtered LiDAR DEM was used to perform a terrain correction on the AGG data the correction dramatically over-corrected for local topography, creating false lows over hill tops (due to using a sharper and higher peak than can be resolved in the survey), and false positives on their flanks (due to using steeper slopes than can be resolved in the survey (**Figure 4.4**). The initial purpose of acquiring an updated DEM to apply to the AGG dataset for VB was driven not just by the desire to apply the most accurate terrain correction possible, but also to apply a more recent DEM than the CDED data that was initially used. The initial CDED topographic dataset had been collected prior to the construction of the VB mine and did not include many major changes to the ground that existed during the time of AGG data acquisition, including the Ovoid open pit and the waste pile sitting over the Southeast Extension). The effect of using this outdated DEM obviously caused artifacts in the CDED terrain-corrected dataset. One example is that by not taking into account the amount of earth removed in the Ovoid open pit we are creating a strong false negative anomaly. As a result, the strong positive gravitational anomaly in the same area cause by the extremely dense (3.8-4.0 g/cc) world-class massive sulphide deposit is heavily masked and is indiscernible from the background signal.

The current application of the LiDAR dataset to the Voisey's Bay AGG terrain correction is an excellent example of how careful preparation of the DEM is essential prior to applying a terrain correction to any gravity dataset. In order to properly prepare a high resolution DEM for this type of processing it must be carefully filtered to a match the resolution of the gravity dataset. This requires a spectral analysis of the frequencies contained in both datasets and subsequent careful low-pass filtering of the DEM. As previously noted, the lack of information

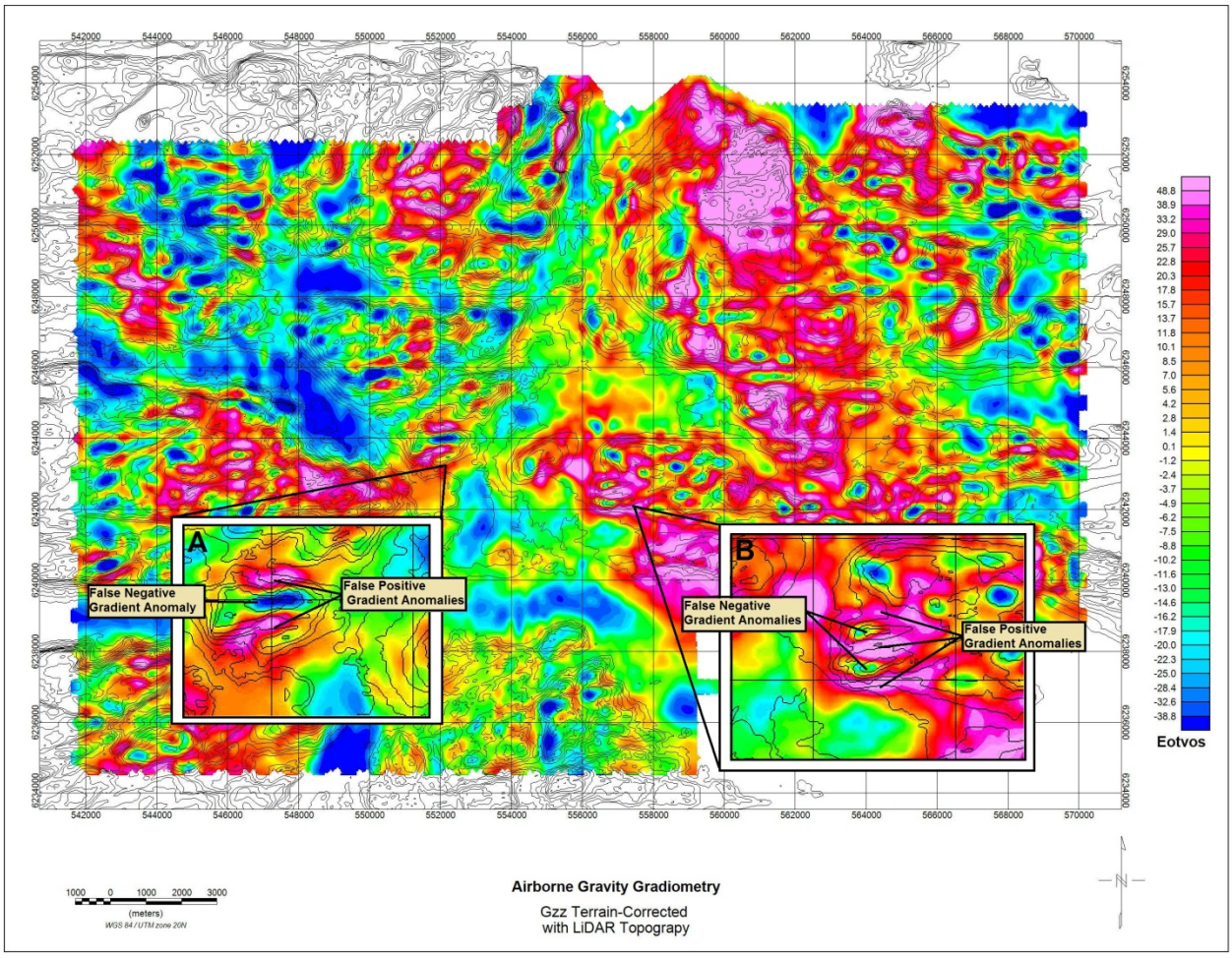

Figure 4.4: AGG Gzz terrain corrected using a LiDAR-derived DEM. In this case, the DEM was not properly frequency-matched with the AGG dataset prior to the terrain correction, resulting in false negative anomalies on hilltops and false positive anomalies on hill-flanks due to the over-correction of the sharper computed correction.

about proprietary filtering completed by the contractor complicates any attempt at frequency-matching a DEM to an AGG dataset by the end-user.

Through comparing ground gravity and AGG data, Lane (2004) shows that the remaining frequency content of AGG data after contractor filtering is consistent with that of a Butterworth filter of varying cut-off wavenumber. Although this does not provide detail about the individual filtering steps during acquisition and processing, it does provide a composite filter representing the effects of both together (Kass and Li, 2008). The characteristics of the cumulative filtering will vary from dataset to dataset based on factors such as data quality and survey height, but has been successfully simulated by filters similar to a 200m length, fourth-order Butterworth filter (Kass and Li, 2008). In order to avoid the adverse data artifacts previously discussed, the same type of filter must be applied to the DEM prior to terrain correction. This process would be highly recommended for future work with the LiDAR corrected AGG dataset at Voisey's Bay, but at the time of the writing of this thesis has not yet been completed. As a result, in considering the spectral content of the AGG dataset in the next section we will deal exclusively with the terrain-corrected product previously creating using the CDED DEM.

4.5: Filtering

In addition to the processing and corrections which must be performed on airborne gravity gradiometry data, filtering maybe applied to the final grid in order to accentuate

features of interest. Due to the nature of gravity gradient measurements the majority of gradient sensitivity lies in shallower depths of the ground. Therefore the terrain corrected Gzz provides us with a very useful and detailed image of the local subsurface density contrasts (**Figure 4.5)**. When working with a traditional gravity survey, it is commonplace to produce images of the vertical derivative of the gravity in order to see such local changes, which is analogous to our Gzz product. In this instance it is desirable to also focus on broader trends in the data representing larger and/or deeper bodies by enhancing the very subtle long-wavelength signals in the Gzz data. One method of highlighting these features is to perform a vertical integration on the Gzz, resulting in a Gz image similar to a traditional gravity survey.

The two primary methods of converting gravity gradiometry data into a vertical gravity product are through direct integration techniques (Gunn, 1975) or equivalent source methods (Dampney, 1969). Both methods amplify long wavelength features within the AGG data, therefore making larger/deeper features more prominent. One important difference between this and regular gravity data is that we are acquiring gradient data directly in the survey, and therefore our data is missing meaningful information from wavelengths longer than the dimensions of the survey. In the case of the Voisey's Bay AGG dataset, the survey features lines as long as 40km. If features of longer wavelength than the dimensions of the survey are of interest, as is sometimes the case in oil exploration or regional mineral exploration, it is possible to combine the high resolution data of an AGG survey with the long wavelength content of a gravity survey if one should exist in the same area. One method of combining gravity and gravity gradiometry datasets is described by (Lane, 2004) involves upward or downward continuing both datasets to a common drape surface, supplementing the long

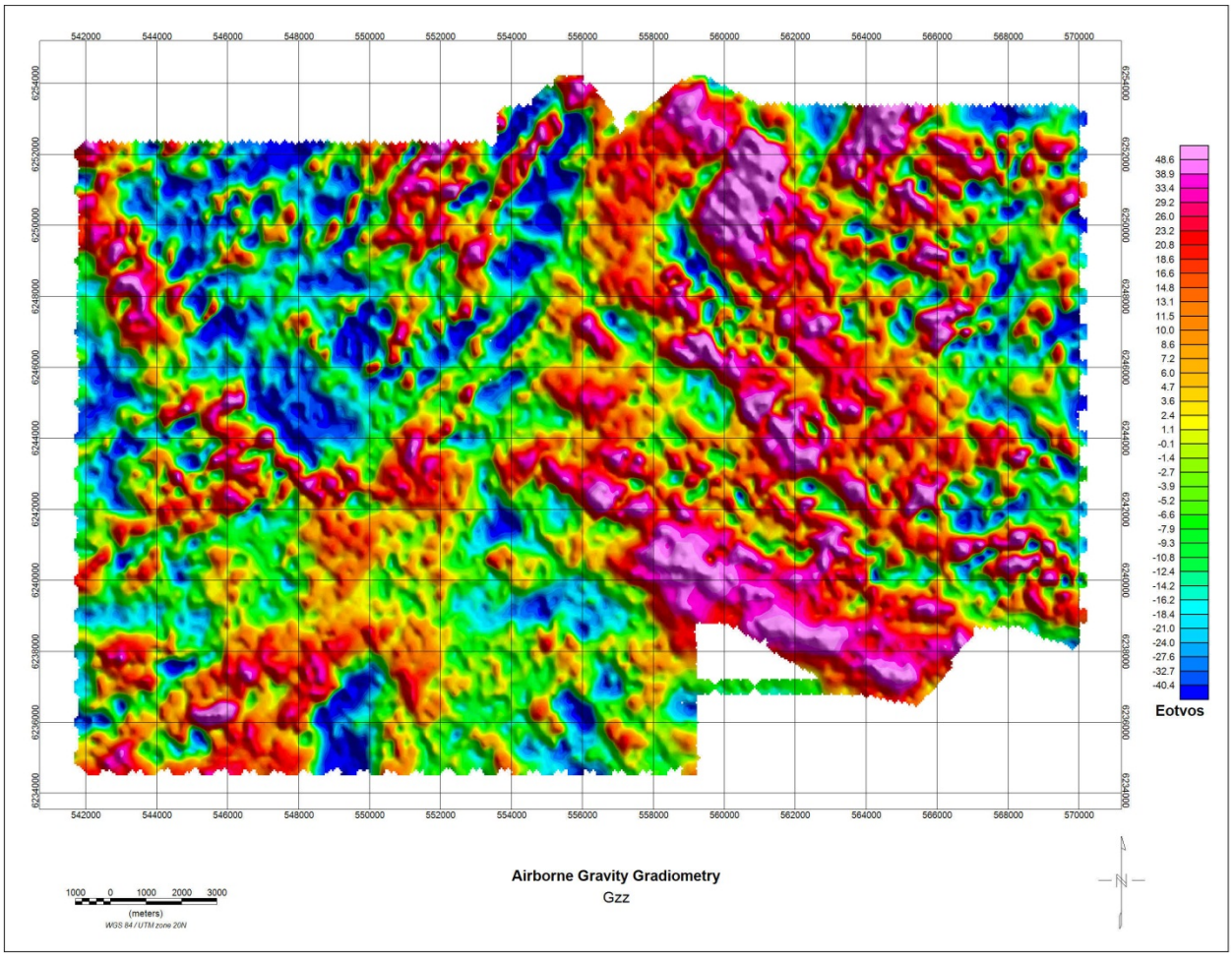

Figure 4.5: Final Terrain Corrected Airborne Gravity Gradiometry Gzz Map

wavelength content of the AGG with that of the ground gravity via cross-over filtering, and obtaining a smooth output data surface by jointly inverting the datasets using an equivalent source technique (Lane, 2004). In the case of nickel exploration in Labrador and therefore the purposes of this study, however, we are primarily concerned with density signatures in the top 2km of the Earth, which is more than sufficiently represented in the current spectral content of the AGG dataset.

The vertical integration map is shown in (**Figure 4.6**). This processing, and all other processing included in this section, was completed using the magmap module of Oasis Montaj. For the purpose of comparison with both the Gz and Gzz products, the Voisey's Bay geology map is shown on the same scale (**Figure 4.7)**, using the geological legend shown in **Figure 4.8**. In the case of the Voisey's Bay environment we can see a large regional density trend dominating the eastern portion of the survey block. This region of high density encompasses the troctolite of the Mushua and Voisey's Bay intrusions. The surrounding paragneiss and orthogneiss country rock are included in the region of lower density in the western and the far eastern portions of the block.

Having satisfactorily enhanced the medium and long wavelength signals in the AGG dataset to a similar level as the shorter wavelength signal, the more traditional problem of removing the regional gravity signal can be approached. The purpose of this processing step is to highlight local features of interest in mineral exploration and remove the gravity response of deeper basement rock beyond the scope of investigation. The separation of the regional and residual gravity signals can be quantitatively achieved through several filtering methods (Hearst

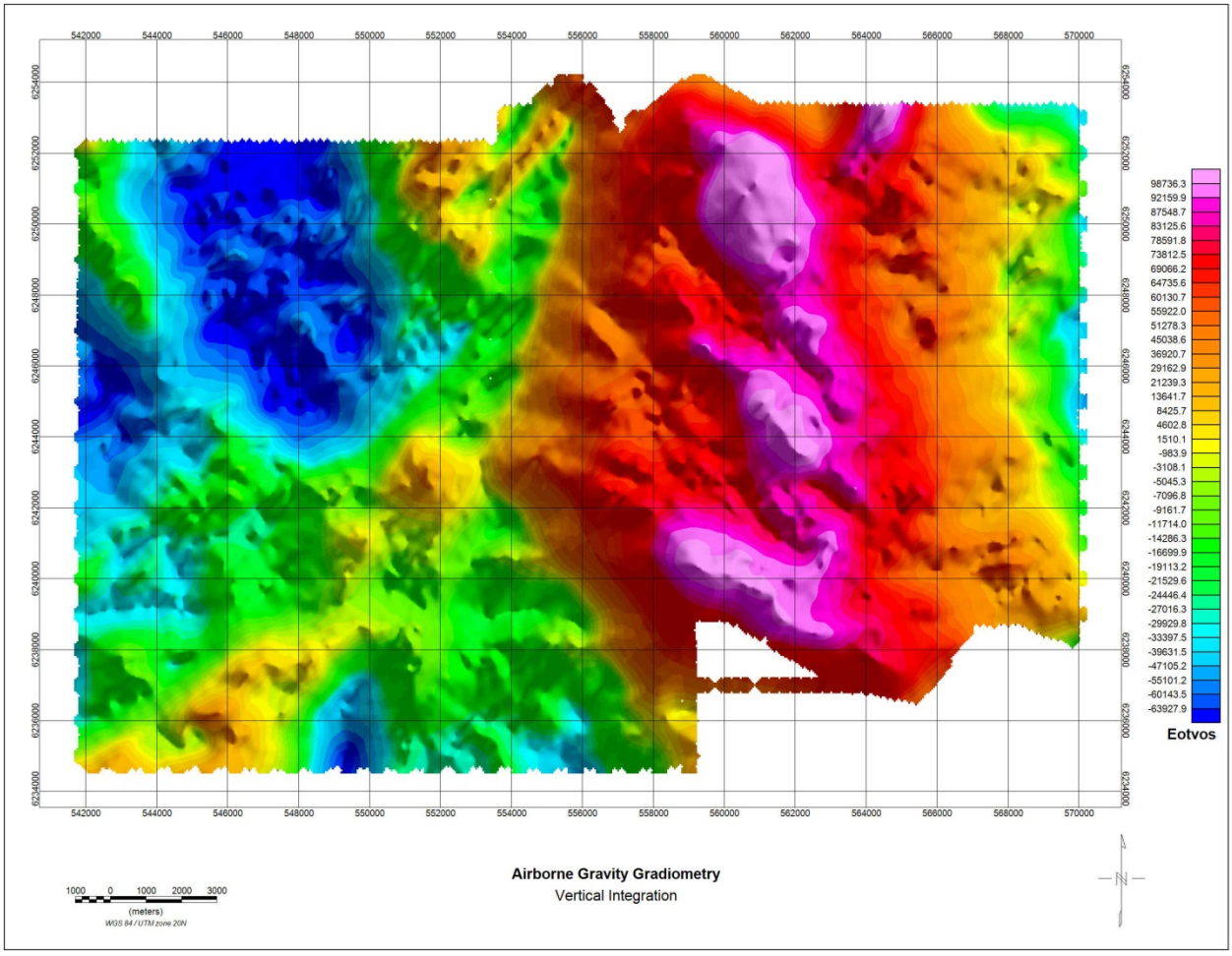

Figure 4.6: Gz map of AGG survey, vertically integrated from Gzz

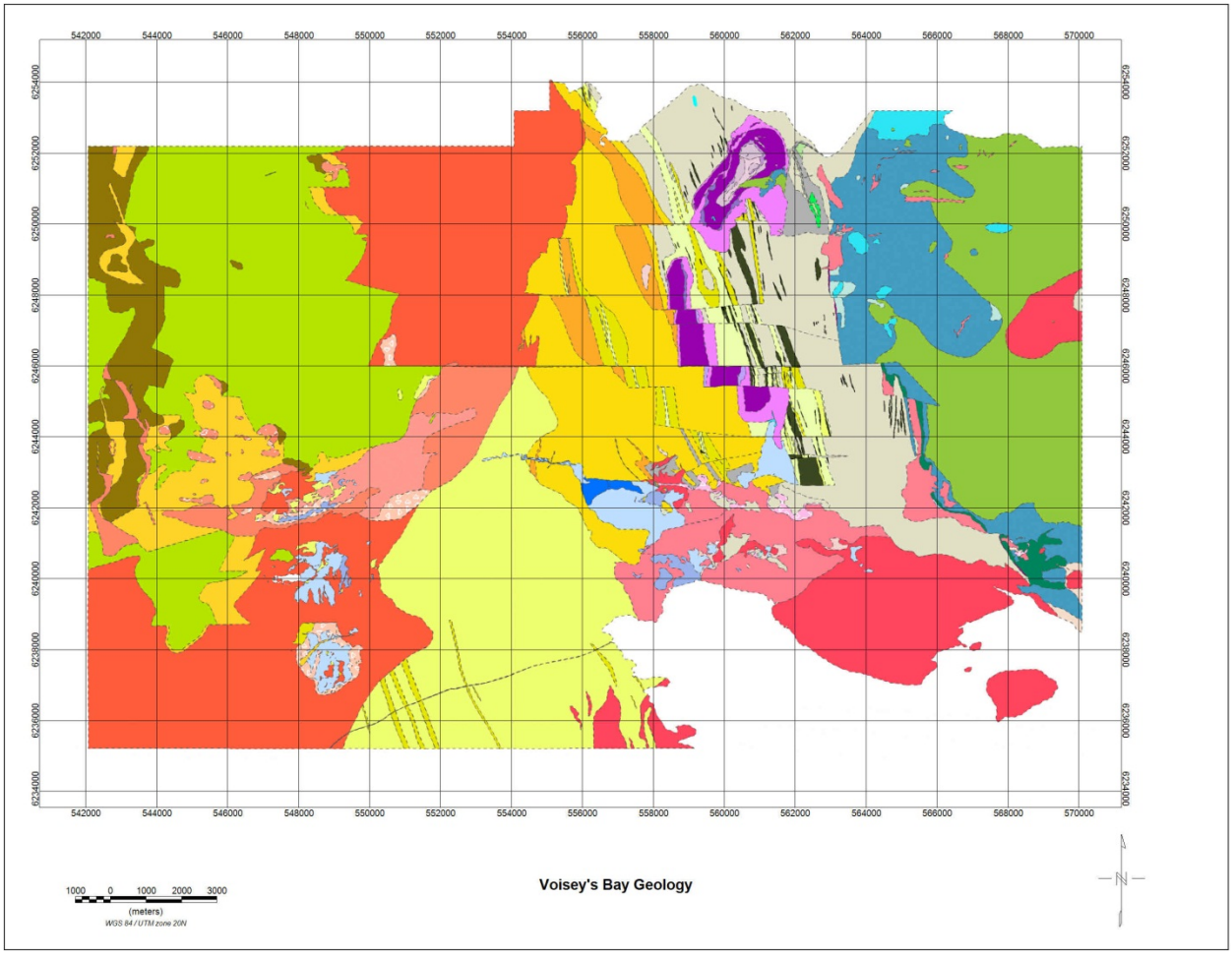

Figure 4.7: Voisey's Bay Geological Map

Figure 4.8: Voisey's Bay Geological Key to accompany Figure 4.7

and Morris, 2001), amongst which some of the most commonly used are wavelength filtering and upper-continuation.

The basis for regional gravity removal via wavelength filtering relies on the generally valid assumption of a correlation between source bodies of specific depth and a finite range of anomaly wavelengths (Spector and Grant, 1970). Although it is true that deeper bodies will always give longer wavelength anomalies, the assumption does not hold true for broad-scale shallow bodies (Hearst and Morris, 2001). For the purposes of removing the response of the deeper geological units in the Voisey's Bay AGG survey and highlighting features likely to be located within the top several km of the Earth, a high-pass filter was selected, with a wavelength cut-off of 15km. The resulting residual gravity map is shown in **Figure 4.9**.

As a means of checking the assumptions involved with the wavelength filtering regional-residual gravity separation and ensuring the resulting map isn't being adversely affected by ringing in the FFT processing, we may go through the same process with the filtering method of upper continuation. This filtering process allows for a better visualization of the background signal being removed. The first step is to upward-continue the data until the signal of the mapped surface geology is effectively removed (Hearst and Morris, 2001). In the case of the Voisey's Bay main block much of the country rock has a great depth extent. With the same intention of highlighting troctolite chambers within the top several kms as the previous processing, an upward continuation of1km was chosen to represent the regional signal (**Figure 4.10**). Although the general trend of higher density existing to the east of the main block is

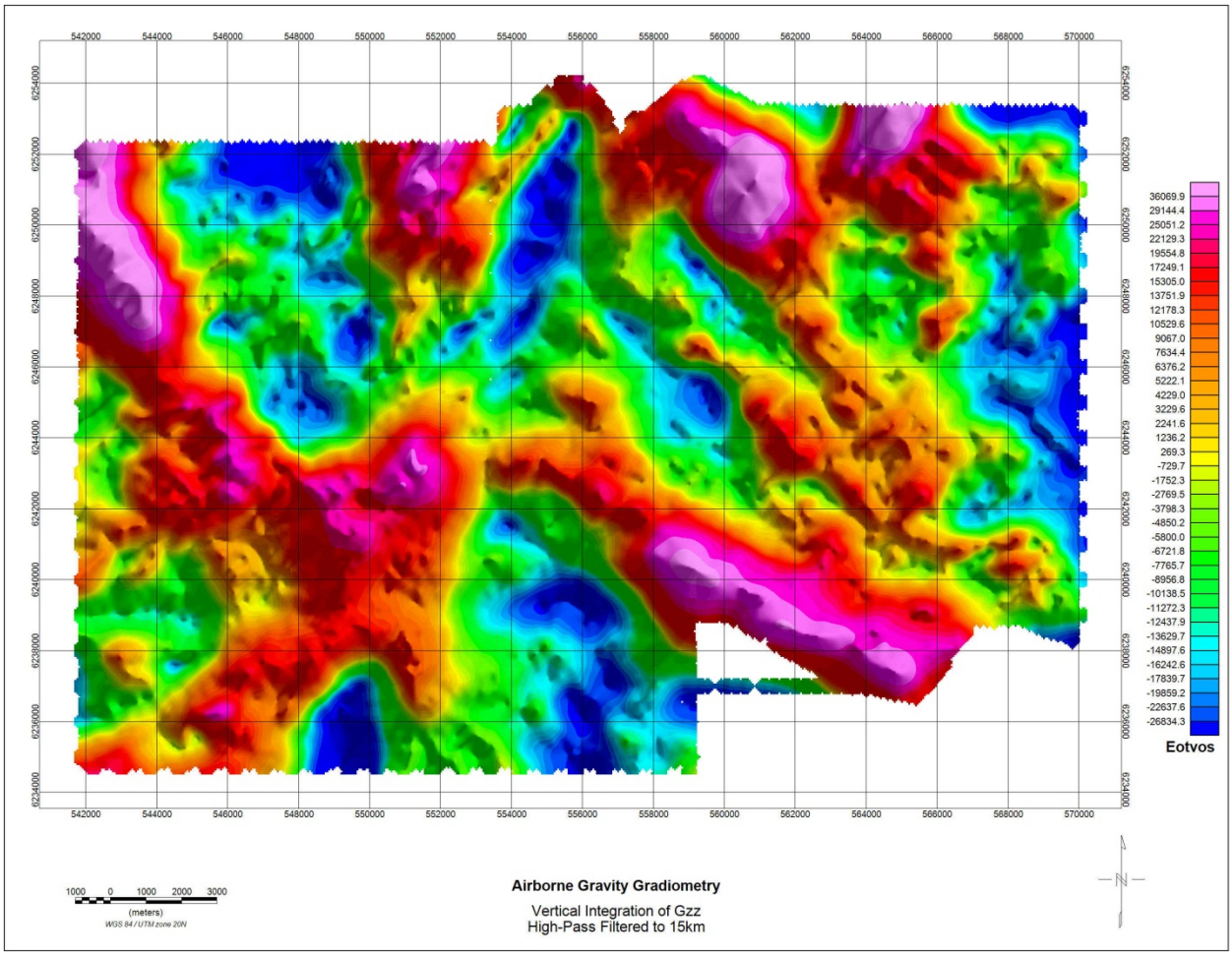

Figure 4.9: Residual AGG Gz grid high-pass filtered to a wavelength of 15km.

present in this figure, none of the detailed geology represented in the surface geological map (**Figure 4.7**) can be seen here. Once this regional signal grid is subtracted from the original grid, a residual gravity grid is produced (**Figure 4.11**). This figure highlights resembles the residual gravity grid produced by high-pass filtering closely, highlighting many of the same features but with some amplitude variance.

Both residual gravity anomaly maps do an excellent job of highlighting the VBI and Mushua intrusions, but also indicate a body of anomalous density to the immediate west of the Reid Brook zone that could represent a buried troctolite chamber. The amplitude of this feature is stronger and more similar to the VBI gravity signature in the wavelength-filtered map, but is also significant in the upper-continuation residual map. This area is overlain with overburden and granite, has a limited amount of drilling, and is directly along trend of the Voisey's Bay mineralized system, giving it compelling potential as a buried troctolite chamber with prospective for economic mineralization.

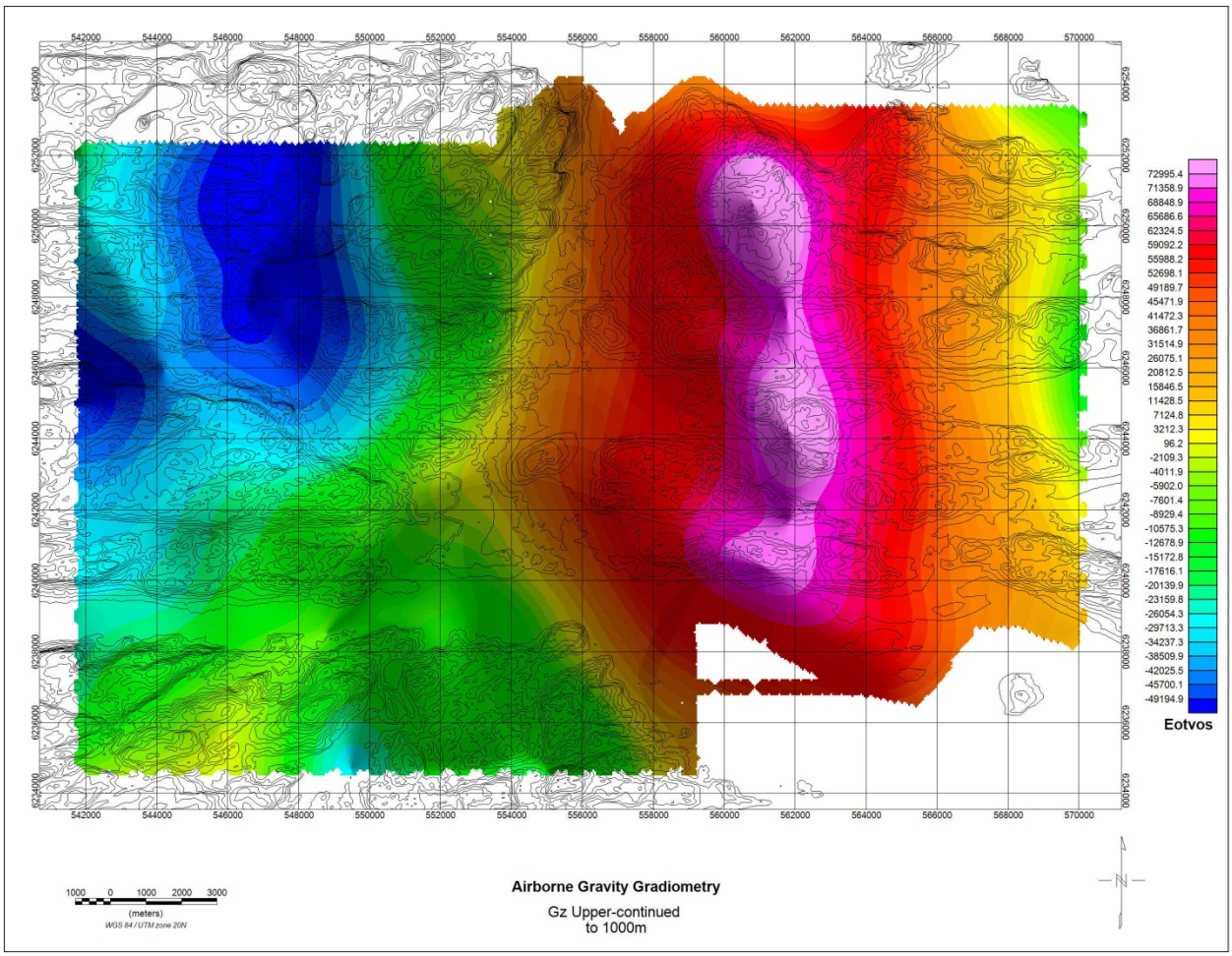

Figure 4.10: Upward continuation of Gz by 1000m. This map contains the longer wavelength features of the Gz dataset that represent the regional geological signals.

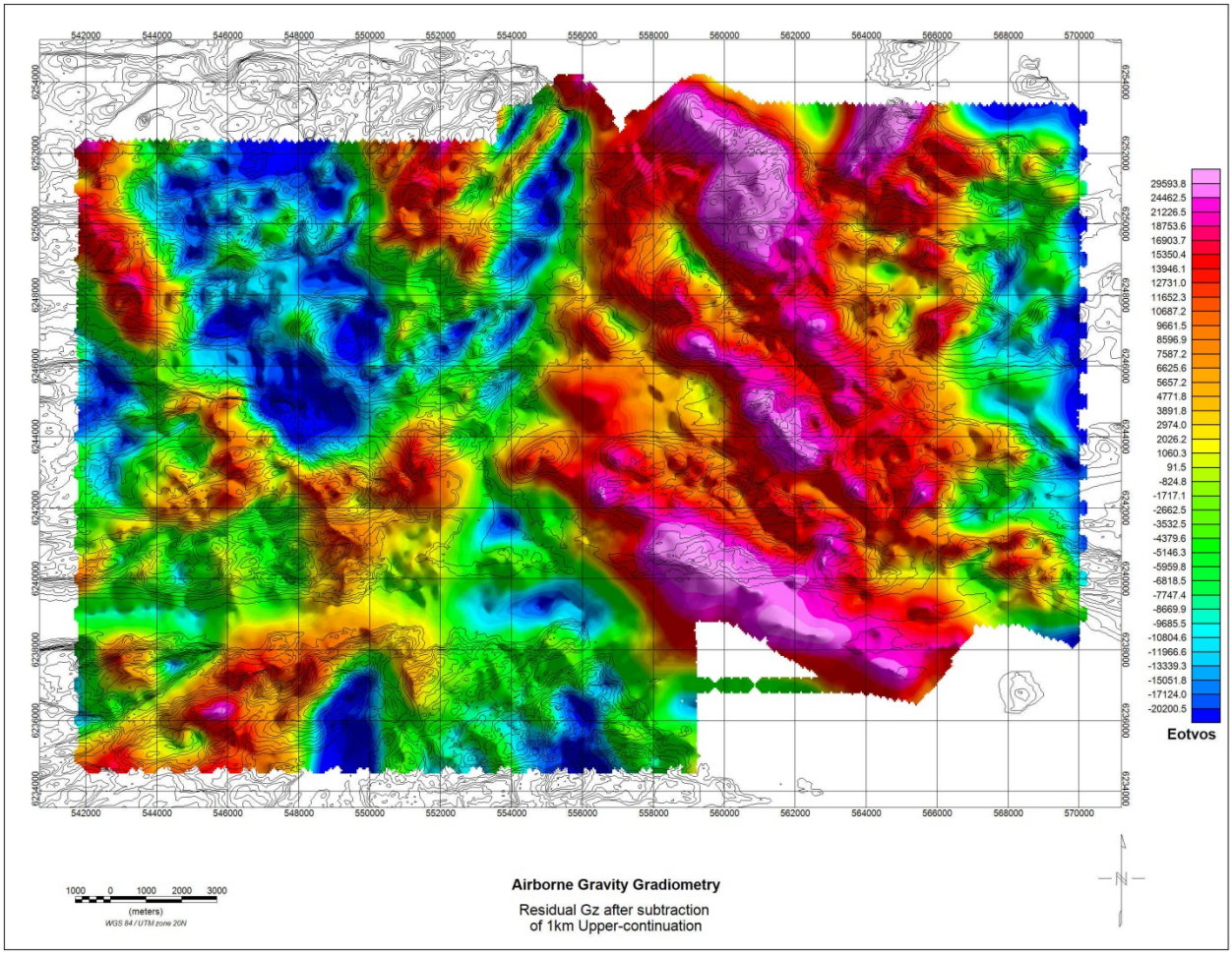

Figure 4.11: Residual gravity map of Gz, after the subtraction of the upward-continuation shown in Figure 4.10 from the Gz grid shown in Figure 4.6. This image contains many of the same residual features as the residual grid derived through the use of a high-pass filter shown in Figure 4.9.

Chapter 5: Spectral Analysis

5.1: Introduction

Chapter 5 of this thesis will be focused on a spectral analysis and comparison of the airborne gravity gradiometry dataset, the historical ground gravity data and an upward continued version of the ground gravity which is meant to represent the response of an airborne gravity survey collected at the same height as the AGG. A qualitative comparison of the datasets will be completed, as well as a consideration of the spatial sampling of each survey. The quantitative analysis methods used will include 2D power spectra and radially averaged power spectra plots, and will attempt to define the resolution capabilities of each dataset.

5.2: Spatial Sampling and Qualitative Features of Gravity Datasets

In the consideration of Airborne Gravity Gradiometery as an exploration and prospecting tool, it is necessary to have an understanding of how it compares to the more traditional method of ground gravity data collection. A primary control on the characteristics of any geophysical dataset is the spatial sampling of the survey, usually defined by the line and station spacing. This can vary greatly amongst ground gravity surveys used in the exploration industry, from detailed surveys with station spacing of 25-100m and line spacing of 100-500 meters to more regional surveys designed for a coarse mapping of large lithological units that commonly use a station spacing of 10-15km. Similarly, the regularity of ground gravity surveys

can vary from an organized grid of pickets and cut lines to extremely irregular sampling along roads, rivers, or wherever a helicopter can easily land.

The line spacing of airborne gravity gradiometry surveys can also vary, with common surveys employing a line spacing of anywhere from 200m to several kilometers (there is no upper limit to AGG line spacing, but surveys with line spacing greater than several kilometers are not generally benefiting from the increased sensitivity of AGG compared to traditional airborne gravity, and are usually relegated to this latter, less expensive method). The contrast in spatial sampling between the two methods exists in the variance of both station spacing and sampling regularity. An AGG survey, like any airborne geophysical method, involves taking consistent rapid measurements while flying through the air at a given speed. The Bell Geospace FTG system employs a sampling rate of 1Hz. At surveying airspeeds of approximately 60m/s, this relates to regular spatial samples of roughly 60m along the flight line. In this way, due to the nature of both surveying methods, significantly less variance in spatial sampling tends to exist across the spectrum of AGG surveys than in ground gravity surveys.

A regional ground gravity dataset was collected by the Geological Survey of Canada in Northern Labrador during the late 70's and early 80's **(see Figure 5.1).** Prior to the large ground gravity program run in Voisey's Bay during the mid-late 90's this was the only gravity dataset available for the region, and is a prime example of wide and irregular station spacing (commonly 5-15km). The Voisey's Bay ground gravity dataset was a significant improvement over this, with much tighter station spacing and less, but still existent, irregularity in station locations **(see Figure 5.2).** This dataset consists of 112 survey lines with station spacing of 25-

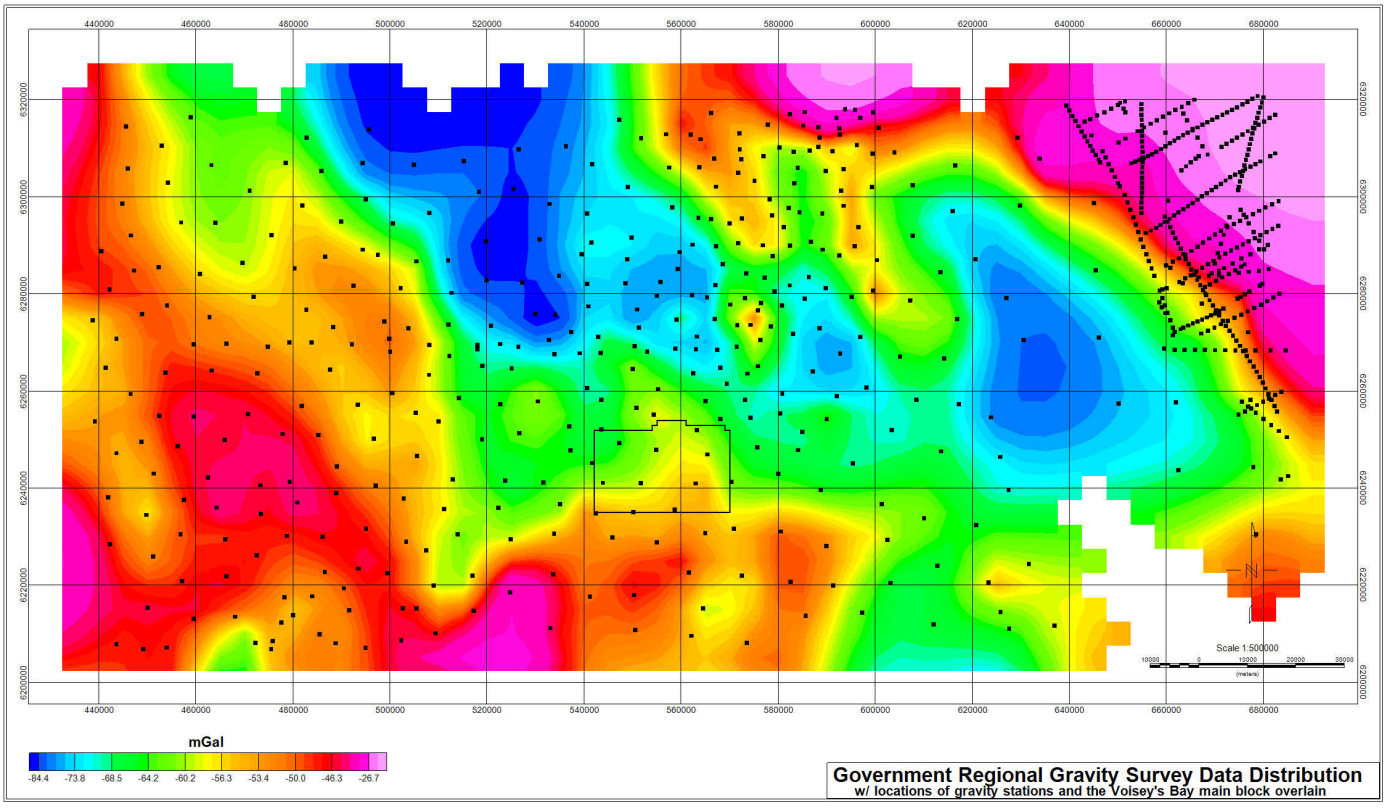

Figure 5.1: The data distribution of the government regional gravity survey in the Voisey's Bay region, overlain with station locations and an outline of the Voisey's Bay main block.

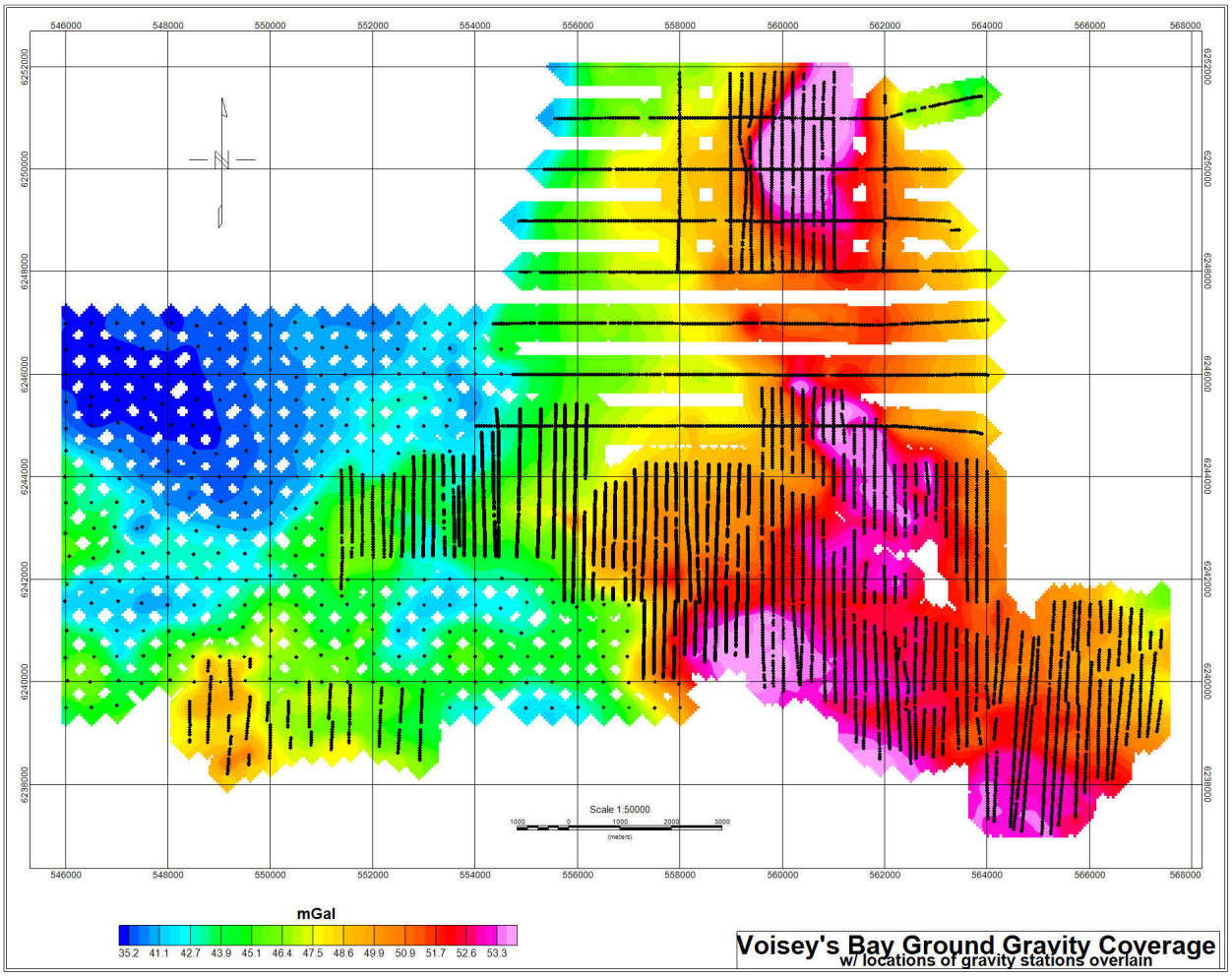

Figure 5.2: The data distribution of the Voisey's Bay ground gravity survey.

50m and line spacing of 100-400m. These lines exist in various locations around the Voisey's Bay block, but are primarily concentrated along the main E-W mineralized trend. There was also a regional gravity grid collected within the block using a station and line spacing of 500m which is incorporated into the dataset. All individual surveys were tied together by the use of a common base station. This mosaic-type of non-uniform data sampling is commonly seen in ground gravity coverage for properties throughout the mineral exploration industry.

The AGG dataset, as discussed in Chapter 3, had N-S lines with a uniform line spacing of 200m throughout the Voisey's Bay block **(Figure 5.3).** This spacing compares favorably with the ground gravity, being equally detailed in some areas but significantly more detailed in others. As also previously mentioned, the station spacing along lines was at regular intervals of approximately 60m. In some areas of the ground gravity survey the sampling is equal or slightly better, but in most areas the AGG station sampling is also substantially better. In addition, the AGG dataset sampling is extremely uniform throughout the survey area and also extends further than the ground gravity.

In qualitatively comparing the features mapped by both surveys **(See Figure 5.4),** we see that both surveys capture the same dominant features throughout their shared survey extent. The three main troctolite chambers on the Voisey's Bay block, Mushua, Gomer, and the Eastern Deeps, are all featured prominently in both datasets. While the location and main characteristics of these large features are shared, we do see a contrast in their level of detail. The contrast between surveys is more pronounced for smaller, yet potentially important, features throughout the area. This variance can be traced back to two primary sources: 1) the

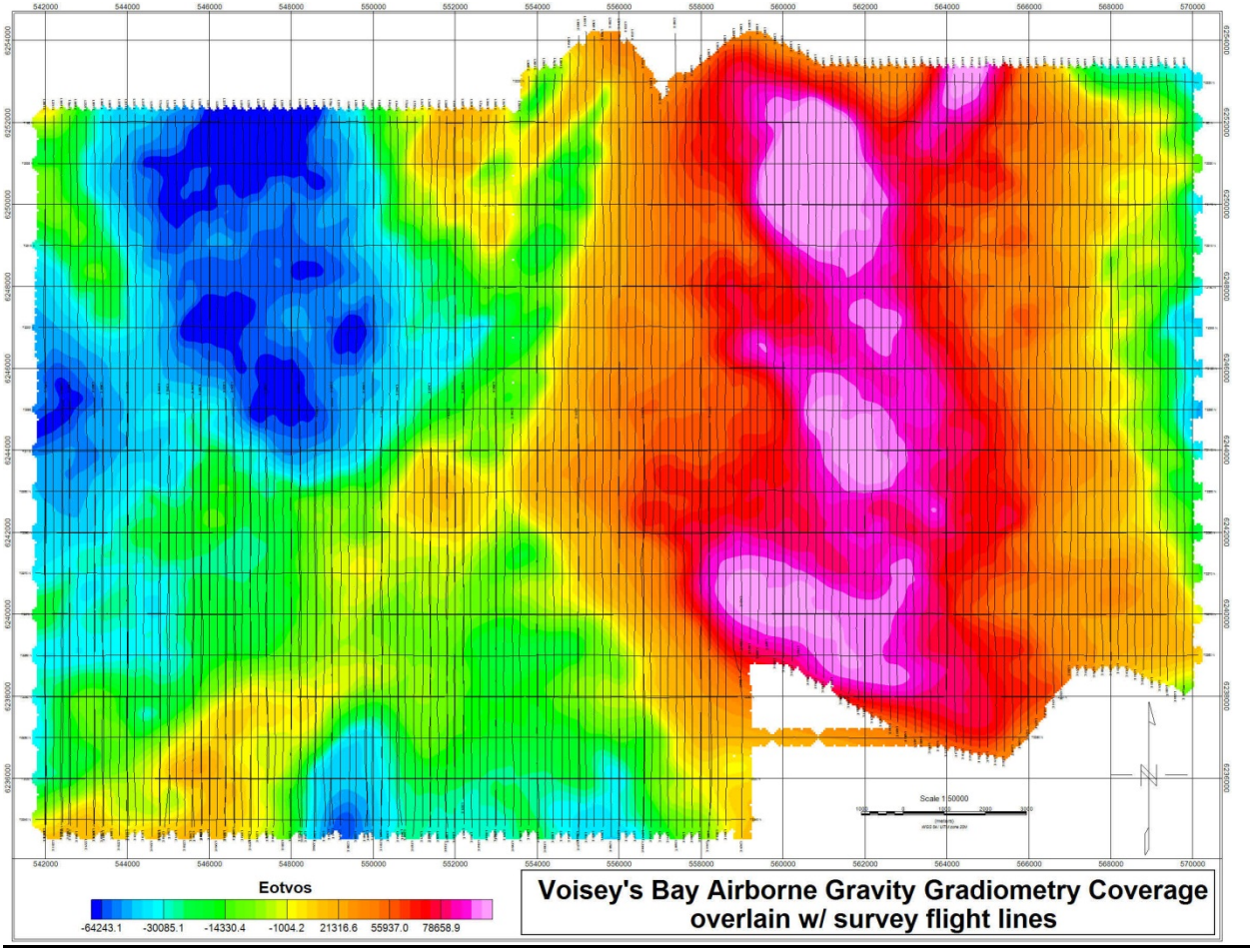

Figure 5.3: Data distribution of AGG survey

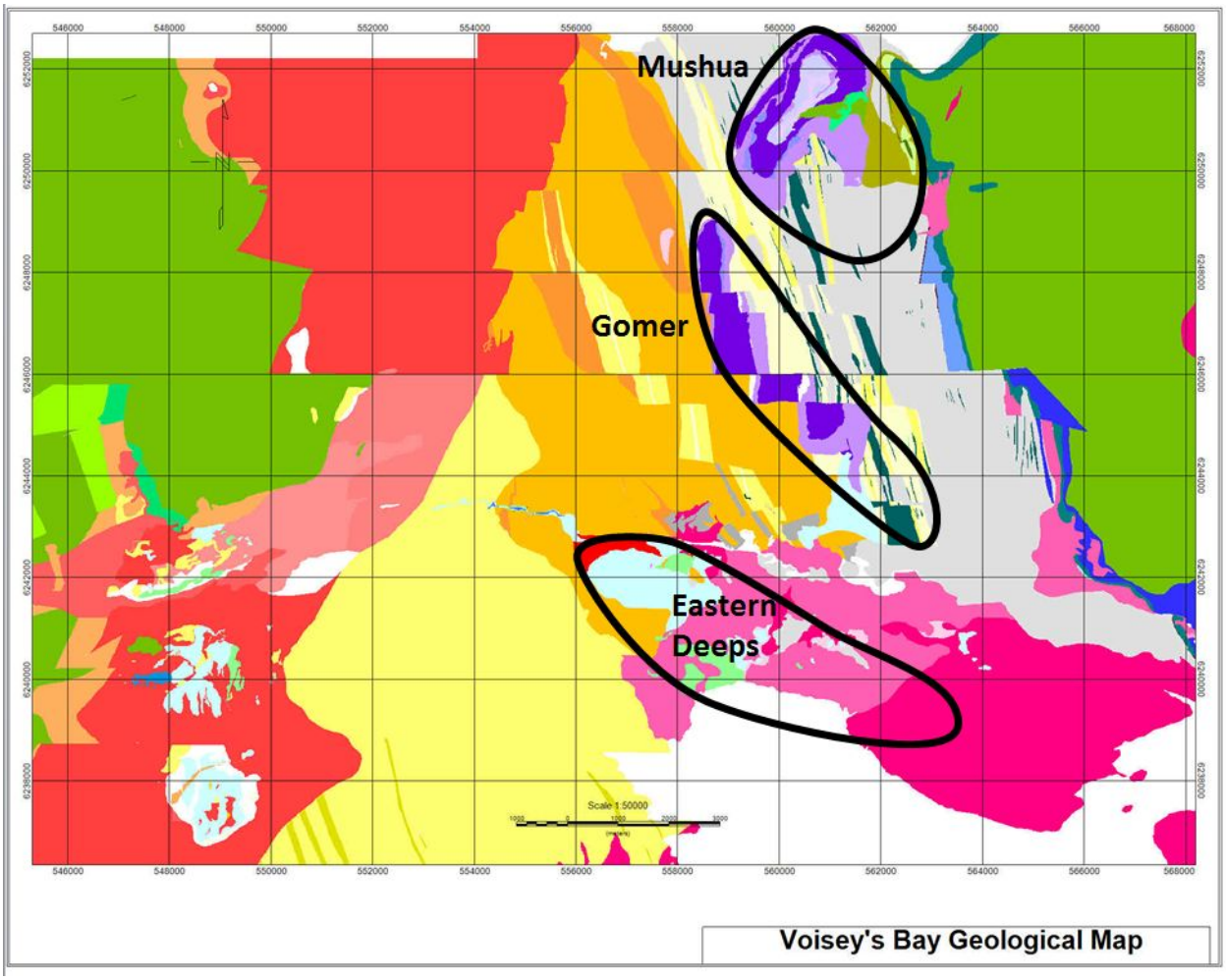

Figure 5.4a: Voisey's Bay Geology map with the three largest troctolite chamber trends outlined.

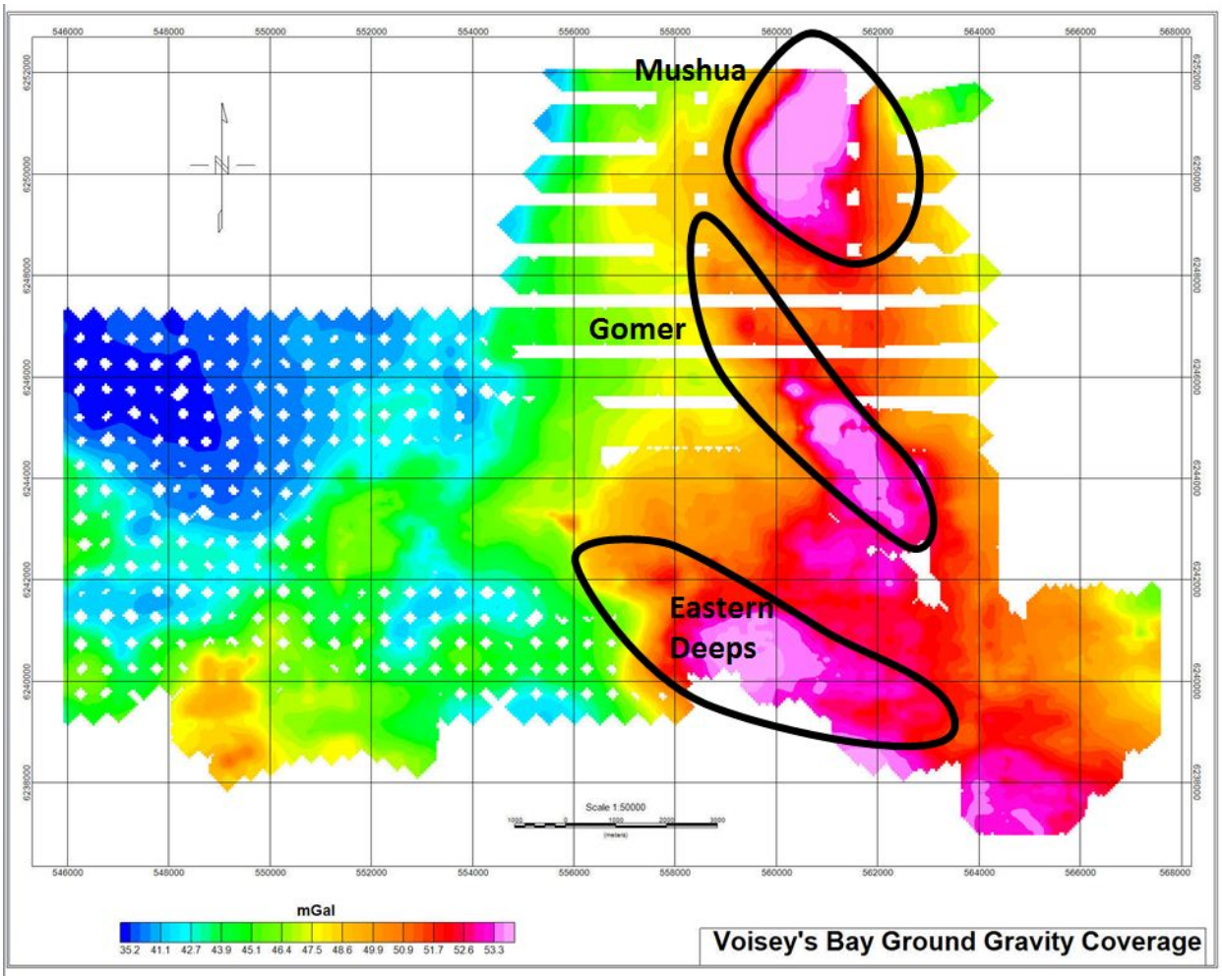

Figure 5.4b: Voisey's Bay ground gravity map with the three largest troctolite chamber trends outlined.

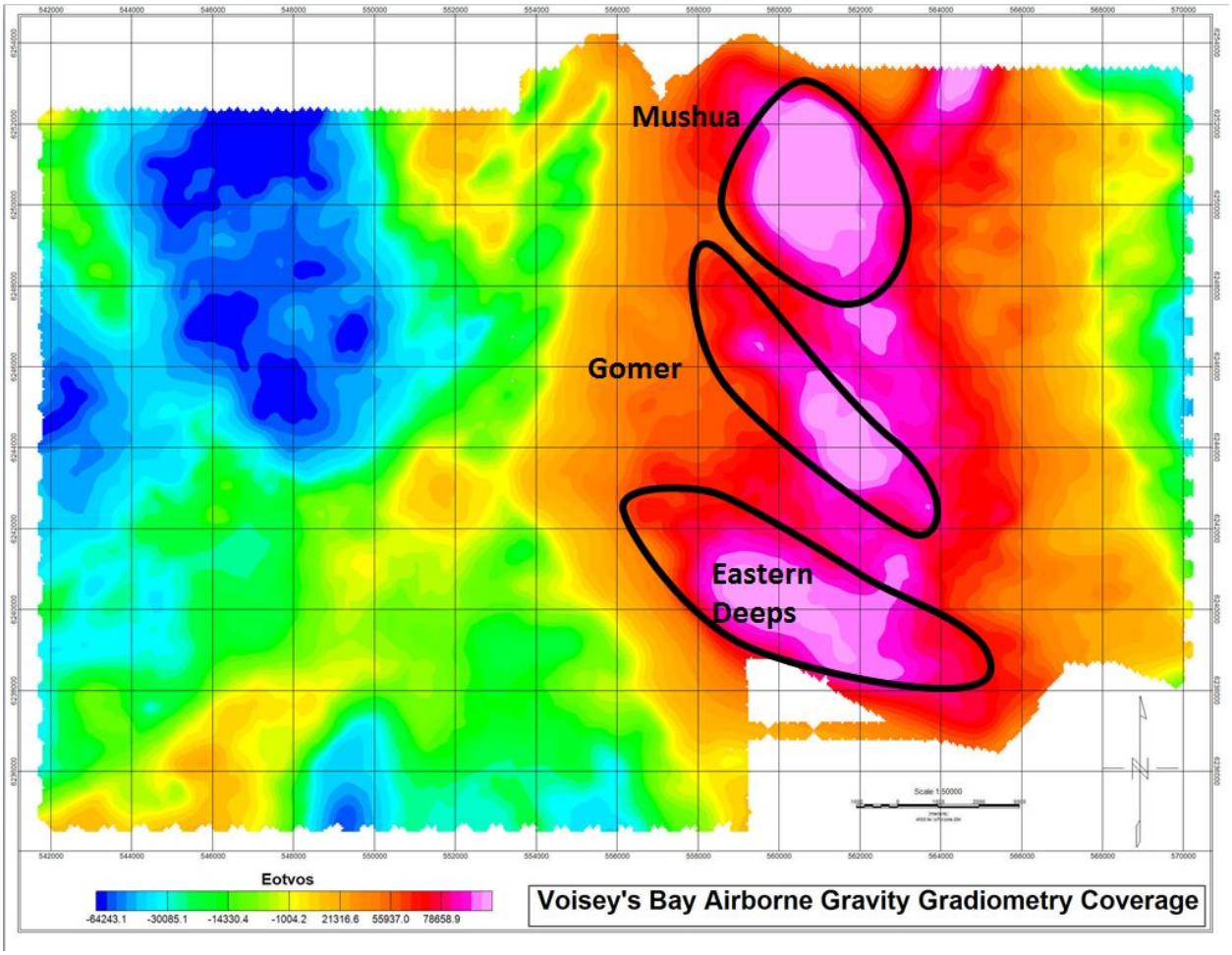

Figure 5.4c: Voisey's Bay Vertically Integrated Tzz map with the three largest troctolite chamber trends outlined.

greater uniformity in spatial sampling of the AGG survey (resulting in a much greater amount of information in areas where the ground survey has poor coverage) and 2) the higher signal resolution of the ground measurements as a function of being closer to the causative geological features (resulting in sharper boundaries and greater high frequency detail of anomalies where the ground gravity coverage is equal or better)**.** Further comparison of both datasets calls for a more quantitative analysis of their respective spectral characteristics.

5.3: Spectral Analysis Methodology

Prior to numerically comparing the ground gravity and AGG datasets as equivalent datasets, some preliminary processing was performed. First of all, a vertical integration was completed on the Tzz component of the AGG, as discussed in Chapter 4. Next, the units of the vertically integrated AGG were scaled to mGal using the simple conversion of 1 Eotvos = 0.1mGal/km. Finally, in order to compare not just the datasets, but the sensor resolution capabilities in both surveys, the ground gravity was upper-continued to the average survey height of 250m used in the AGG survey.

In order to complete a quantitative analysis of the spectral content included in the ground gravity and AGG datasets we must first transform the data into the frequency domain. To accomplish this we will make use of the Fast Fourier Transform (FFT) method within Oasis Montaj. The FFT is a method for decomposing an image into a series of sine and cosine

functions of varying frequencies. The lowest frequency in such a transformation is zero which represents the DC component of the signal and is the average value found within the dataset. The highest frequency found in an FFT transformation is determined by the Nyquist cut-off frequency of the dataset. The Nyquist frequency represents the limit of resolution for a dataset as determined by the spatial sampling increment of a survey and is represented by the function:

$$f_{max} = \frac{1}{2\Delta x}$$

Any frequency higher than the Nyquist will be aliased, meaning folded back into the lower frequency parts of the spectrum.

From a geophysical survey standpoint, the actual maximum frequencies which are possible to resolve within the data are determined by the station and line spacing. In most surveys data is generally over-sampled along the direction of the line, and under-sampled across lines. When we grid geophysical data we attempt to choose a cell size which compromises between both sampling rates, attempting to be small enough to avoid aliasing data along the line and to be large enough so as to avoid creating artifacts due to excessive interpolation across adjacent lines. The critical choice of cell size, and therefore behavior of the interpolation algorithm, is what ultimately defines the Nyquist frequency for the gridded data.

Given the spatial variance and non-uniformity of stations in the ground gravity dataset described in section 5.1, the choice of cell size required some trial and error. After trying a wide range of possibilities, a cell size of 50m was selected because it seemed to offer the most effective compromise of being faithful to densely populated areas of data and not creating

unwanted artifacts between measurements in sparsely populated regions. All further analysis of the 50m cell ground gravity grid from this point onward should be taken with the caveat that, in general, ground gravity survey sampling and the corresponding cell size can commonly vary a great deal (there are specific areas of this survey area which could be accurately represented by a cell size as large as of 250m), and the spectral character can be expected to vary as a direct result.

The choice of a cell size for the AGG dataset was much more straightforward, due to the regular spatial sampling, but still required some trial and error. A cell size of 50m was also selected for this dataset as a compromise between representing the detailed 60m in-line measurements and the 200m spaced flight lines. The fact that we were able to represent both datasets accurately with the same choice of cell size is advantageous for our comparison, as we would otherwise be introducing another uncommon variable into the power spectrum of each dataset. The Nyquist cut-off frequency of 100m will also be identical for both datasets.

The restrictions on FFT input grids include that the grid must be of a square or rectangular shape and that there cannot be gaps in the data. In practical terms this means that for an entire survey area to be transformed through the FFT process, all gaps within the dataset must be interpolated, and any gaps within the chosen rectangular or square area that do not include data must have extrapolated values. Square grids have an advantage of minimizing possible side effects from having different wave number samples in the X and Y directions (source: Geosoft Technical Documentation “Preparing Grids for MAGMAP FFT Processing”, 2013). For survey grids which are of irregular shape, such as both the Voisey’s Bay ground

gravity and AGG surveys, this step has the potential to introduce significant contamination of the power spectrum because of the difficulties in a large amount of extrapolated data not sufficiently representing the characteristics of the rest of actual data. There are numerous methods to tackle this problem, but for the purposes of this study the choice was made to instead select the largest square data sample possible within the survey area so as to most accurately represent the spectral character of both datasets. Because the ground gravity survey covers a smaller area, its bounds were the controlling factor in the selection of our data sample area. The largest square sample area possible to fit inside the ground gravity survey area was 8770x8770m **(See Figure 5.5)**. This sample area also has the advantage of including areas of both dense and spare ground gravity measurements, making it a good representative sample of the spectral character of this dataset.

The next step taken in preparing the gravity grids for the FFT process was to accommodate the implicit FFT assumption that the data is periodic; therefore the data on the Eastern border of the grid are neighbors to the data located on the Western border. This assumption also applies to data on the North and South borders. If no treatment of the grid occurs to make the transition between these borders smooth then the borders are effectively seen as step functions in the frequency domain, which causes the contamination of the power spectrum in the form of a concentration of power along both axes in the frequency domain (St. George's Cross) (Billings and Richards, 2010). In order to smooth the transitions between these edges and avoid contamination the grids are expanded by an amount and extrapolated to matching values. In this case both gravity grids were expanded by 10%, filled using a square multistep expansion, and have a 1st order trend removed (**Figure 5.6)**. The resultant grids had a

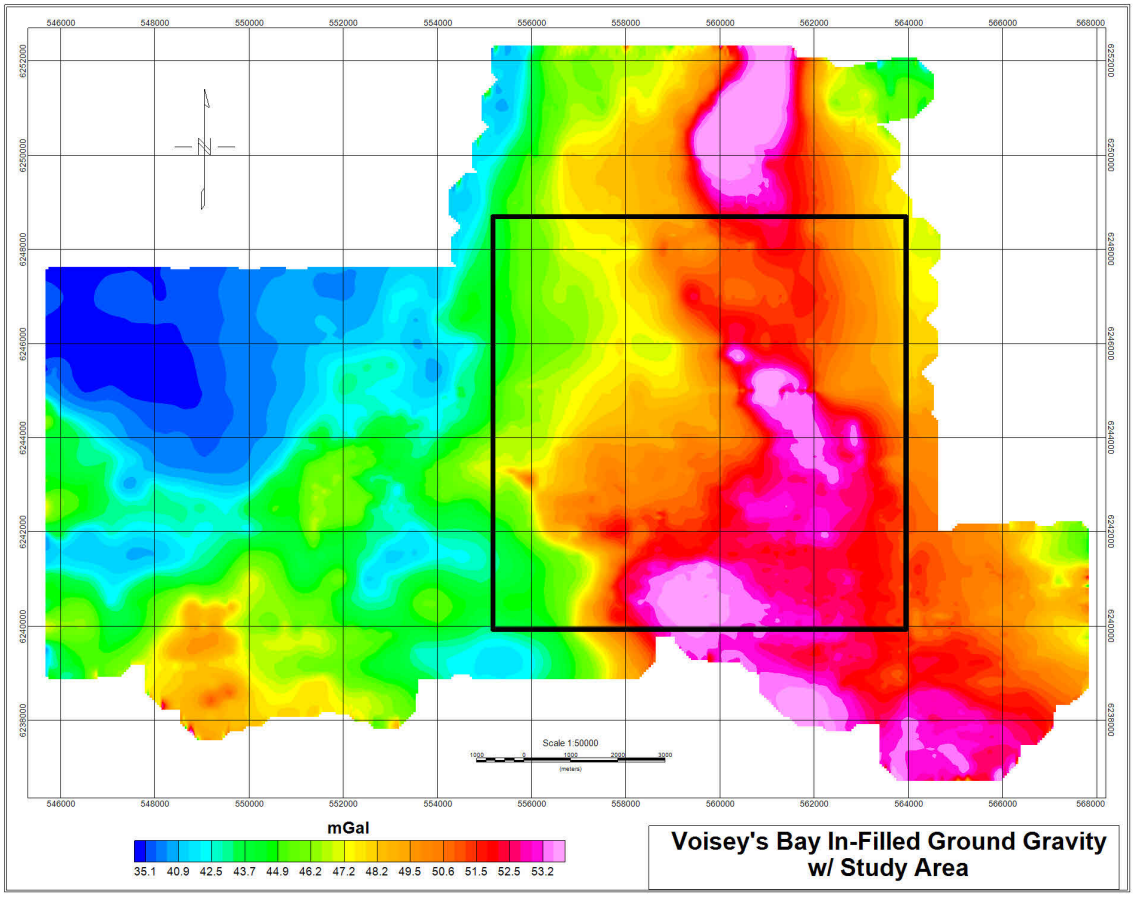

Figure 5.5: In-filled Ground Gravity Grid with an outline of the study area

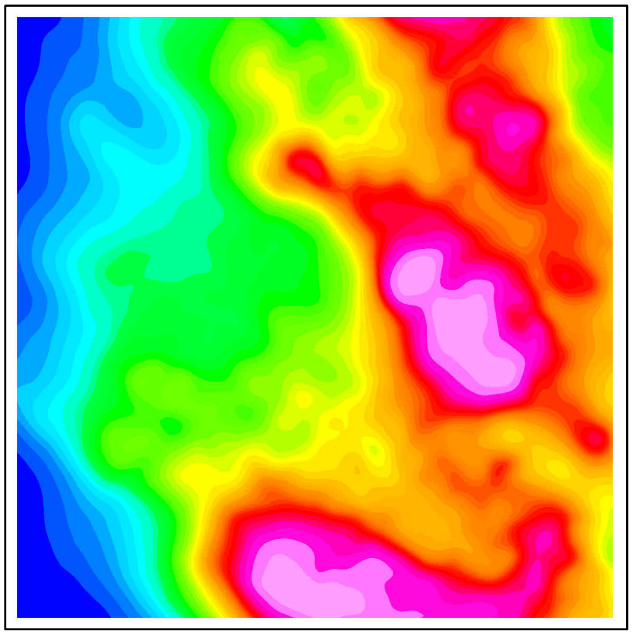

Figure 5.6a: Gravity grid masked to study area extents

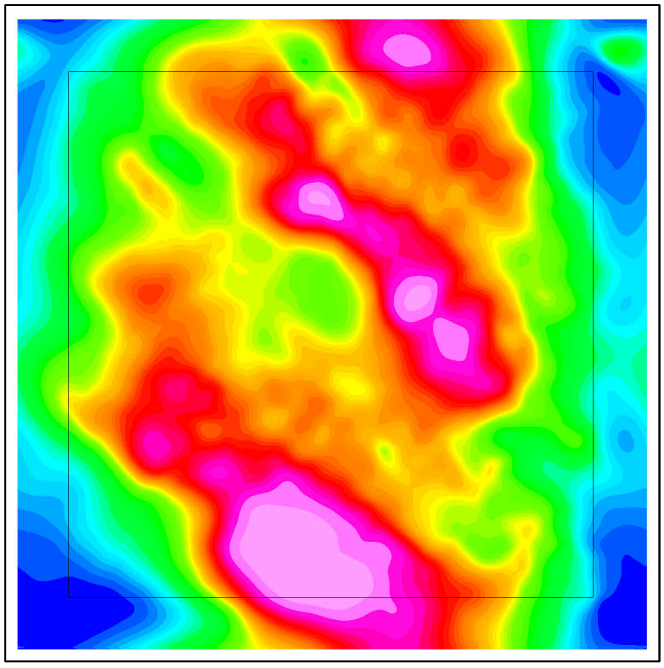

Figure 5.6b: Masked gravity grid extended by 10% using multi-step expansion

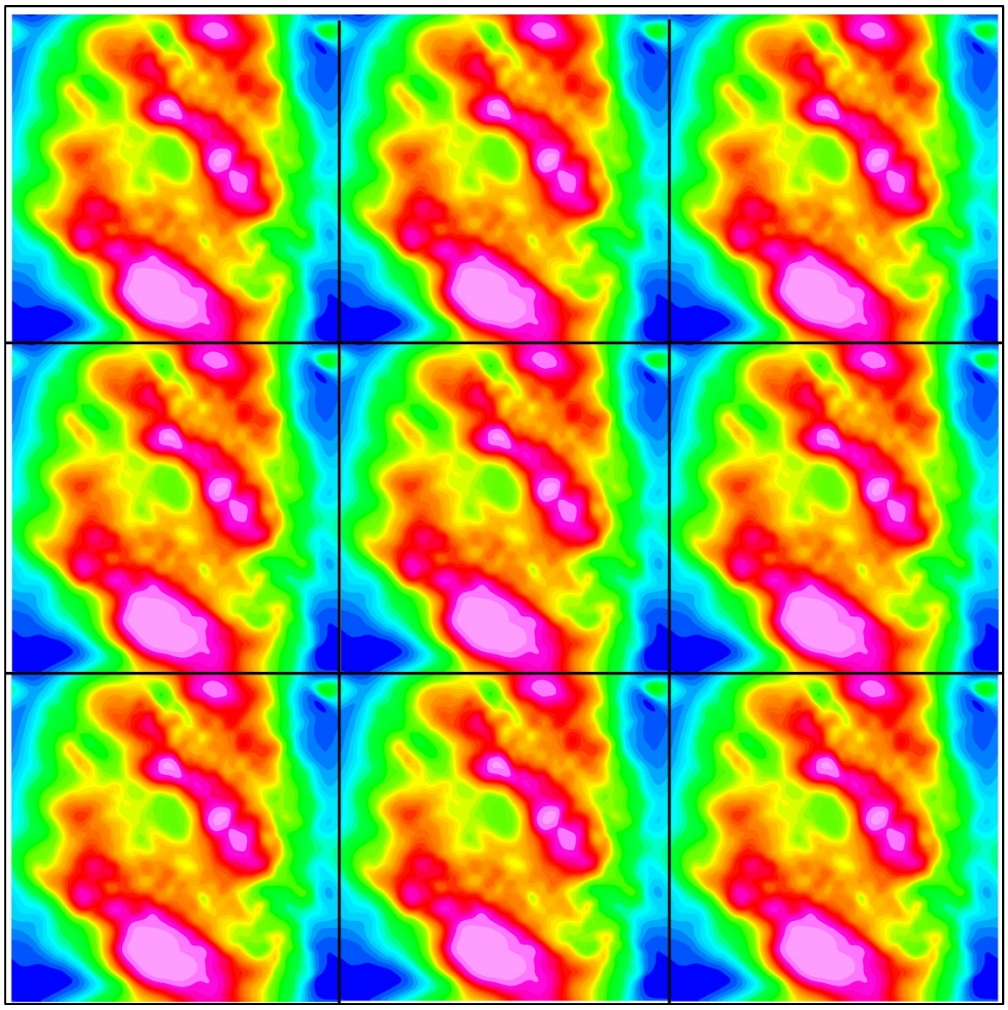

Figure 5.7: Conceptual array of gravity grids prepared for FFT processing.

smooth transition between E-W and N-S border data in which the least amount of foreign spectral character possible was added **(Figure 5.7)**, and were fully prepared for the FFT processing and further quantitative analysis**.**

5.4: 2D Power Spectral Analysis

The following analysis will be focused on three gravity grids: 1) the vertically integrated airborne AGG, 2) the ground gravity, and 3) the ground gravity upper-continued to 250m. The choice of examining these grids is for the dual purposes of comparing the spectral character of the AGG survey with the ground gravity survey in order to consider what information we could typically expect from these types of datasets in general, and comparing the resolution of the AGG sensor to what we could expect from the ground gravity sensor at a matching survey height.

Geophysical image data transformed to the frequency domain are commonly plotted as logarithmic 2D power spectra. This type of plot represents the amplitude of the different sine and cosine spectral components within an image as a function of their wavenumber, and is logarithmically plotted due to the large variation of amplitude within these components. The wavenumber, or spatial frequency, is the number of wavelengths over some unit of distance for a given periodic signal, and is analogous to frequency being the number of signal wavelengths for a given amount of time. A 2D power spectra plot features a zero wavenumber signal at its center and an increases wavenumber value in all directions out to the edges of the plot. Wavenumber is inversely proportional to wavelengths, meaning that wavelengths decrease

while moving away from the center of the 2D power spectra plot and frequency increases. The convention of plotting 2D power spectra within Oasis Montaj takes advantage of the natural symmetry in the Fourier Transforms of image data, in that only half a frequency range is needed to completely characterize the power spectrum. As a result only the right-hand portion of the 2D power spectrum is displayed, with the zero-wavenumber being represented at the center of the left-edge of the plot (Billings and Richards, 2010).

The 2D power spectrum of the ground gravity grid, shown in **Figure 5.8**, depicts the highest concentration of energy being located in the lower frequency ranges. This is not surprising as most potential field datasets are dominated by low frequency energy. The plot also provides a great deal of information on the spectral character of this grid. Aside from the low frequency signal, there is also a significant amount of energy persisting into the higher frequency ranges. One noteworthy feature is the much higher concentration of energy contained along the Y axis than the X. This is a reflection of the high concentration of spatial measurements being taken in the N-S direction (the vast majority of the data). There is also a concentration of power along the X axis corresponding to a wavenumber of 0.05, and therefore a wavelength of roughly 200m. This represents a high amount of variation in the E-W direction of the grid corresponding to the majority of the survey lines being spaced 200m apart. There is a gap in the power content along the x-axis between this feature and the Nyquist frequency of 100m, which contains another smaller concentration of energy. This second, more subtle, concentration appears to be building towards the Nyquist, and is due to the station spacing of 50m in the 4 long E-W lines included in the study area. Overall, the more complex character of this power spectrum is reflective of the irregular spatial sampling.

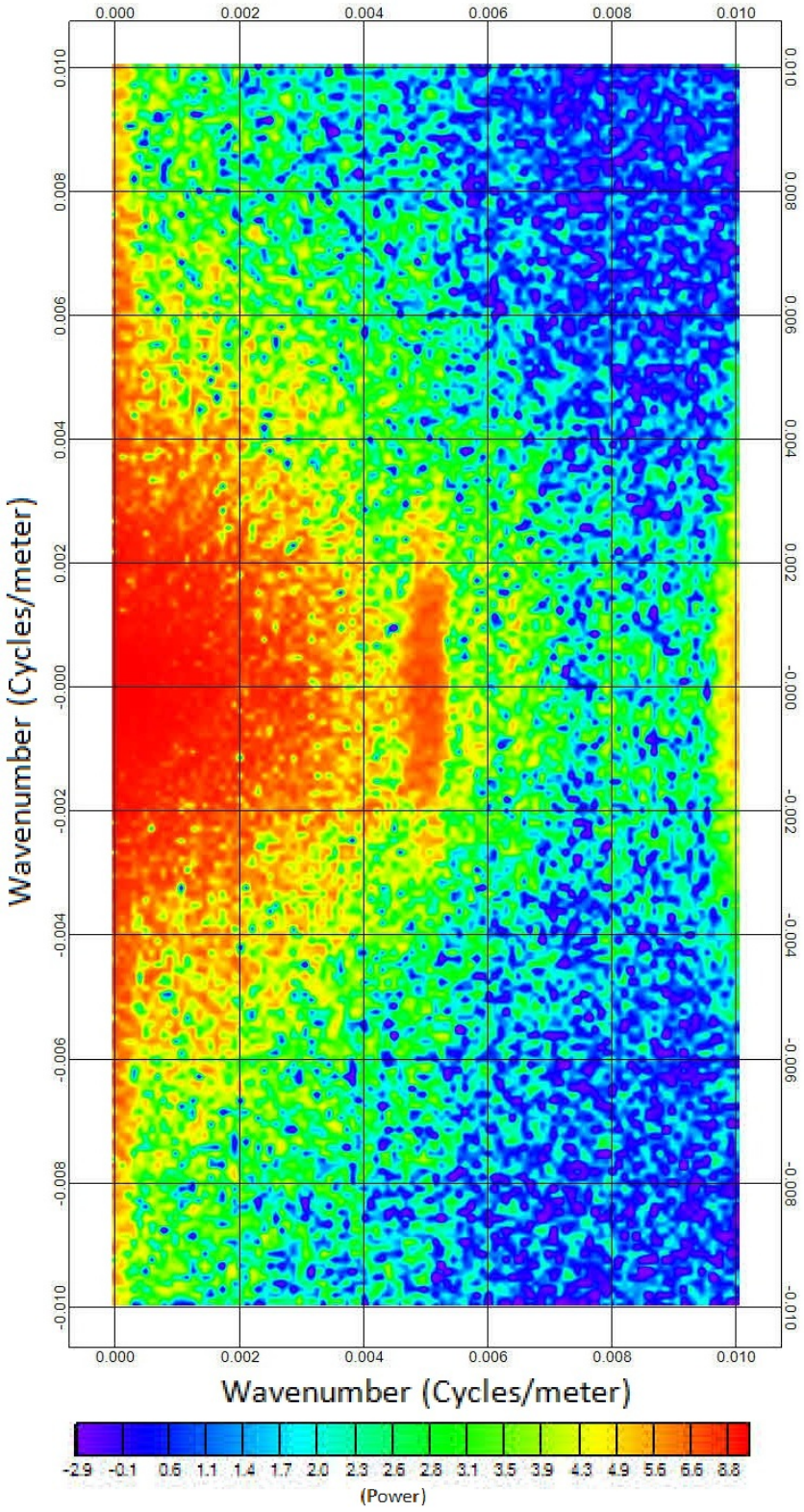

Figure 5.8: 2D Power Spectra of the ground gravity grid

Next, the 2D power spectrum of the upper-continued ground gravity is shown in **Figure 5.9**. Being that an upward continuation filter acts effectively as a smooth low-pass filter, it is of no surprise that the concentration of energy for this grid is in the low frequency range. Almost all of the non-uniform character shown in the unfiltered ground gravity grid has been removed along with its sensitivity to higher frequency content. The physics of the upward continuation filter is attempting to represent the same measurements of the ground gravity survey being taken 250m above the ground. At this distance above the ground only longer wavelength features may be observed and as a result the irregular spatial sampling ceases to be the dominant feature in defining the spectral characteristics of the data.

Finally, the 2D Power Spectrum plot of the vertically integrated AGG grid, as shown in **Figure 5.10**, has the typical concentration of energy in the lower frequencies but also moderate amounts of power located through the mid-frequency range and decreasing towards the Nyquist cut off frequency, which represents a 100m wavelength signal corresponding to the choice of a 50m cell size and is the highest frequency feature within this transform. Although it is not apparent in this plot, the AGG dataset has a lower-limit on its frequency detection capabilities as defined by the longest dimension of the survey area. This survey featured lines as long as 40km, which is the upper limit of wavelength detection for this AGG dataset. Another feature of interest in this plot is the roughly equivalent concentration of power along the Y and X axes which indicates similar variations in data in both the N-S and E-W directions. This is a sharp contrast to the ground gravity power spectra, which was strongly affected by the details of station and line spacing and direction. While this is likely partially due to an effective choice of cell size, it is also due to small variations in the spatial sampling having a less

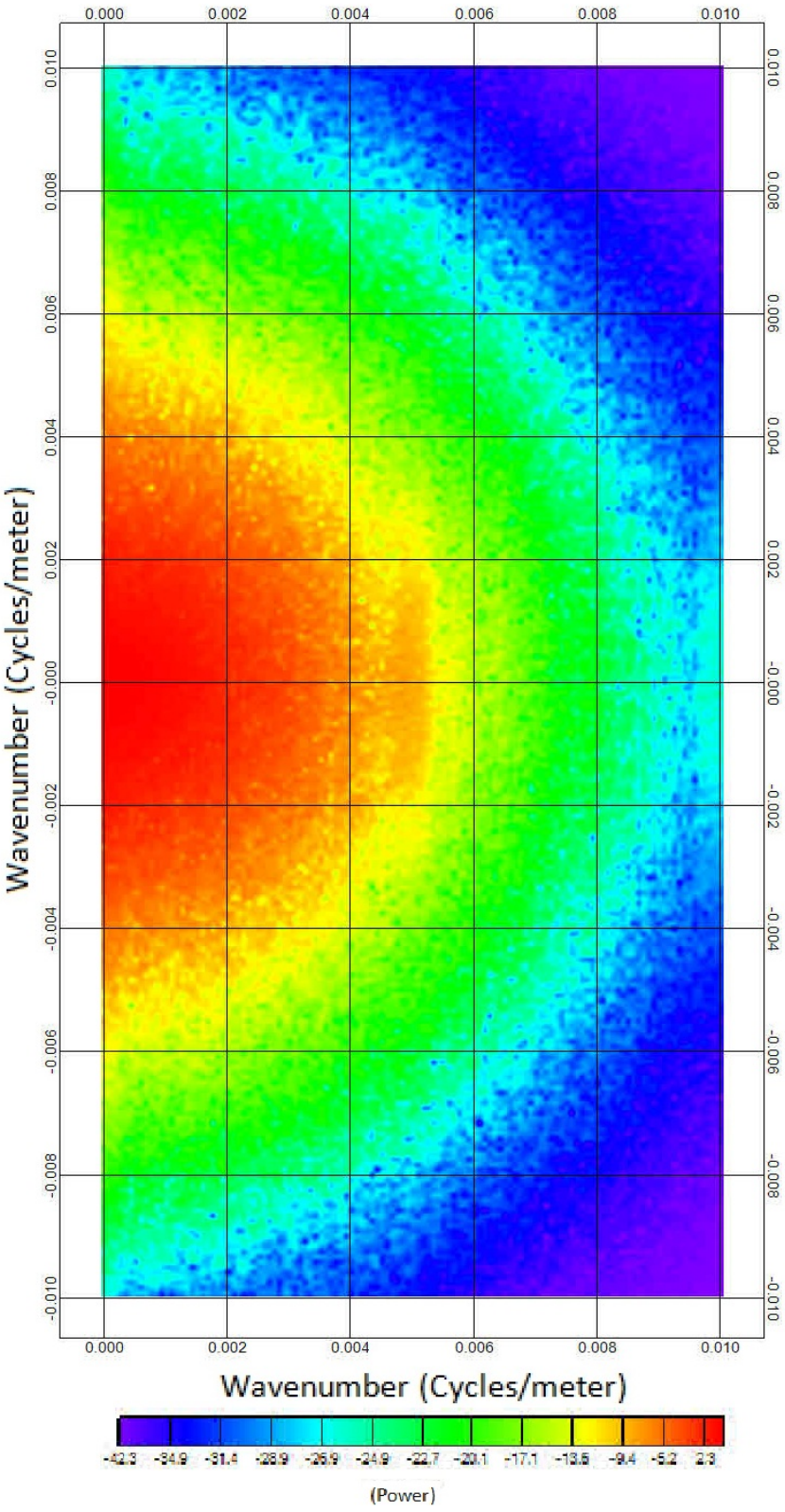

Figure 5.9: 2D Power Spectra of the upper-continued ground gravity grid

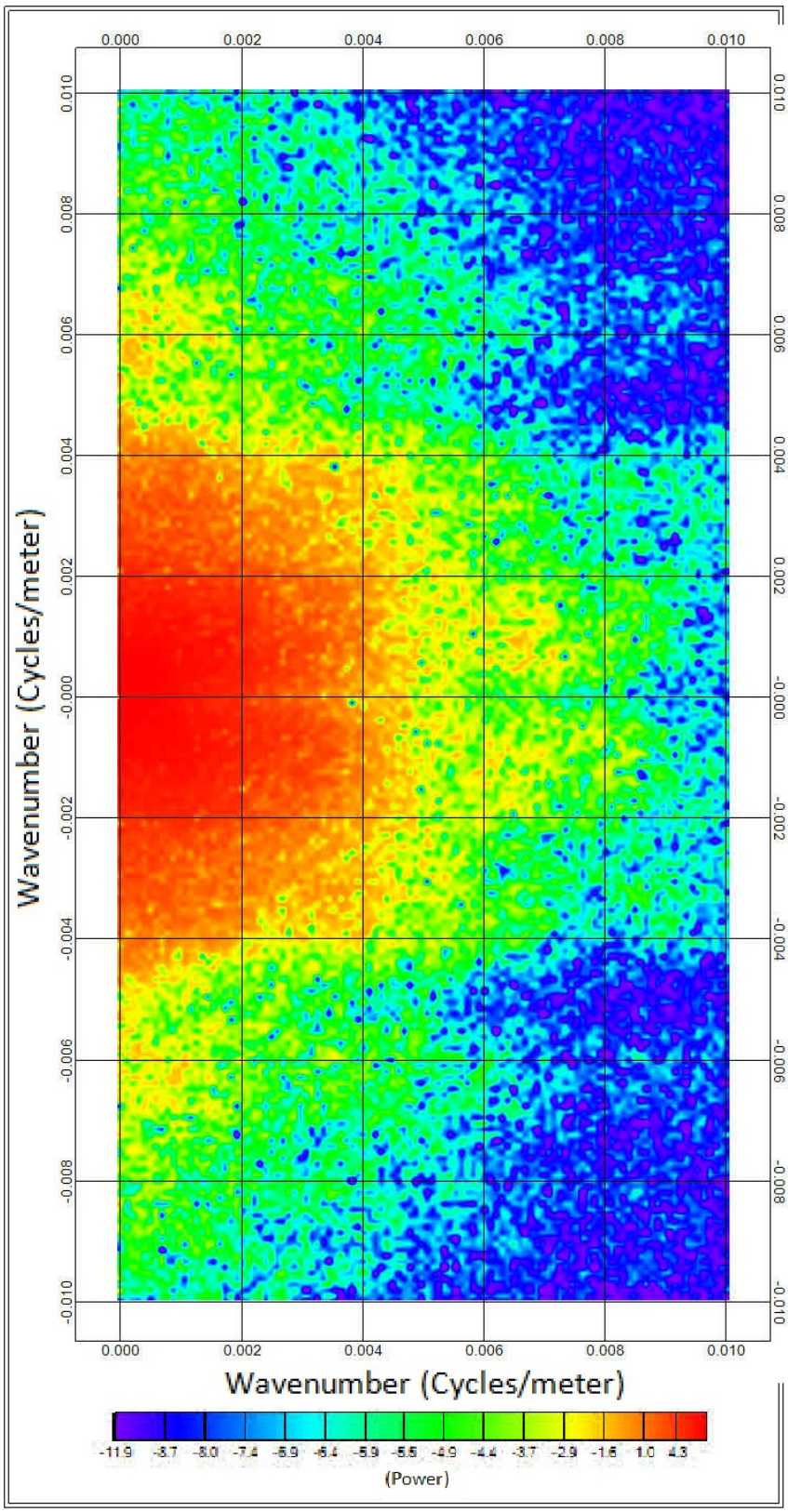

Figure 5.10: 2D Power Spectra of the vertically integrated AGG grid

dominant role in the definition of the spectral character of a survey when the measurements are made at a distance from the source.

Having completed a qualitative interpretation of each 2D power spectra, we can now perform a more quantitative comparison between them. **Figure 5.11** shows the 2D power spectra of all 3 grids plotted adjacent to one another and colored with the same color stretch so as to directly compare the signal amplitude contained within each dataset. The most striking, but not surprising, observation shown in this figure is the broad-band signal strength of both the AGG and upward-continued ground gravity grids are overshadowed by that of the ground gravity grid. The power of low frequency features (>500m) are equal across all three grids, but the power amplitude of the unfiltered ground gravity dataset decreases much slower in the mid to high frequency range than either of the other grids. Due to the nature of gravitational force, it increases in magnitude with proximity to the causative body. Being on the surface of the Earth while measuring a geological signal allows for a greatly stronger signal than that of a measurement taken 250m in the air, and therefore collecting high resolution information is made significantly easier.

Another interesting comparison can be made between the vertically integrated AGG and the upper-continued grids (shown in **Figure 5.12** with a common color scale). Because the non-uniform spatial sampling is playing a much smaller role in the spectral character of the upward-continued ground gravity grid, a comparison of sensor capabilities between the traditional ground gravimeter and the AGG system becomes much easier. Although in the previous comparison we saw that the amplitude of the AGG data decays much faster than the ground

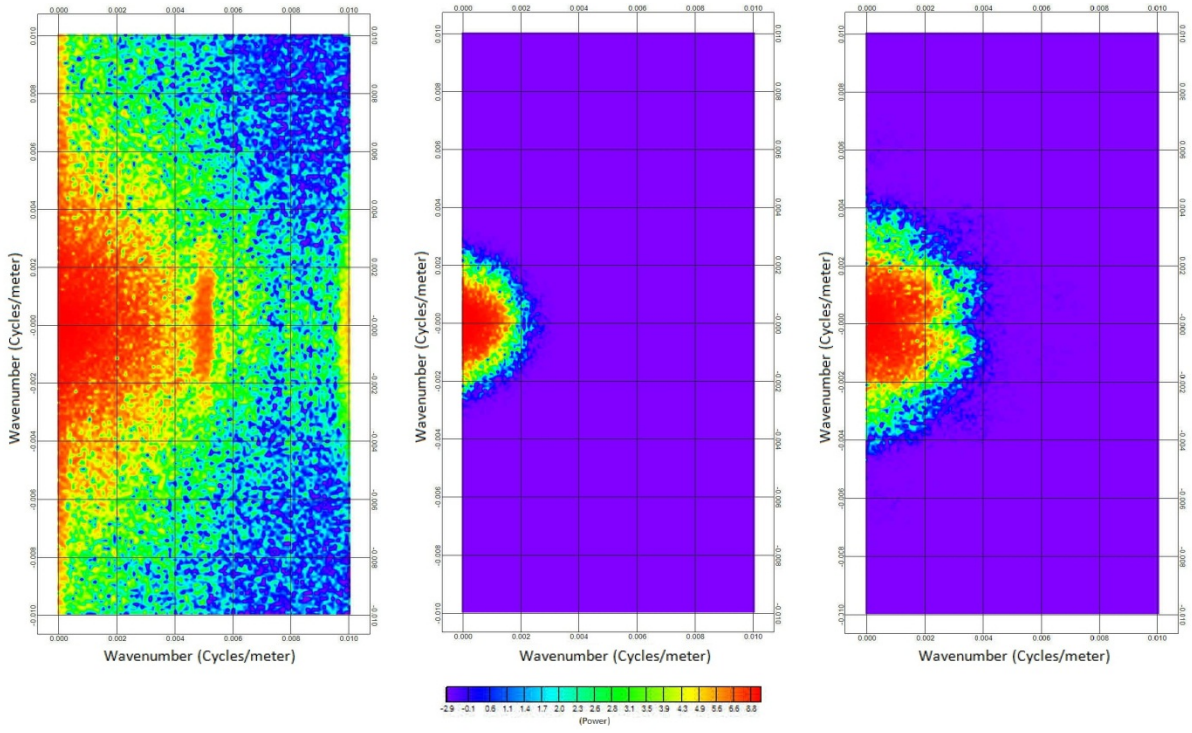

Figure 5.11: 2D Power Spectra for the ground gravity grid, upper continued ground gravity, and vertically integrated AGG grids, respectively from left to right and all colored with a common color scale.

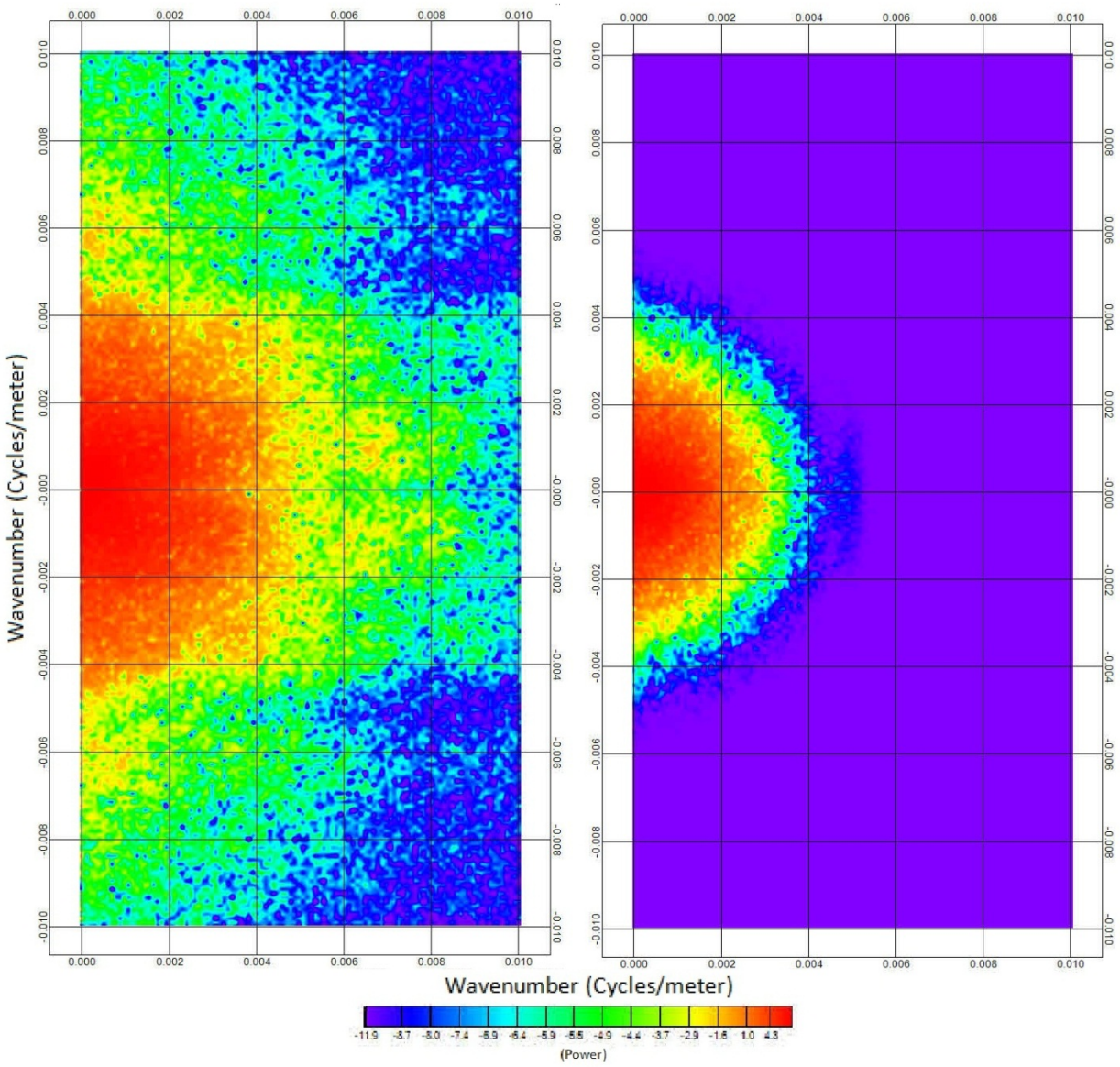

Figure 5.12: 2D Power Spectra of vertically integrated AGG and upper-continued ground gravity grids, respectively from left to right, and colored with a common scale.

gravity dataset with increasing frequency, this is not true of measurements taken from the same height with both sensors. The spectral power of the upward continued gravity decreases extremely rapidly as frequency increases in comparison to the AGG, and is extremely insensitive to features smaller than ~250m.

5.5: Radial Power Spectral Analysis

A second approach to plotting power spectrum data is to make use of a radially averaged power spectrum plot, which is the directional-independent mean spectrum, i.e. the average of all possible directional power spectra. This type of plot offers a convenient way to view and compare information contained in 2D spectra in 1D. This has a special significance when applied to a 2D geophysical grid in that we are able to consider the frequency content of a dataset in both the in-line, cross line, and all other directions at once. While considering the power spectra in each of these directions independently is very important, especially for considering the effect of spatial sampling, the radially averaged power spectrum plot allows us to consider the spectral content of the entire dataset as a whole.

Shown in **Figure 5.13** is the radially averaged power spectra data for all three grids. Similar to our observations using the 2D power spectrum plots, we see the highest concentration of energy in the lowest frequencies and a general decay of energy with increasing frequency in all three grids. Also similar to our previous observations, we see this decay happening fastest in the upper-continued ground gravity and slowest in the unfiltered ground gravity, with the vertically integrated AGG grid falling in between. The upper-continued

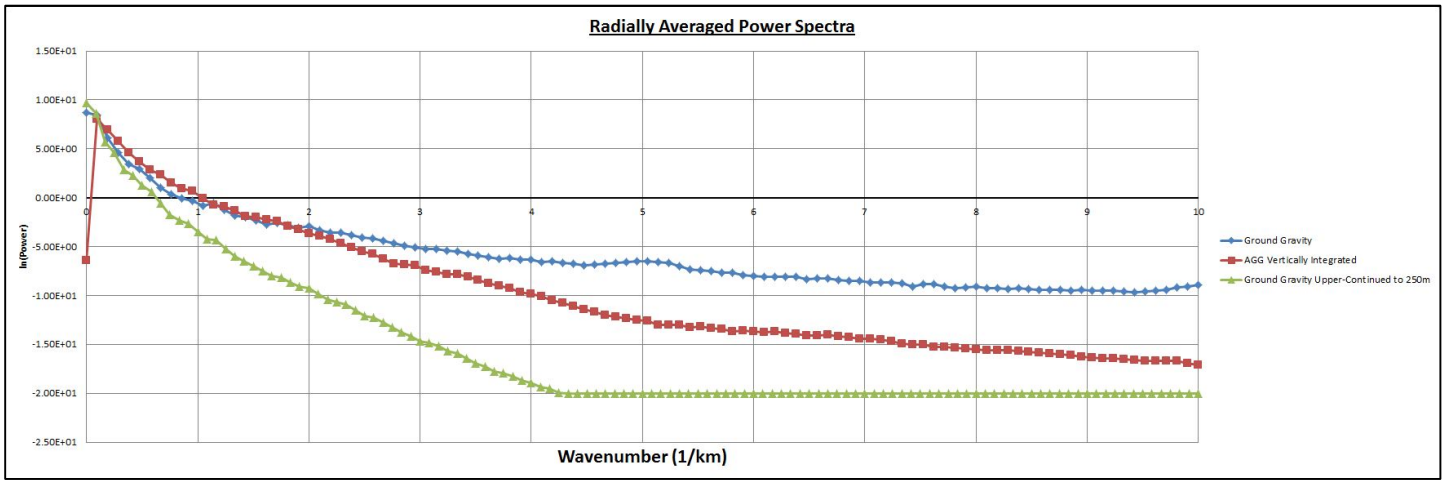

Figure 5.13: The Radially Averaged Power Spectra for all three grids

plot decays to its minimum value for wavelengths of approximately 250m and smaller, and then appears to maintain that same level of energy throughout the spectrum up until the Nyquist cut-off frequency. This seemingly lack of decay is an artifact of the upper-continuation filter, which only reduces the power to the limit of a miniscule value but not past it, whereas in real gravimeter data collected at 250m we would see a continued rapid decrease in signal strength with increasing frequencies. Another interesting feature which may appear to be an artifact upon first glance is that while the energy of the vertically integrated AGG builds as it moves to lower frequencies, it undergoes a sudden and dramatic decrease in power before the zero wavenumber limits. This is actually not an artifact, but a result of AGG data being limited in the longest wavelength signal by the dimensions of the survey grid, as previously noted.

For a closer analysis on the variances between the radially averaged power spectra of the three gravity grids in question it is possible to plot the differences between spectra. Shown in **Figure 5.14** is the difference in radial averaged spectra between the ground gravity grid and the vertically integrated AGG. The sharp decrease in the power of the AGG as it approaches a wavenumber of zero is a more obvious feature in this plot. Another feature of interest is that the radially averaged power of the AGG grid is actually greater than that of the ground gravity for wavelengths between 5km and 600m. This dominance of the AGG power for the high to mid-frequency range is strictly due to the superior spatial sampling of this survey. For wavelengths smaller than 600m the effect of the distance from the source begins to become a more dominant factor than the spatial sampling, and the power of the AGG decreases quickly in comparison to the power of the ground gravity. The trade-offs in resolution between both datasets are highlighted through this analysis. The lack of resolution in the AGG dataset is

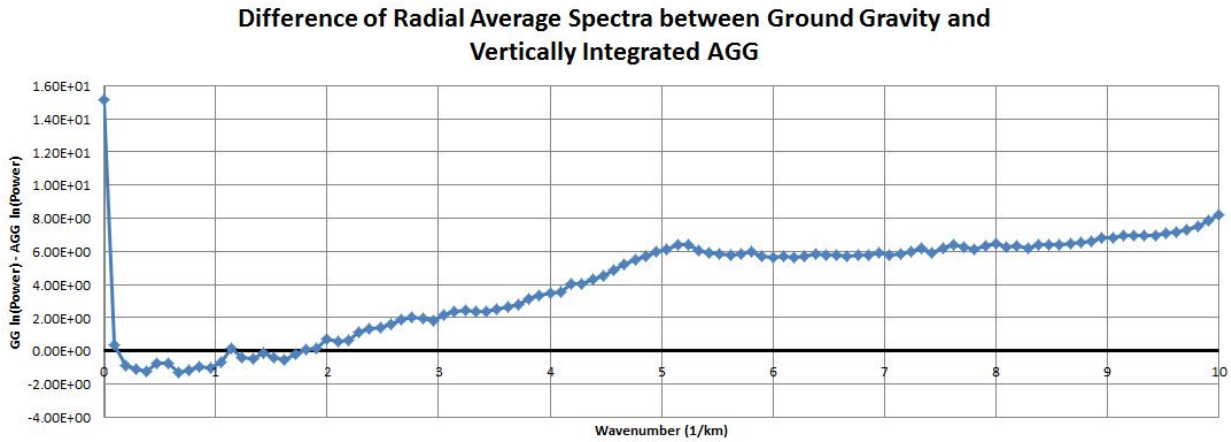

Figure 5.14: The Difference in Radially Averaged Power Spectra between the ground gravity and vertically integrated AGG

caused by the distance from the ground, which is an advantage of the ground gravity survey. On the other hand, the limitations on resolution in the ground gravity survey are caused by the variable and sometimes sparse data distribution, whereas the AGG survey's coverage is both complete and uniform. Ideal circumstances for both surveys would involve denser and regular sampling of the ground gravity data, and a lower flight height for the AGG survey (as originally planned), both of which could be expected to increase resolution in the respective surveys dramatically.

A difference plot between the radially averaged power spectra of the vertically integrated AGG and the upper-continued ground gravity is shown in **Figure 5.15**. The difference in power between the two datasets appears to increase up until a point and then begin to decrease. This apparent decrease is, once again, simply a function of the upward continuation filter bringing the power to a minimum value and not smaller. The most important observation in this plot is that it lacks the back and forth character of the previous difference plot. The AGG sensor is superior to the gravimeter sensor throughout the entire frequency spectrum, and increasingly so as the frequency rises.

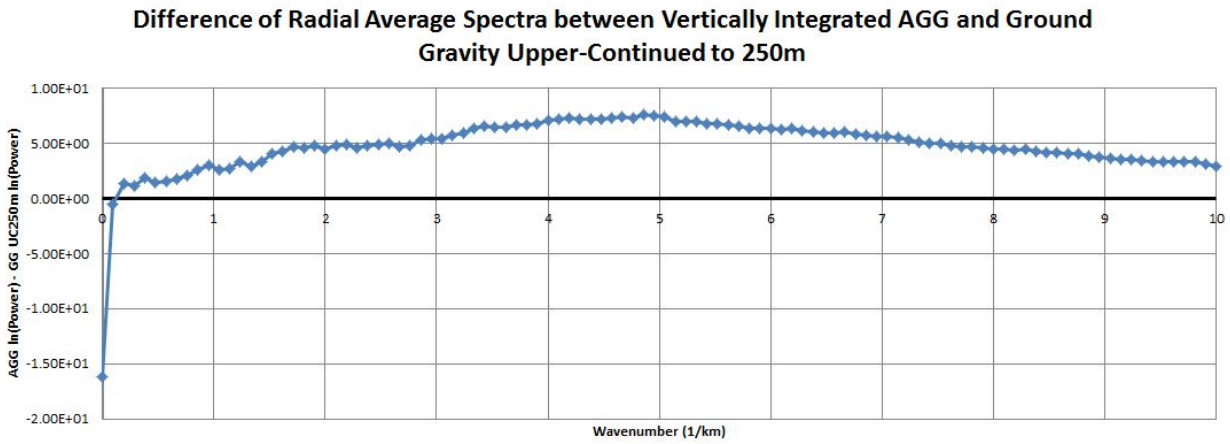

Figure 5.15: The Difference in Radially Averaged Power Spectra between the vertically integrated AGG and the upper-continued ground gravity

Chapter 6: Inversion

6.1: Introduction

In this chapter the AGG, ground gravity, and upward-continued ground gravity datasets will be compared in the context of their final interpretive results. The interpretation technique of choice in this case is geophysical inversion using software from the University of British Columbia's Geophysical Inversion Facility (UBC-GIF). Inversion theory and methodology will be discussed in terms of the components of the model objective function, the optimization of the inversion solution, and the discretization of the Earth. Final inversion results for all three datasets are shown and discussed.

6.2: Inversion Theory

Thus far we have considered the theory, acquisition, and processing of airborne gravity gradiometry (AGG), as well as how this technique can fill an important role in nickel exploration by attempting to delineate hidden troctolite chambers in the area surrounding Voisey's Bay, Labrador. In order to evaluate the quality and content of the gravity dataset produced from the AGG survey, we compared its spectral and spatial character to that of a traditional ground gravity survey in the same area, as well as that of an upward continued version of the ground gravity dataset. In the context of mineral exploration, however, the ultimate measure of effectiveness for any geophysical dataset is whether that data has the potential to impact our

understanding of the geological environment and advance the exploration program closer to a discovery. The link between collecting geophysical measurements and relating that information to the subsurface in a meaningful way is the key process of interpretation, and in this section we will explore how all of the factors previously discussed can impact our final density model and affect the outcome of the interpretation.

Potential field datasets are amongst the most commonly used in exploration due to the fact that they are logistically easier and cheaper to collect than many other surveys, and are useful in the exploration of many different commodities. These are commonly found on both regional scales, often collected by governments to encourage resource exploration, and project scales, to better outline specific prospects. Depending on the level of analysis of a potential field dataset and the nature of the study, the interpretation of the data may either involve a qualitative approach of inferring information about geology by examining 2D maps or may involve a more quantitative method of using the data to derive physical property model. Traditionally 2D or 3D forward modeling was used to calculate the response of some physical property model in an attempt to identify discrepancies between inferred geological scenarios and the geology required to reproduce the observed data. Over the course of the past two decades computing power has advanced to the point of being capable of handling the forward modeling of very large 3D geophysical datasets. In addition, methods have been developed to calculate inverse solutions that predict physical property distributions that give rise to observed geophysical responses (Williams, 2006). These methods are referred to as geophysical inversion, and were the interpretive method of choice in this study.

6.3: Misfit and Errors

An obvious goal of any inversion model is to produce a solution which is not just geologically reasonable, but also mathematically reasonable in the sense of reproducing the response of the observed geophysical data to within a limit. This capability is introduced to the inversion through the use of the "data misfit", which provides a measure of how closely the predicted response of the recovered inversion matches the observed to geophysical response in the field data, and is given by the function:

$$\varphi_d = ||W_d(\mathbf{Gm}-d^{obs})||^2$$

$$W_d = \mathbf{diag}(\frac{1}{\sigma_i}) \qquad \text{(Williams, 2006)}$$

where Gm is the predicted response of the recovered model and σ_i is the standard deviation associated with the *i*th data point (Williams, 2006).

Due to the nature of geophysical measurements we know that our data will always contain some level of inevitable noise, and for this reason it is important that the inversion does not attempt to match the observed data exactly. Instead the inversion attempts to match the observed results only to a degree of accuracy that is consistent with the errors in the observations, making our assignment of an appropriate level of noise a critical factor in the inversion. Should the assigned noise levels be too high then an excessive amount of the observed data will be disregarded and information will be lost in the model. If the defined noise levels are too low then our final inversion model will attempt to create a density

distribution model that not only reproduces the observed data but also the noise signal as well. If the source of noise in our data is truly random, then it will follow a Gaussian distribution and the misfit can be expected to have a value of N, equal to the number of data.

The error involved in the measurements of an Airborne Gravity Gradiometry system is frequency dependent. For the Voisey's Bay survey, Bell Geospace's FTG system had an estimated accuracy of ~10 Eotvos (or roughly 0.001 mGal) for shallow features of 300m or less. Because the dynamic range of the vertically integrated Tzz data is approximately 10mGals, this is equivalent to a 0.0001% noise level. Additional noise may have been introduced through GPS positioning errors and the terrain correction using the CDED DEM.

The noise estimate of a historical ground gravity dataset, however, is considerably harder to derive. The Voisey's Bay ground gravity dataset was collected in the mid-90's with a Lacoste-Romberg gravimeter, and the terrain correction applied was using the traditional method of estimating the surrounding landscape with inclinometers. One best-practice recommendation included in (Williams, 2006) is that most ground gravity datasets standard deviation will commonly fall within the 1-2% range. Upward-continued datasets, however, will have a naturally lower dynamic range, and should have correspondingly lower standard deviations applied. Correspondingly, errors of 1% and 0.1% were chosen for the ground gravity and upward-continued inversions, respectively.

6.4: The Model Norm

Inversion is a mathematical procedure that involves estimating the geophysical response of an initial model, evaluating the validity of the model by using misfit and acceptability criteria, and then iteratively adjusting the model parameters until the some predefined criteria are satisfied. Once the criteria have been sufficiently mathematically satisfied, a final inversion model is produced and is subsequently evaluated by the operator to determine whether or not it is a geologically feasible solution. The inversion software used in this study is the GRAV3D program created by the University of British Columbia Geophysical Inversion Facility.

A primary difficulty in the inversion and interpretation of potential field data is its inherently non-unique nature. This non-uniqueness originates from two sources, the first of which is that any potential field measured from the surface of the Earth, and thereby restricted to a single bounding surface, can be reproduced by an infinite amount of different equivalent source distributions, according to Gauss' theorem. These endless possible source distributions include even the geologically unrealistic case of a single thin layer directly beneath the surface of the Earth, meaning that potential field data contains no inherent depth information (Li and Oldenburg, 1996). The second source of non-uniqueness is that any measured geophysical dataset will include a finite number of measurements which can, even in the absence of noise related error, be reproduced in an infinite number of ways with equal accuracy (Li and Oldenburg, 1996).

To attempt to deal with the problem of non-uniqueness, the UBC-GIF method of geophysical inversion attempts to quantify the infinite number of models that could reproduce the observed geophysical data by two adjusting two basic attributes: "smallness" (the difference between the reference and recovered models) and "smoothness" (a measure of how the difference between the reference and recovered models vary between calls in each of three orthogonal directions) (Williams, 2006). The purpose in using these features as a means of guiding the inversion process is to push the inversion in the most geologically realistic direction possible: the simplest or most compact solution that can explain all given observations. The reference model may vary between a carefully built model that includes prior geological information or a uniform half-space with a zero value. This model quantification is completed through the use of the model norm, which is represented by the model objective function:

$$\varphi_m(m) = \alpha_s \int_V w_s [w_r(z)(m-m_{ref})]^2 \, dV + \ldots$$
$$\alpha_x \int_V w_x [\frac{\partial}{\partial x} w_r(z)(m-m_{ref})]^2 \, dV + \ldots$$
$$\alpha_y \int_V w_y [\frac{\partial}{\partial y} w_r(z)(m-m_{ref})]^2 \, dV + \ldots \quad \text{(Li and Oldenberg, 1996)}$$
$$\alpha_z \int_V w_z [\frac{\partial}{\partial z} w_r(z)(m-m_{ref})]^2 \, dV$$

The initial component in this function measures the "smallness", while the last three components measure the "smoothness" of the difference between the initial and recovered models in the x, y, and z directions. The alpha terms α_s, α_x, α_y, and α_z are user-defined terms which determine the influence of each component in determining the geologically realistic

geometric bias that the final recovered model will attempt to fulfill. Each inversion in this study makes use of equal default alpha terms of 1, as there is no directional preference in our desired model or geophysical dataset.

Another very important term within the model objective function is $\mathbf{w_r}$, which represents the depth weighting (Williams, 2006). Due to the fact that potential field data contains no inherent depth information, inversion calculations tend to concentrate solutions near the surface of the model regardless of the true depth of the causative bodies. This is a result of the inversion code kernels attempting to imitate physical forces which become rapidly weaker with distance from the source ($\frac{1}{r^2}$for gravity and $\frac{1}{r^3}$in the case of magnetics). In order to compensate for this effect, a depth weighting function is utilized that attempts to counteract the decaying response of potential fields with distance and thereby normalize the probability of a solution at depth to one at shallow depths. The definition of the depth weighting function is given by:

$$\boldsymbol{w_r^2(z)} = \frac{1}{(z+z_0)^{\beta}} \text{ (Williams, 2006)}$$

Here z is the depth to the center of the cell and z_0 and β are adjustable parameters used to match the weighting function to the kernel's decay with depth. If the distance between a cell and observation point is large relative to the dimensions of the cell, as will be the case for most cells in the model, then β will approach the exponential decay of the gravity or magnetic response of a sphere: β = 2 for gravity data and β = 3 for magnetic data. The parameter z_0 is usually calculated automatically to match the kernel's decay (Williams, 2006).

6.5: Optimization

Having considered the inverse problem in terms of its two primary criteria, the model objective function ($\boldsymbol{\varphi_m}$) and the data misfit ($\boldsymbol{\varphi_d}$), it is now possible to clearly state the goal of the inversion is to find the model (m) that minimizes the model norm while also produces an acceptably small misfit. This statement provides the context to reconsider the inverse problem as a simple mathematical single optimization. A suitable recovered inversion model can be derived by minimizing:

$$\boldsymbol{\varphi} = \boldsymbol{\varphi_d} + \boldsymbol{\beta}\boldsymbol{\varphi_m} \qquad \text{(Williams, 2006)}$$

The term $\boldsymbol{\beta}$ **in this equation** is called the regularization parameter or Tikhonov parameter. It is a user-defined parameter which specifies the emphasis of data misfit versus the model objective function. The value of $\boldsymbol{\beta}$ is not known at the start of an inversion, but it is instead sought so that when the optimization objective function has been minimized, the final recovered model will have a misfit that is equal to or less than some predetermined error tolerance.

Obviously, the choice of $\boldsymbol{\beta}$ is a key aspect in guiding the mathematical constraints of an inversion and defining what type of solution is ultimately required. The range of possible $\boldsymbol{\beta}$ values and how they each may impact an inversion could conceptually be considered by carrying out the minimization of our objective function for a range of $\boldsymbol{\beta}$ values and then plotting the results. This type of plot is referred to as a Tikhonov curve, as shown in **Figure 6.1**.

Referring to this figure, we can see how as $\boldsymbol{\beta}$ values get very small, the objective function is heavily favored over the misfit. The result of such an inversion would be a recovered model whose predicted response looks more like the observed geophysical response, including the noise. The model norm would also be significantly larger in this case, resulting in a model that is much more complicated and contains excess erroneous structure which is likely related to creating a solution to account for the response of the noise in the data. On the other hand, in the scenario where $\boldsymbol{\beta}$ is much larger than is optimal results in much larger values of misfit. The predicted response of the final recovered model will look much less like the observed data, and the model will be much simpler due to low model norm values. This is, in effect, creating a model that doesn't just ignore noise that exists in the data, but also a significant amount of the data itself. An optimal $\boldsymbol{\beta}$ will guide the inversion towards a solution that does not contain artifacts through over-fitting for noise in the data, but does include as much detail as reasonably possible from the observed data. Although there are several different methods commonly used to determine the value of $\boldsymbol{\beta}$, this study makes use of the Chifact determination method (UBC-GIF website, 2005).

The Chifact method relies upon the assumption that noise and error within the geophysical dataset are random, and therefore behave according to a Gaussian distribution. If this assumption is correct, the misfit, $\boldsymbol{\varphi_d}$, will roughly equate to the number of data points, N. With this in mind, it is possible to try a range of $\boldsymbol{\beta}$ values within the inversion and then select the resulting model that used a $\boldsymbol{\beta}$ value yielding $\boldsymbol{\varphi_d}$ **= N.** To allow for greater control over the

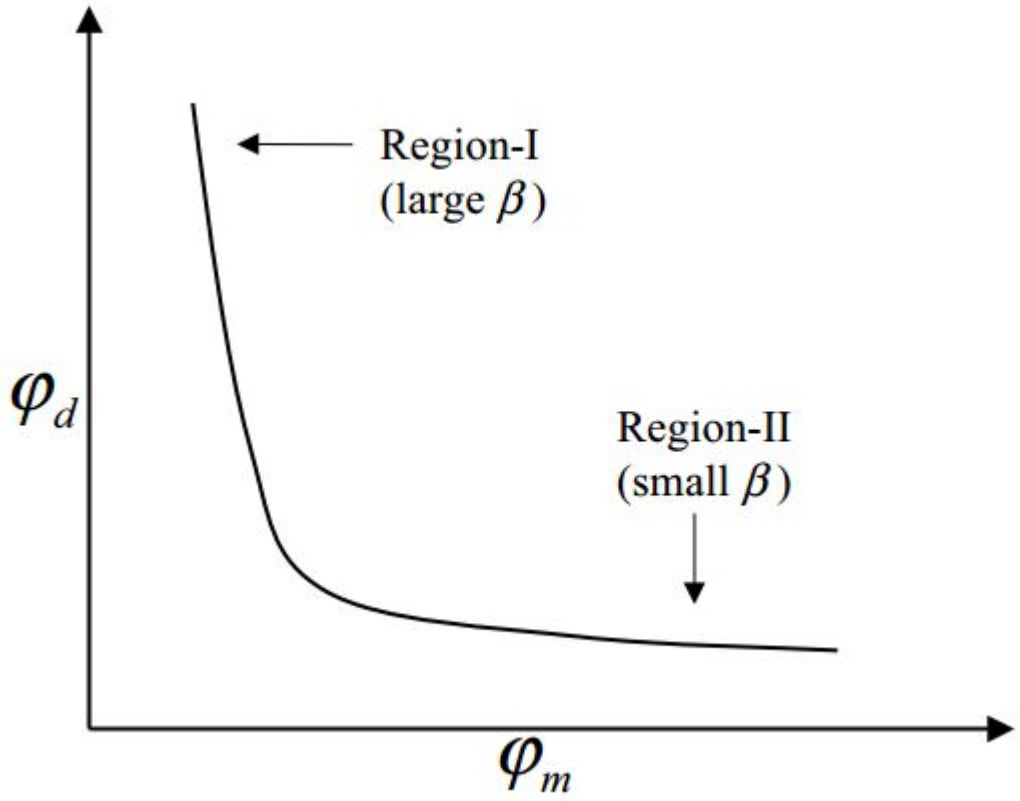

Figure 6.1: A Tikhonov curve representing the range of solutions with varying β values. Region-I represents an area of a larger than optimal β value in which model solutions would be much smoother and would look less like the observed geophysical data. Region-II represents an area of a smaller than optimal β value in which model solutions would contain excessive structure and would attempt to recreate the response of noise in the data. (Oldenburg and Li, 2005).

inversion results, it is even more useful for the user to be able to manipulate how closely the predicted data must match the measured observations. For this purpose $\boldsymbol{\varphi_d}$ **= Chifact x N** is used instead, where Chifact is a user-defined parameter. The use of Chifact allows for misfit adjustments that coincide with prior knowledge of noise and errors, or other factors that may result in a need for the misfit to be greater than N.

6.6: Discretization

Although the physical property distribution within the Earth is continuous, to quantitatively model the response of the Earth we must be able to represent it in terms of a finite mathematical geometry. In order to do this, we simplify the subsurface by discretizing it into 3D rectangular cells called voxels, which each contains uniform physical properties. The choice of voxel size should be dependent on the resolution of the survey in question. In this case, bearing in mind the resolution of each dataset previously discussed, the choice of cell size for the input grids, and the required resolution to image gravity responses which may be related to troctolite chambers, a voxel size of 100x100m was chosen for the x and y directions and a constant size of 50m was chosen for the z direction.

Because computing resources are not infinite, a maximum depth extent must also be defined for the discretized volume. In the case of potential fields, extremely long wavelength features may originate from sources very deep within the earth. For the purposes of mineral exploration and this study, however, the area of focus is limited to the top 2km. In order to account for longer wavelength features from regional sources, extra "padding" voxels are

added to the model in all direction. These voxels become increasingly larger in size in the x, y, and z directions with distance away from the main inversion mesh due to the fact that their contributions will only a very course effect on the modeled response and also to make the overall calculation less computationally intensive. A general rule of thumb for the use of padding distance is that it should be at least twice the depth extent. As a result a padding distance of 4km was chosen for the inversions in this study.

One important feature in the creation of the mesh model in a UBC-GIF inversion is the capability to include *a priori* information within the mesh design. This type of information can include information such as a physical property distribution as dictated by geology observed through surface mapping or drilling. Although there is a great deal of surface mapping and drill-hole information in Voisey's Bay, no geological constraints were used in the inversions reported in this study. One justification for this is that the technique of airborne gravity gradiometry was, in this case, being used and evaluated to potentially locate nickel-bearing troctolite chambers that were hidden under overburden or sheets of granite with variable thickness. We are attempting to replicate a greenfields exploration approach. Although the inclusion of a thin layer of physical properties representing a green-fields-level of mapped geology at the surface of our voxel model would not preclude solutions of anomalously dense rock underneath these features, it also wouldn't likely affect the final models in a way that is meaningful to the resolution of interest for this study.

In the absence of geological constraints, there are still further mathematical constraints that may be taken advantage of. The output of the UBC-GIF Grav3D Inversion program is a 3D

model mesh of relative density, meaning the model represents density contrasts rather than absolute densities. The initial input mesh model is a zero value half-space, masked to the known topography. It is possible to mathematically constrain the output values by "bounding" the possible output density contrasts to a user-defined limit in order to best represent known densities in the study area. Although the vast majority of rock types in the Voisey's Bay area fall in between 2.6-2.9 g/cc, the massive sulphide bodies commonly have densities of 4.0 g/cc. Although the abundance of massive sulphide is very limited in comparison to other lithologies, it is very common to have a mixture of a varying amount of sulphides within the troctolite bodies, creating a corresponding mixed range of possible density values. As a result, a range of 1.5 g/cc was used as a bounding limit to the inversions in this study.

6.7: Inversion Results and Discussion

Using the inversion parameters discussed above, inversions were completed for the study area discussed in chapter 5 (**Figure 5.4**) on the grids of the ground gravity, the upward-continued ground gravity, and the vertically integrated Tzz component of the airborne gravity gradiometry. While all the final recovered models from these inversions identified the major density trends that relate to the main concentrations of troctolite in the study area, each model also varied greatly in terms of resolution, structure, and geometry.

As discussed, the output of the UBC-GIF Grav3D inversion code is in the format of a 3D mesh of rectangular cells which are each assigned with values of subsurface density contrast meant to represent the distribution of physical properties within the Earth. The density contrast values were somewhat varied among the recovered inversion models; however the bulk of the models all fell within roughly the same range. As a result, and for ease of comparison, all inversion figures referred to in the following discussion were colored with a common color scale (**Figure 6.2)**.

The final inversion results for the ground gravity are shown in **Figure 6.3**. As previously discussed, an error of 0.1 mGal was used as an initial parameter for this inversion. The initial misfit of the model response to that of the data was 4.68E+05, which was reduced to a misfit of 7.66E+03 after 8 inversion iterations. As a general rule of thumb for potential field inversions, the data misfit should be reduced by at least a couple of orders of magnitude by the final recovered model, which is the case in this inversion. Referring to **Figure 6.3** we can examine the final model results. In **6.3a**, an elevation slice of the model at sea-level is shown (because the topography varies between 0 and 500m in this area, this is the highest elevation at which we can see a slice through the entire model). Immediately the main gravity trends of the Eastern Deeps, Gomer, and the southern extent of Mushua captured by our study (as identified by **Figure 5.4,** area easily recognizable. In **6.3b** the voxel model has been filtered to values of 0.07 g/cc and higher, leaving us with the highest density contrasts in the study area. Imposed upon this is a semi-transparent image of the Voisey's Bay surface geology. The Gomer gravity trend matches up extremely well, contains a high level of detail, and the majority of the density being coincident or to the immediate east of the mapped troctolite (due to the eastern dip of

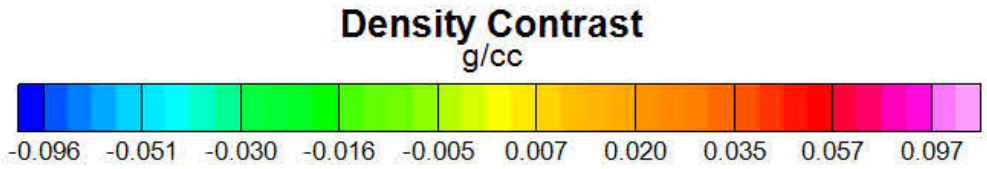

Figure 6.2: Color stretch used in describing all following gravity inversion results in this chapter. The UBC-GIF Grav3D code outputs inversion results in terms of density contrasts rather than absolute densities, and is measured in units of g/cc.

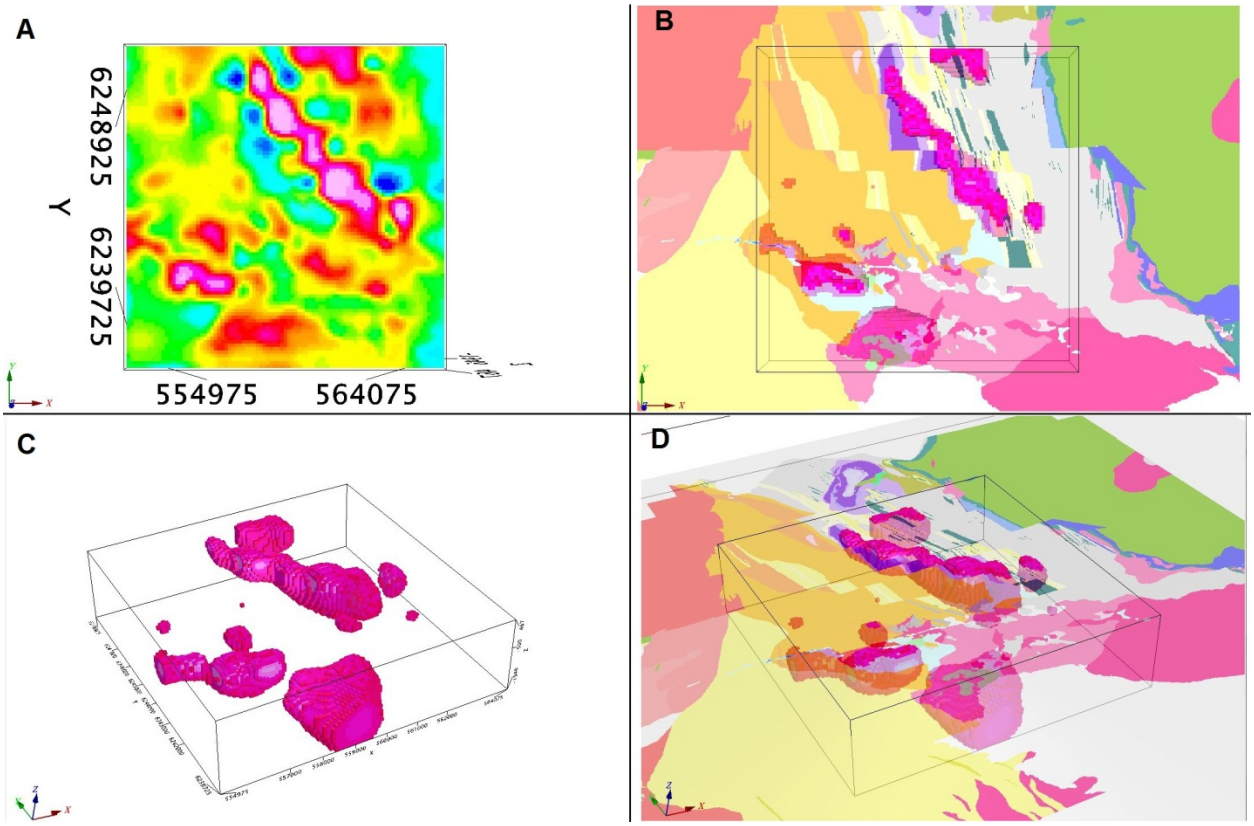

Figure 6.3: Ground Gravity 3D Inversion (A)plan view of 3D model at 0m elevation, (B)plan view of 3D model density contrast values > 0.07 g/cc overlain on semi-transparent geology map, (C) angled and northeast-facing view of 3D model density contrast values > 0.07 g/cc, and (D) angled and northeast-facing view of 3D model density contrast values > 0.07 g/cc overlain on semi-transparent geology map.

this unit). There is a high density contrast associated with the deepest portion of the Eastern Deeps Chamber (which is also the location of all Eastern Deeps massive sulphides) that leads to a thin and highly detailed density trend that follows the Voisey's Bay main mineralized trend west through the Ovoid and into the Reid Brook area. There is an even stronger and larger density body to the immediate south and east of the Eastern Deeps chamber, which correlates to the continuation of the troctolite body at depth. This, as well as the other inversion features, can be further visualized by examining **6.3c** and **6.3d**, which include angled views of the filtered voxel model and reference to the geology surface map. Although the troctolite crosses the Red Dog fault at this location (hence the large offset to the east), there is no evidence of an actual physical separation from the Eastern Deeps chamber in drill results. The Mushua gravity trend is not fully represented in the chosen study area, but there appears to be some density representing the response of the Mushua intrusion at depth here.

Although with some experience it is possible to gauge the performance of an inversion by visually examining the final model, another method of evaluation lies in the behavior of the model norm and data misfit values during the iterative inversion process. It is possible to plot these two values against one another to create a Tikhonov curve, as shown for this inversion in **Figure 6.4**. This figure represents an incomplete Tikhonov curve that includes data on only the range of solutions our Chifact method covered in this particular inversion, as such it is difficult to quantitatively gauge where our final $\boldsymbol{\beta}$ value lies on the complete spectrum of possible solution. That being said, the fact that the $\boldsymbol{\beta}$ for our final solution occurs after the inflection point of the Tikhonov curve, and does not seem to have excessively large model norm values (and therefore needless structure) is encouraging. The expected behavior for the data misfit

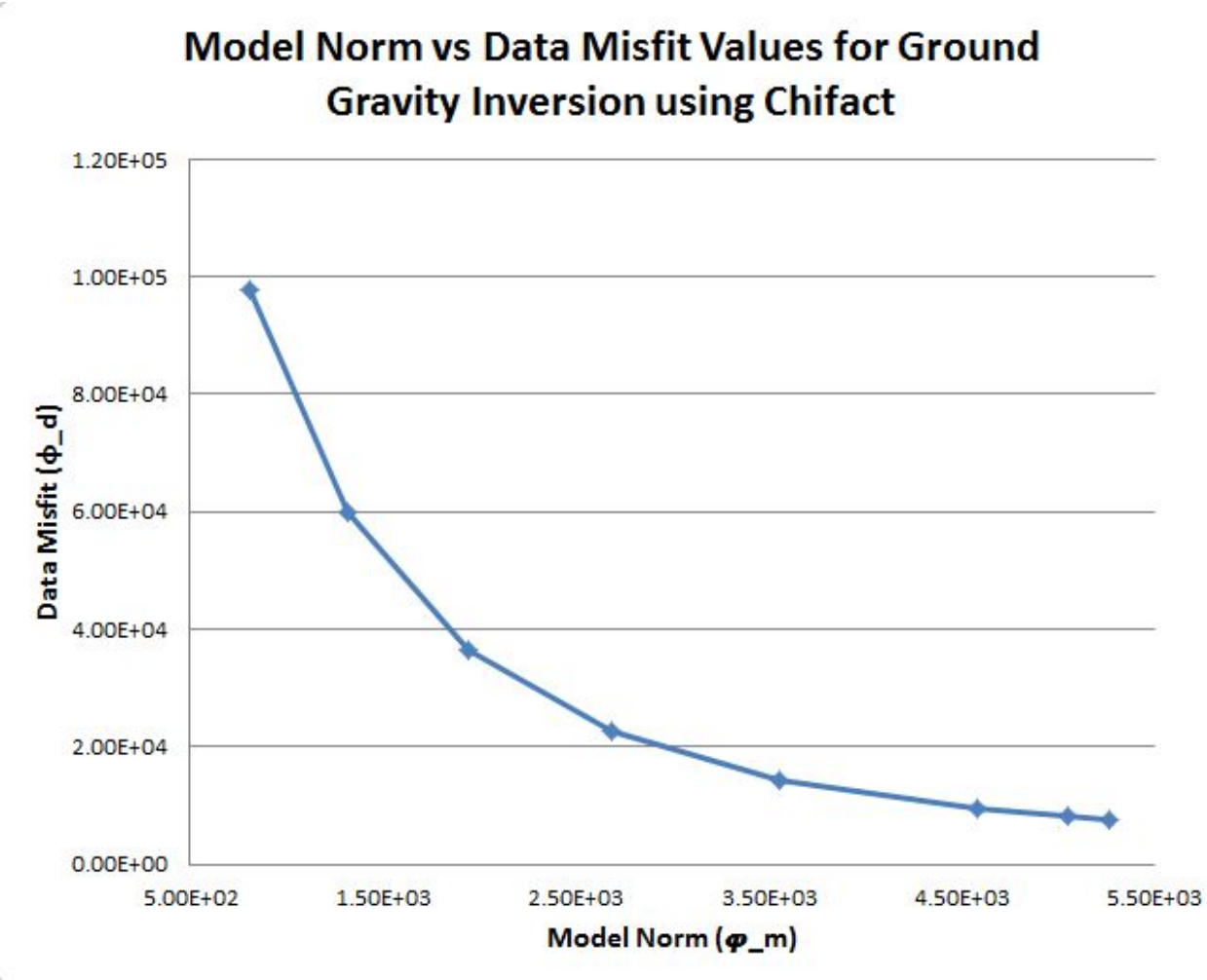

Figure 6.4: Tikhonov Curve plot for the model norm vs the data misfit during the inversion of the ground gravity data.

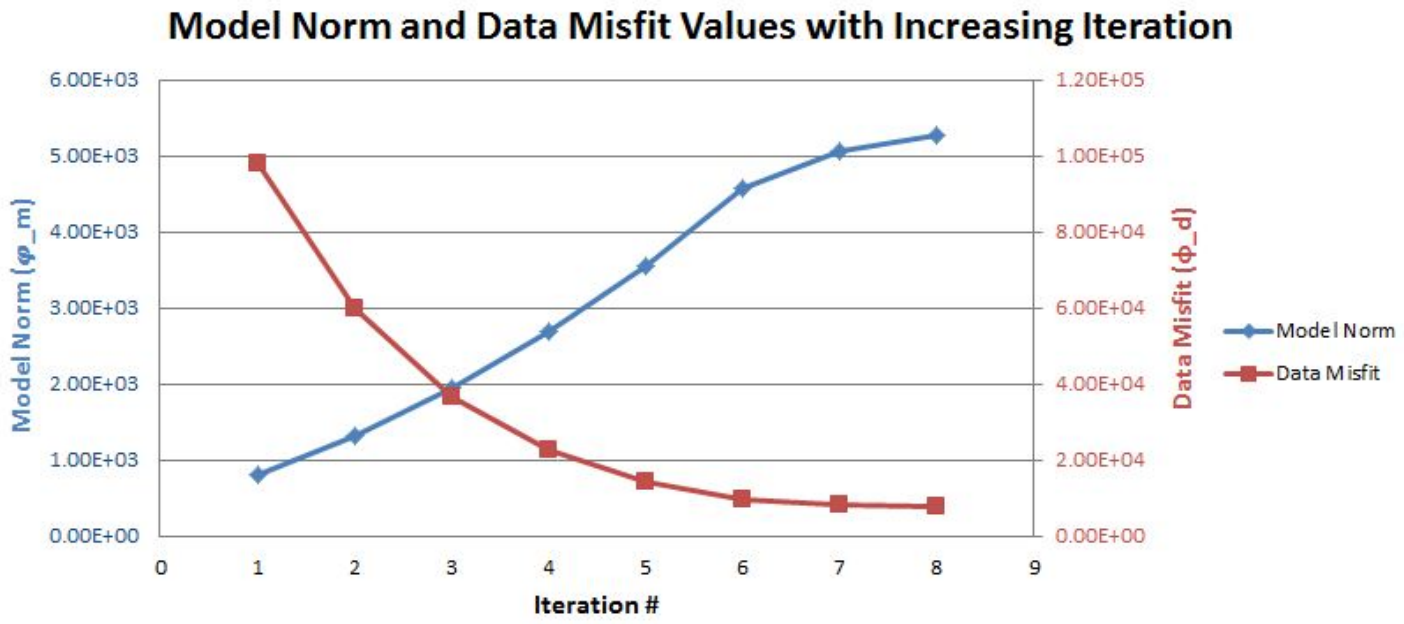

Figure 6.5: A plot of the model norm and data misfit plotted individually against the iteration number for the inversion of the ground gravity data.

parameter over the course of an iterative inversion is for the data misfit to start out very high, decrease rapidly, and then stabilize as the inversion converges. The model norm, on the other hand, is expected to start out at a low value, increase rapidly, and then stabilize as the solution approaches convergence. Although this behavior can be seen in the Tikhonov plot, it is best exemplified when examining both series of values when plotted independently against the inversion iteration number, as seen in **Figure 6.5**.

Next, the final 3D inversion model of the upward-continued ground gravity is shown in **Figure 6.6**. The noise level parameter used for this inversion, as previously discussed, was 0.01 mGal. This noise bar is a full order of magnitude less than that of the ground gravity dataset prior to the upward-continuation, and is a result of the signal, and therefore standard deviation, being significantly less after the filtering. The initial misfit between the observed data and the response of the zero-value half-space was 1.87E+06, which was reduced to a final misfit of 8.01E+03 after 8 rounds of iteration. Referring to **Figure 6.6**, the primary gravity trends of the Eastern Deeps and Gomer, as well as Southern Mushua, are also visible here. The final inversion model correctly identifies the location and approximate depths of the primary troctolite bodies in the study area, but with significantly less detail than the ground gravity inversion model, as expected. The Tikhonov curve is shown in **Figure 6.7**, and the plot of model norm and data misfit against inversion iterations is shown in **Figure 6.8**. Although the general behavior of the inversion matches that of the ground gravity inversion, there is one significant difference. Although the data misfit decreases to a point and then stabilizes nicely, the model norm seems to be starting to stabilize but doesn't reach quite the same level of stabilization by the time the data misfit is reach, as seen in the previous inversion. One explanation for this

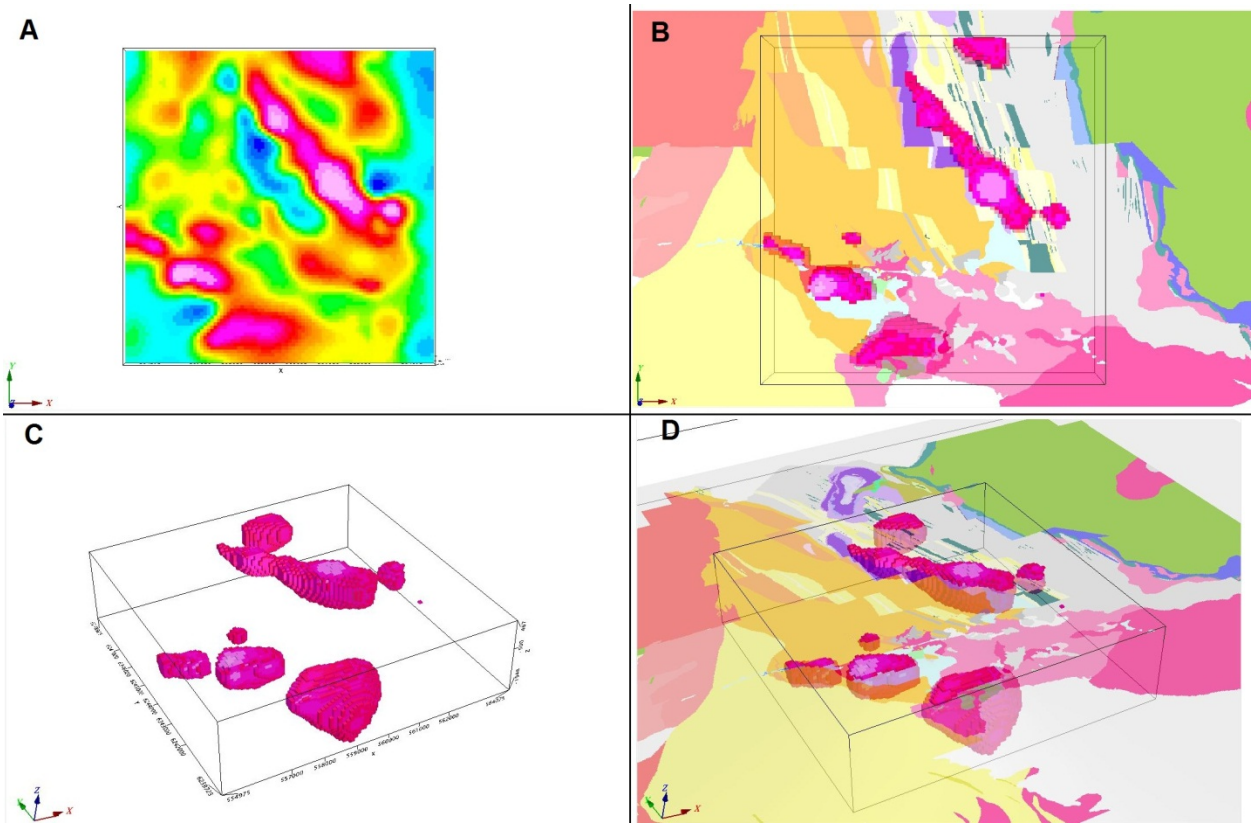

Figure 6.6: Upper-Continued Ground Gravity 3D Inversion (A)plan view of 3D model at 0m elevation, (B)plan view of 3D model density contrast values > 0.07 g/cc overlain on semi-transparent geology map, (C) angled and northeast-facing view of 3D model density contrast values > 0.07 g/cc, and (D) angled and northeast-facing view of 3D model density contrast values > 0.07 g/cc overlain on semi-transparent geology map.

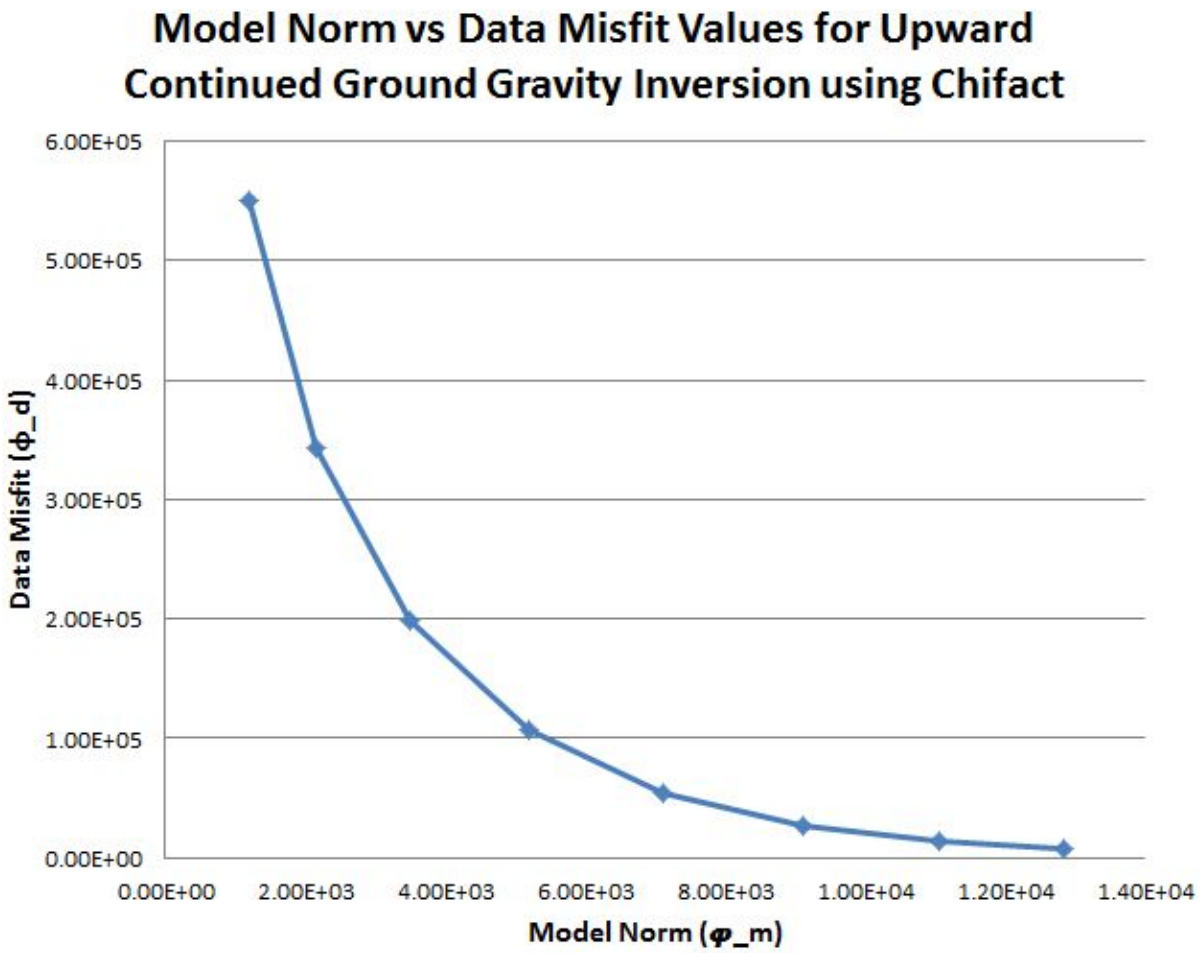

Figure 6.7: Tikhonov Curve plot for the model norm vs the data misfit during the inversion of the upward continued ground gravity data.

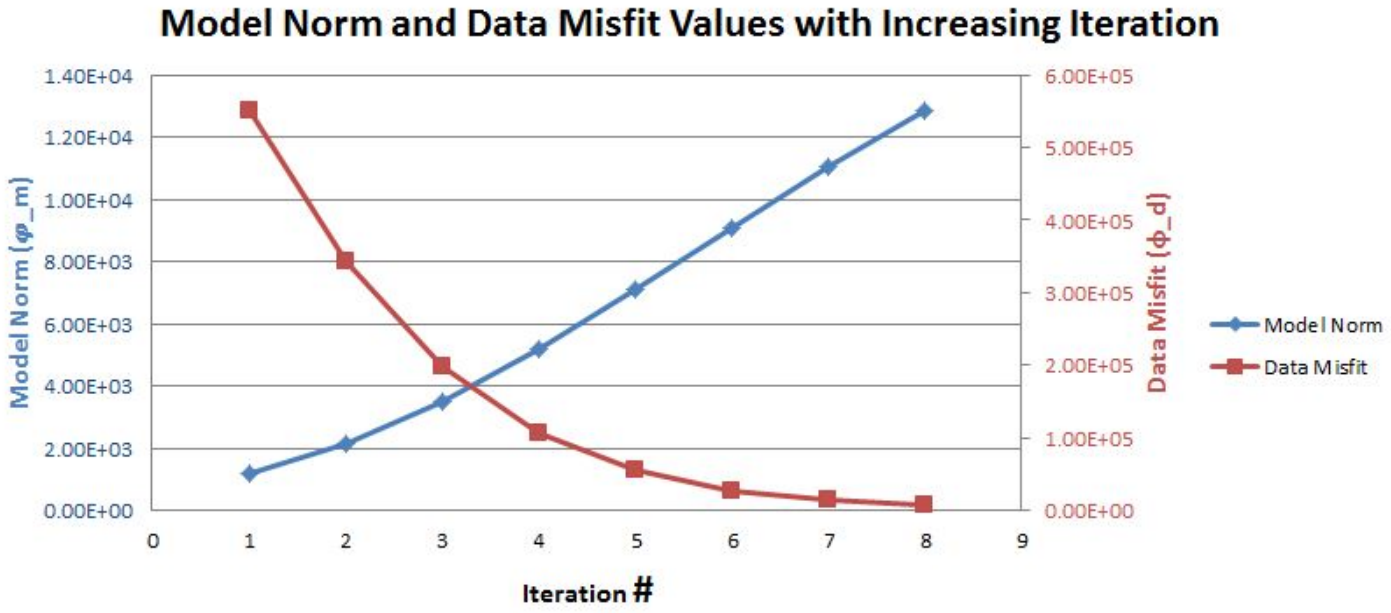

Figure 6.8: A plot of the model norm and data misfit plotted individually against the iteration number for the inversion of the upward continued ground gravity data.

behavior is that through the upward continuation of the ground gravity data, most of the high frequency signals (including much of the noise) was also removed. Although the error values were estimated at an order of magnitude less than the ground gravity survey, it is possible that the decrease in error was greater still. Due to the general lack of detail in the dataset, the current solution was thought to be very similar to the likely result of pushing the error bar further, and was judged to be sufficient for this study.

Finally, the inversion results for the vertically integration airborne gravity gradiometry are shown in **Figure 6.9**. The error level previously discussed of 0.001 mGal was initially used for this inversion, however the final inversion results were poor when using this parameter and included a great deal of "over-fitting" signals which were likely noise, even with higher Chifact inputs. This is likely a result of the potential added noise of GPS error and the terrain correction derived from the CDED DEM. After trial and error, a noise level of 0.05 mGal was settled on, which falls directly between the previous two inversions, and seemed to produce geologically reasonable and yet sufficiently detailed inversion results. The initial and final misfits of this model were 3.22E+05 and 7.67E+03, respectively, and the inversion process included 8 different iterations. By examining **Figure 6.9**, we can see that, similar to the previous inversions, the AGG inversion has no problem identifying the major troctolite bodies within the study area. A similar signature to the Eastern Deeps exists within the model, and a density trend following the main mineralized system through the Ovoid and into the Eastern Deeps. This latter feature is particularly interesting in this case because the inverted data was terrain-corrected with the CDED DEM which did not represent the open-pit over the Ovoid, and therefore suppressed the signature of the massive sulphide Ovoid body in the gridded image.

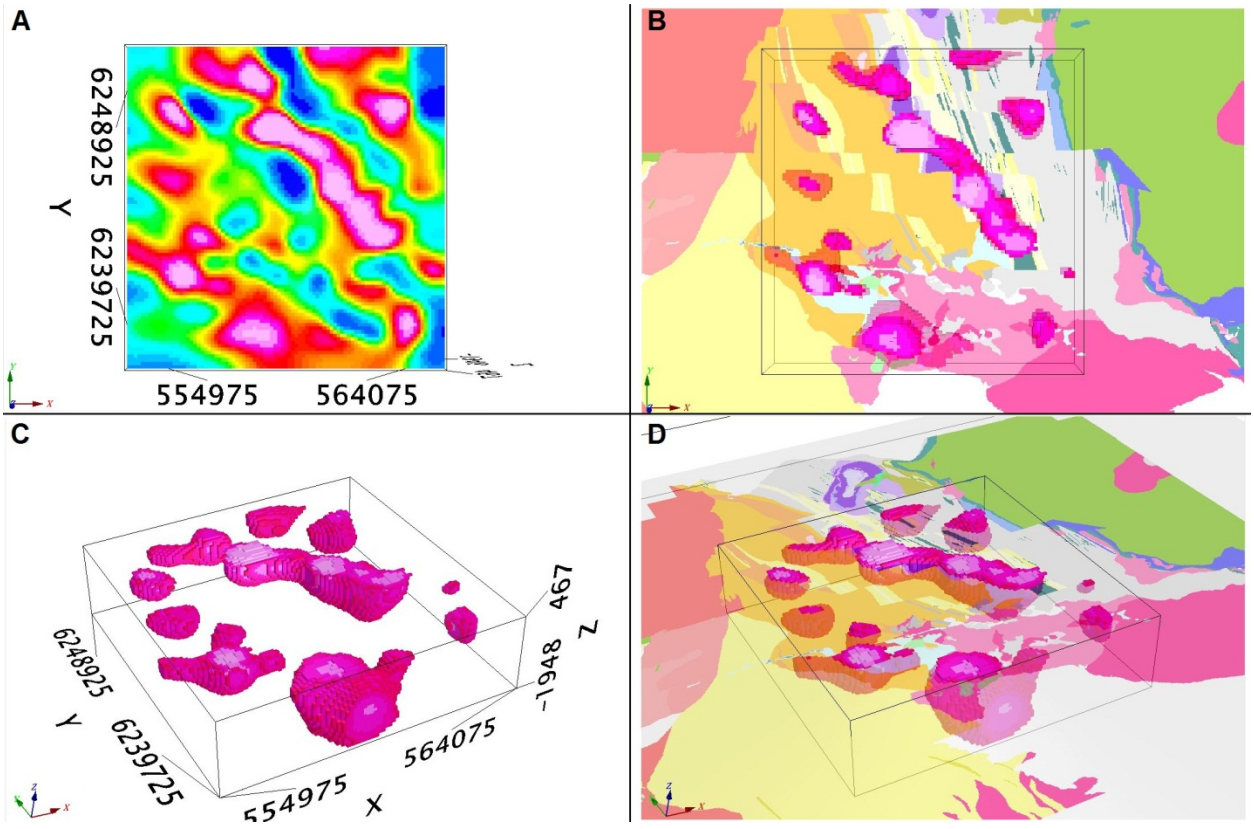

Figure 6.9: Vertically Integrated Airborne Gravity Gradiometry 3D Inversion (A)plan view of 3D model at 0m elevation, (B)plan view of 3D model density contrast values > 0.07 g/cc overlain on semi-transparent geology map, (C) angled and northeast-facing view of 3D model density contrast values > 0.07 g/cc, and (D) angled and northeast-facing view of 3D model density contrast values > 0.07 g/cc overlain on semi-transparent geology map.

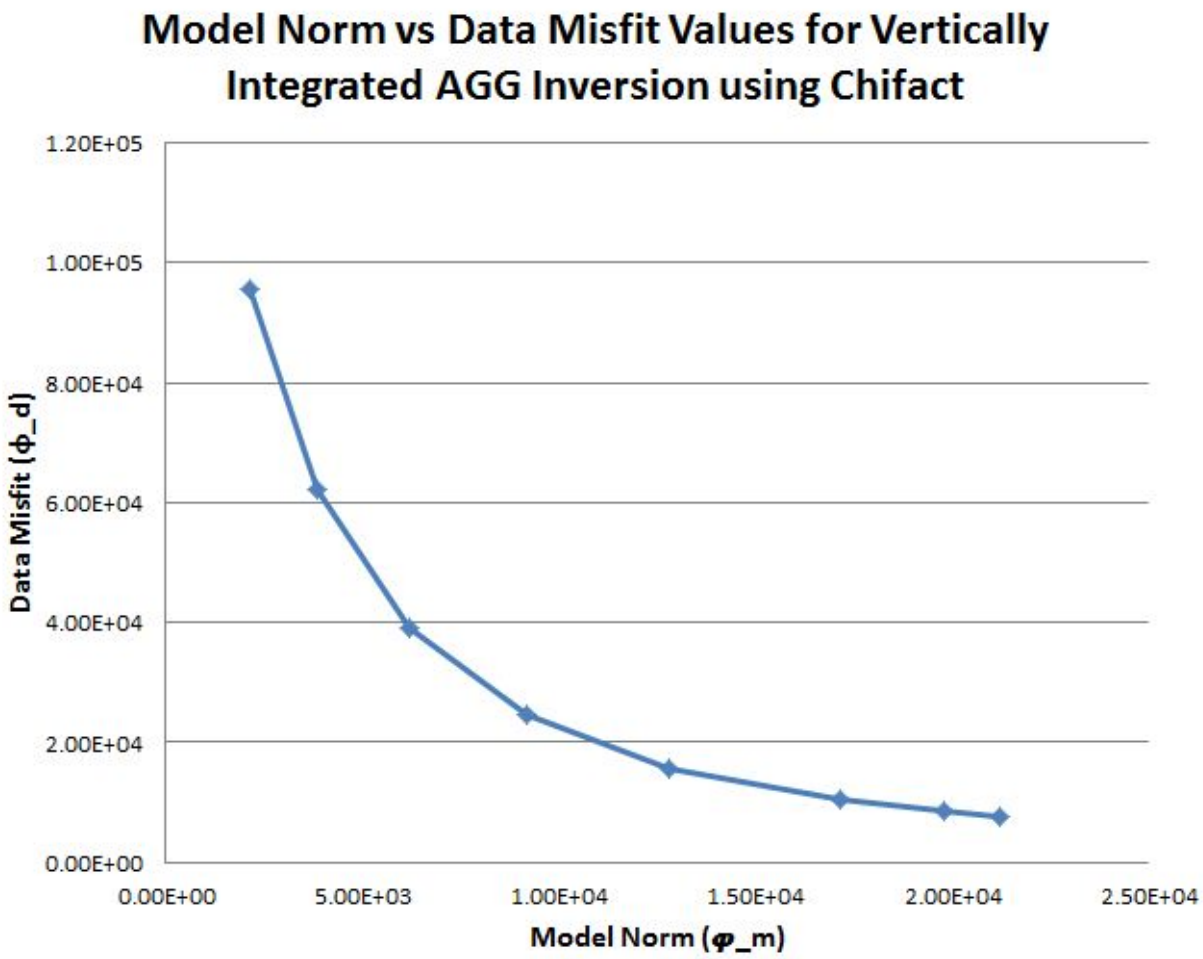

Figure 6.10: Tikhonov Curve plot for the model norm vs. the data misfit during the inversion of the vertically integrated Gzz.

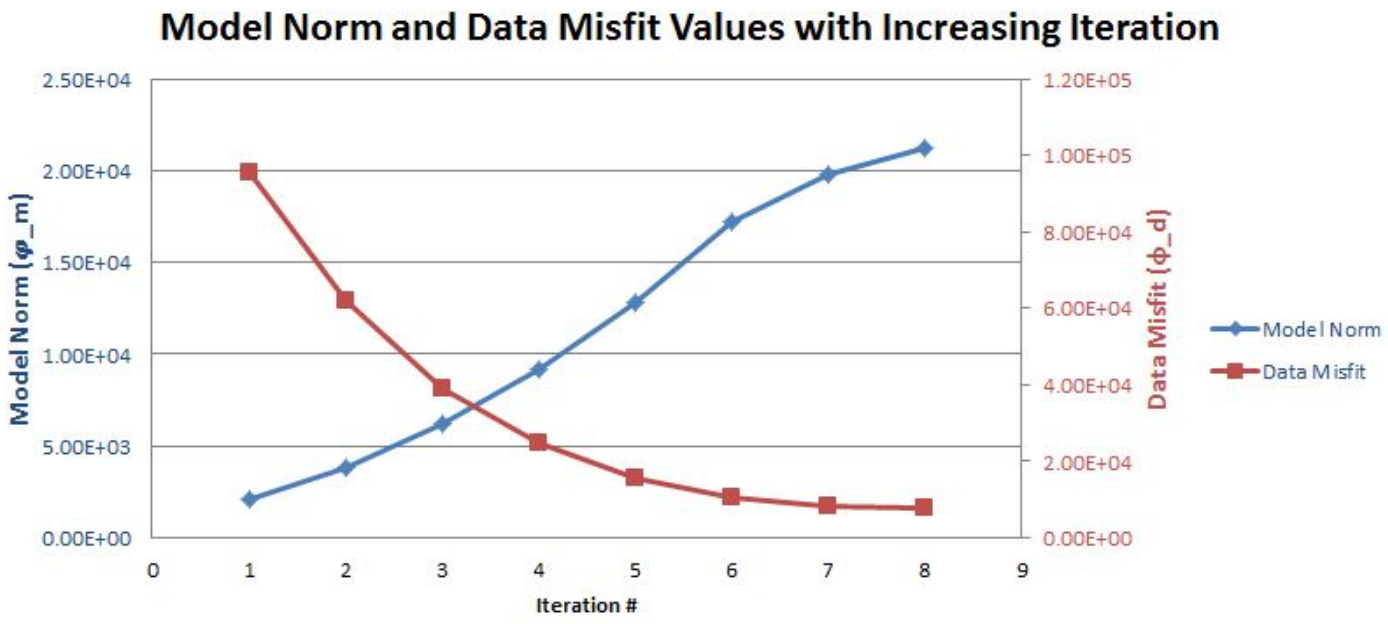

Figure 6.11: A plot of the model norm and data misfit plotted individually against the iteration number for the inversion of the vertically integrated Gzz.

The inversion, however, seems to have no trouble identifying this density trend despite its suppression. In other areas, particularly to the northern extend of the study area which features the southern extent of the Mushua intrusion, we see a higher level of character in this inversion than in the previous two. This appears to better represent the extent of the Mushua intrusion at depth, likely due to the superior spatial sampling of the AGG dataset in this area. As with the other two inversions discussed, the plots of the Tikhonov curve is shown in **Figure 6.10**, and the plot of model norm and data misfit against inversion iterations is shown in **Figure 6.11**. The parameter behavior observed in these plots is very similar to that seen in the ground gravity survey, indicating that the error estimate was likely an accurate one and the final inversion solution is likely an appropriate one.

In order to more directly compare the inversion results from the three different gravity products, grid slicing was completed at specific depths under the topography for each model. Although a range of depth slices were produced, this discussion will be focused on depth slices from 100m, 500m, 1000m, and 1500m. **Figure 6.12** shows images of (A) the surface geology map masked to the study area extents, (B) a 100m depth slice of the ground gravity inversion 3D model, (C) a 100m depth slice of the upward-continued ground gravity inversion 3D model, and (D) a 100m depth slice of the vertically integrated AGG inversion 3D model (all using the common color scale from **Figure 6.2**). The ground gravity data contains the most detail here, due to its superior resolution resulting from the closer proximity to the signal source. The upward-continued ground gravity inversion identifies all major density trends, but lacks the resolution of both other inversions, as well as the extra features provided by the superior spatial sampling of the AGG dataset. One interesting note regarding the 100m depth slice of

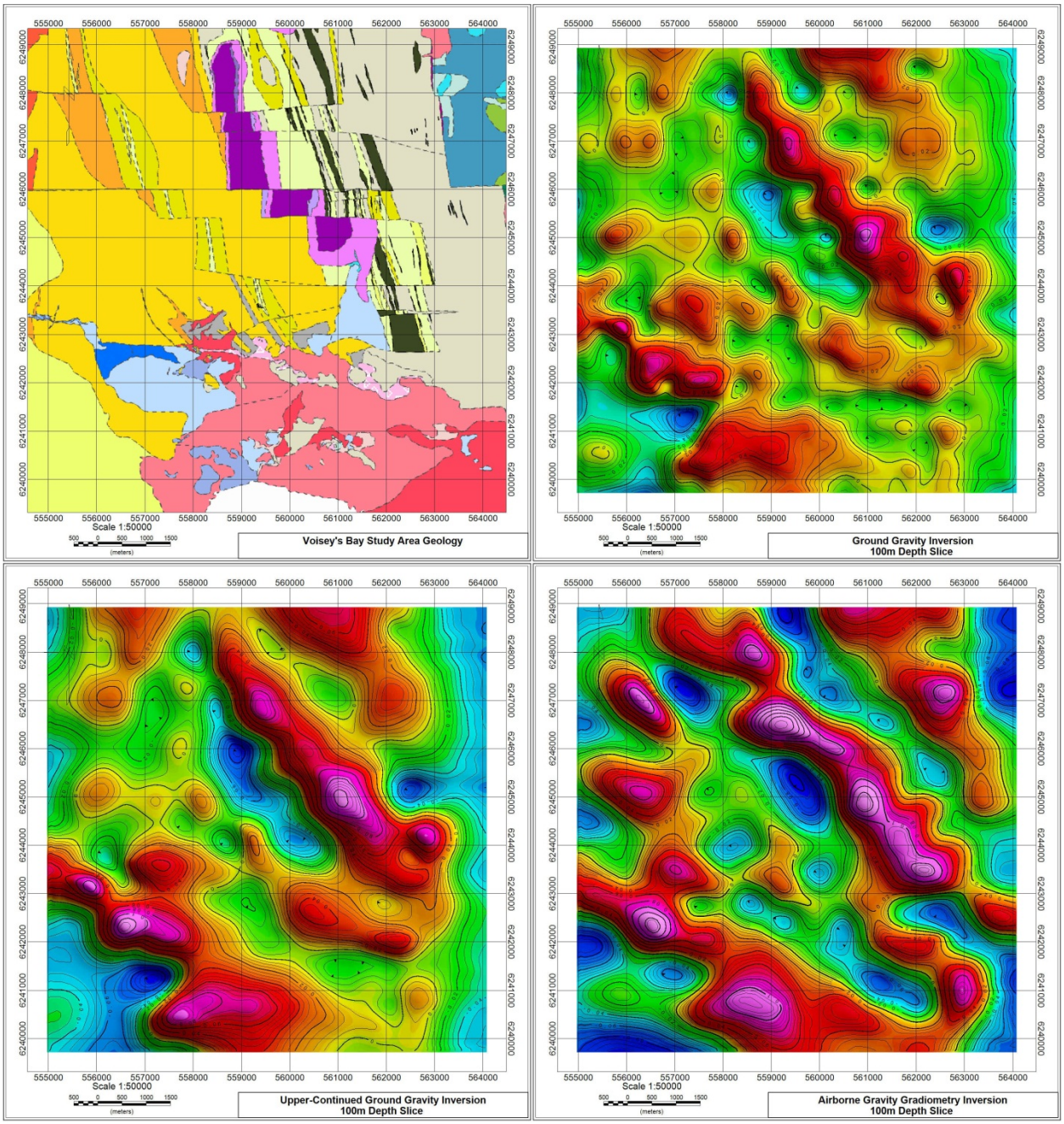

Figure 6.12: Comparison of gravity inversion results, (A) Voisey's Bay surface geology over the study area, (B) 100m depth slice of the ground gravity inversion 3D model, (C) 100m depth slice of the upper-continued ground gravity inversion 3D model, (D) 100m depth slice of the vertically integrated airborne gravity gradiometry inversion 3Dmodel

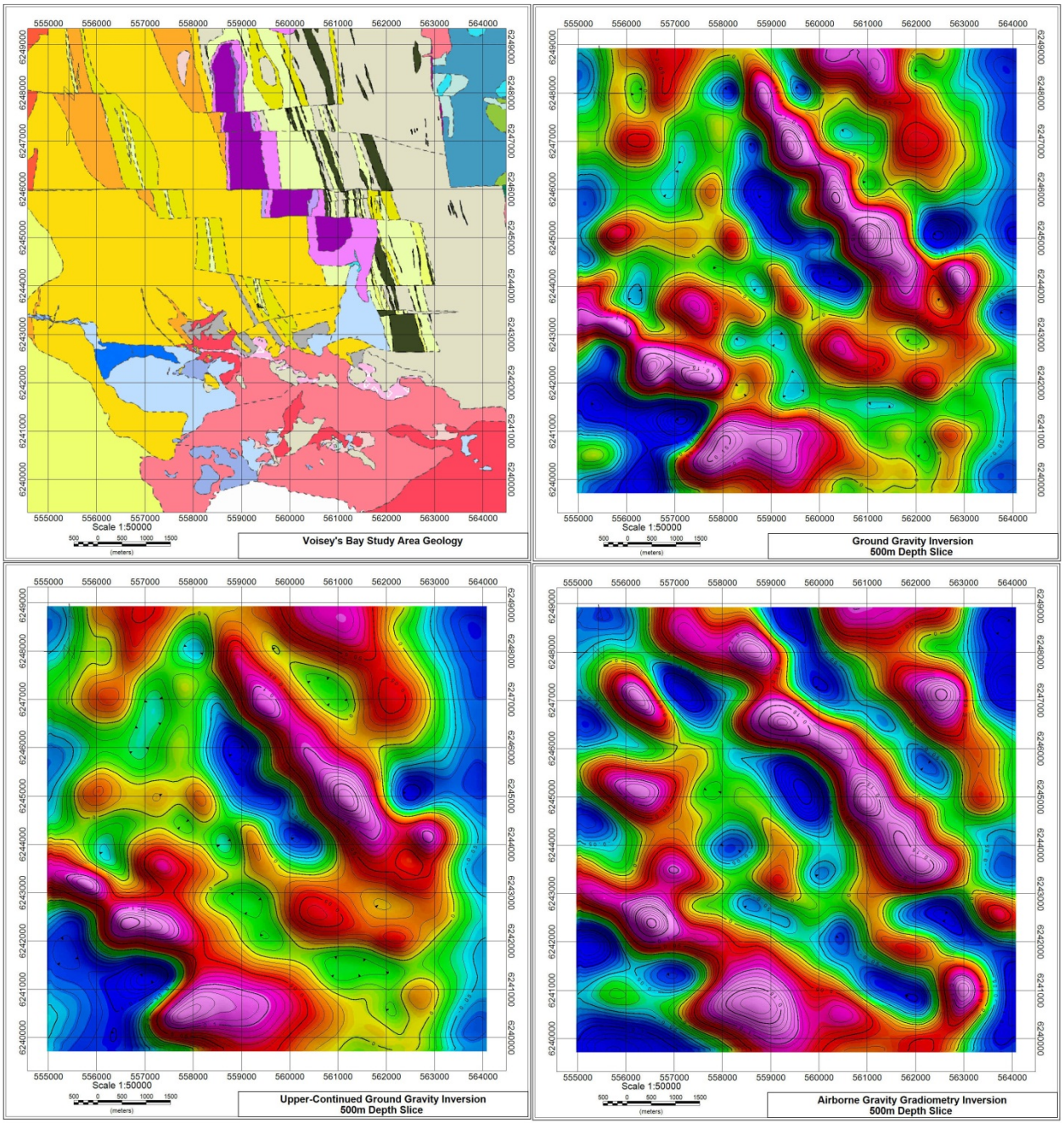

Figure 6.13: Comparison of gravity inversion results, (A) Voisey's Bay surface geology over the study area, (B) 500m depth slice of the ground gravity inversion 3D model, (C) 500m depth slice of the upper-continued ground gravity inversion 3D model, (D) 500m depth slice of the vertically integrated airborne gravity gradiometry inversion 3Dmodel

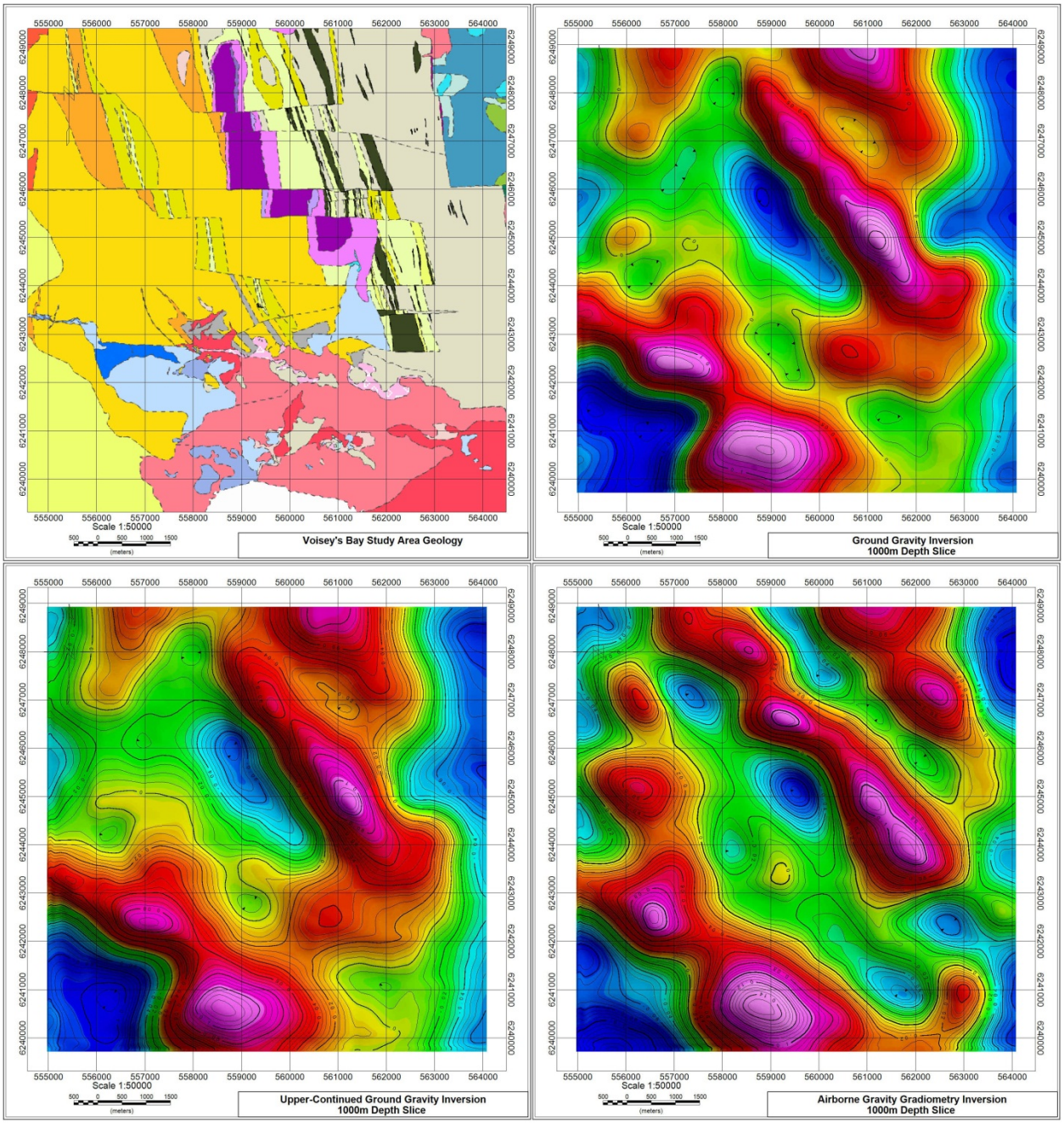

Figure 6.14: Comparison of gravity inversion results, (A) Voisey's Bay surface geology over the study area, (B) 1000m depth slice of the ground gravity inversion 3D model, (C) 1000m depth slice of the upper-continued ground gravity inversion 3D model, (D) 1000m depth slice of the vertically integrated airborne gravity gradiometry inversion 3Dmodel

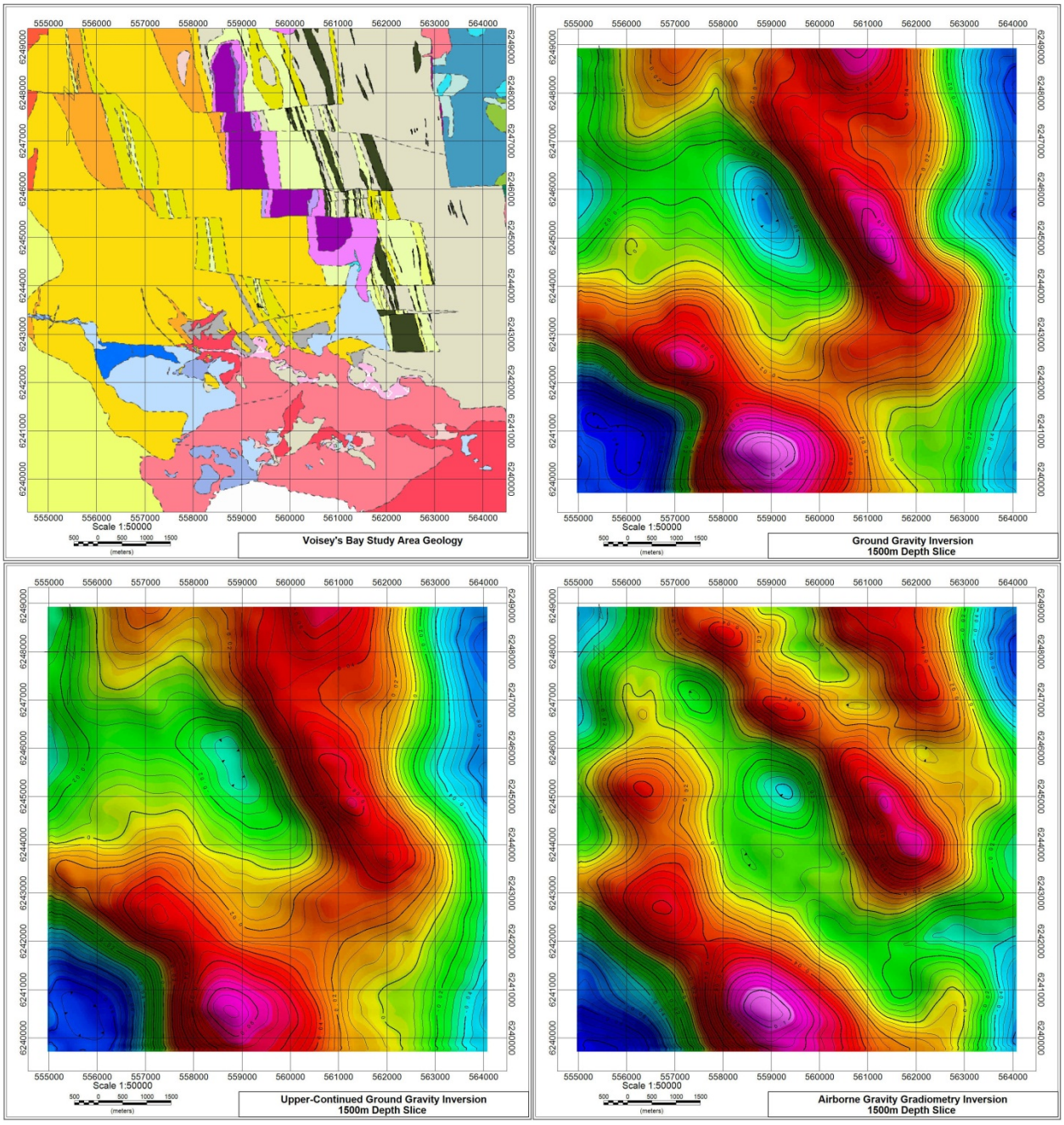

Figure 6.15: Comparison of gravity inversion results, (A) Voisey's Bay surface geology over the study area, (B) 1500m depth slice of the ground gravity inversion 3D model, (C) 1500m depth slice of the upper-continued ground gravity inversion 3D model, (D) 1500m depth slice of the vertically integrated airborne gravity gradiometry inversion 3Dmodel

the AGG inversion model is that it appears to bring high-amplitude anomalies closer to the surface than the other two inversions. This may be a result of the previously noted difference in spatial sampling.

In **Figure 6.13** we see depth slices from each model at 500m. The ground gravity inversion model is free from the near-surface over-fitting previously observed, and has a superior resolution for most of the features observed here. The AGG inversion model has superior resolution to the upward-continued gravity, particularly along the Gomer trend, and includes many density features missed by the limited spatial sampling of the ground gravity dataset, particularly along the Mushua trend. At 1000m depth, shown in **Figure 6.14**, the higher-frequency content of each dataset begins to play a significantly lesser role and the inversion results begin to look much more alike. The south-east portion of the Gomer trend is featured as higher in amplitude in all models, due to its greater depth extent in this direction. Similarly, the portion of the Eastern Deeps troctolite on the south-east side of the Red Dog fault begins to overshadow the density response of the rest of the system.

Finally, **Figure 6.15** depicts depths slices from the three inversions at 1500m. The continued convergence of the results from all three inversions is seen here, as the ground gravity and upward-continued ground gravity are almost identical except for slightly higher amplitudes in the former. This is, of course, due to the fact that at this depth the inversion is attempting to represent wavelengths in the data which were barely affected by the upward-continuation, and as depth increases we could expect to eventually see inversions from both grids becoming identical. One interesting difference between these two models and the AGG

inversion result is that there are differing conclusions represented here as to the connectivity of the Mushua and Voisey's Bay troctolites at depth. The ground gravity appears to indicate a potential joining, or at least overlapping, of the two chambers at depth, whereas the AGG inversion model depicts the two as being strictly separate.

Through the examination of these inversion results, it is possible to make several definitive statements about the quality of interpretation possible to make from each gravity dataset. First of all, the airborne gravity gradiometry survey contains a much greater amount of information than an airborne gravity survey would at a similar flight height. The AGG inversion contains many more detailed than the upward continued ground gravity dataset, and would be of much more use in the exploration or detailing of features smaller than 800m-1km. Second of all, although the ground gravity dataset holds a distinct advantage of being closer to the ground and therefore having much greater signal strength from the geology, the more complete coverage of the AGG survey combined with its significantly more sensitive system produces a final inversion model which is competitive in areas of good ground gravity coverage, and superior in areas of poor ground gravity coverage. As previously noted, an ideal scenario for either of these surveys would involve more uniform closely spaced stations for the ground gravity and a lower flying height for the AGG survey (which was made impossible in this case due to local topography). Although it should be noted that even with a ground gravity survey with a very high density of data sampling, the only anomalies which would be better resolved are those smaller than 200-400m, which is smaller than most troctolite chambers of interest in this scenario. In the often non-ideal world of exploration, and in the case of both datasets

examined in this study, a uniform AGG survey is generally a more reliable method of exploration than a non-uniform and sparse ground gravity survey.

Chapter 7: Conclusion

Notable advances in airborne gravity gradiometer sensors and deployment capabilities have taken place in the past decade and wide acceptable of the technique now exists throughout both the hydrocarbon and mineral exploration communities. The emergence and continued popularity of AGG has provided a new way for potential field data to be collected at a meaningful resolution and in a fast and cost-effective manner. The result of this is the potential for subsurface density mapping playing a role in exploration success in projects which may not have been able to incorporate gravity techniques otherwise. The study of the capabilities and characteristics of AGG data conducted in this thesis has demonstrated the many advantages of this geophysical method, as well as some important limitations.

In Chapter 2 a complete review of airborne gravimetry, including both airborne gravity and airborne gravity gradiometry, was completed. The advantages of AGG over traditional airborne gravity stem from the fact that it has the capability to remove linear accelerations from the movement of the aircraft. My removing the signal created from the movement of the aircraft the primary source of noise in the survey is also removed, providing a significantly higher resolution in measuring the acceleration of the Earth's gravity. A review of all current technology was performed, as well as a discussion of several global research initiatives aimed towards building significantly more sensitive AGG sensors in the future. We also reviewed the common sources of error and uncertainty in gravity surveys, noting that primary sources of error commonly exist not just in instrumental and aircraft noise, but also in accounting for the exact position of the plane through GPS measurements and the gravity contributions from the

surrounding terrain by the collection of a detailed digital elevation model. Clearly, if future AGG surveys are to benefit from sensors that measure at significantly higher resolution then these other controlling noise factors must also be studied closely.

Chapter 3 presented the case study of AGG being used in a nickel exploration program in Northern Labrador. The portion of the AGG survey considered in this thesis was the area covering the main Voisey's Bay mineralized trend. Several economic mineral deposits are contained within dense troctolite host rock at Voisey's Bay, which sometimes forms large chambers. Prospective chambers may be as small as 400-500m and could possibly be overlain by thin granitic sheets, which obscures geological mapping, but makes for an ideal gravity target. Due to the required resolution, and the limitations of other geophysical techniques in this area, AGG is an ideal exploration tool. A forward modeling exercise making use of physical rock properties from Voisey's Bay confirmed the ability of AGG to detect hidden troctolite chambers against the less dense country rock, and also reveals its limitations of being a poor direct detector of massive sulphide bodies within such a chamber.

In Chapter 4 the acquisition and processing of the AGG data revealed some inherent limitations on survey resolution. Due to the removal of high frequency noise from the data during and immediately after acquisition, all geologic signals smaller than the filtered wavelength (usually between 200-400m) are also removed. The limit on the long-wavelength content of the survey is controlled by the largest dimension of the survey, which is a factor of the portion of the gravity field that an integration process is capable of reconstructing from the measured gradient. A terrain correction was applied to the AGG dataset in a way which helped

gauge the most appropriate background density value. Complications arose from the use of a DEM created from a high resolution LiDAR survey because the DEM had not been properly frequency matched with the filtering completed on AGG dataset. The dangers of using such a DEM in the terrain correction were revealed in the form of artifacts being present in the resulting grid, particularly on slopes and hilltops. The limitation of dealing with a sparely sampled, highly variable, and thick overburden layer was also examined. Without additional information about the overburden-bedrock interface it is impossible to adequately correct for the less dense overburden without also risking the introduction of artifacts in the data. As a result, the evaluation of the AGG data for the remainder of the thesis concentrated on a portion of the survey unaffected by overburden and terrain corrected with a lower resolution, but frequency matched DEM. Vertical Integration and regional removal filtering were completed on the AGG in order to facilitate interpretation and comparison with other datasets.

In Chapter 5 a quantitative approach was taken to the analysis of the AGG, and it was compared to the historical ground gravity dataset at Voisey's Bay to gauge the differences in resolution between both surveys. Also included in the analysis and comparison was an upward-continued version of the ground gravity, which was meant to represent an airborne gravity survey flown at the same height as the AGG. The spatial sampling of the ground gravity and AGG datasets plays a significant role in any discussion regarding resolution. The AGG, as with any airborne survey, is flown at regularly spaced lines while taking periodic measurements (1Hz sampling rate in this case). The ground gravity dataset, as is often the case with large ground gravity surveys, contains extremely variable and non-uniform sampling. As a result, although the ground gravity survey has the distinct advantage of being located much closer to the

ground, in certain areas the lack of spatial sampling gives the AGG a significant resolution advantage. As a means of quantitatively examining the resolution and signal strength of all three datasets being examined, a 2D power spectral analysis was completed. Although all three datasets showed similar signal strength in long wavelength features wavelengths (several kms or more), the signal of the ground gravity data appears to decrease much slower as moving into the range of higher frequencies than either of the airborne datasets. The AGG dataset did, however, overshadow the resolution capabilities of the upward continued version of the ground gravity, and could therefore be expected to compare similarly to an airborne gravity survey. Another approach of examining the power spectrum of each data set was taken through the use of radially averaged power spectra plots. An interesting relationship which became apparent in this analysis was that the AGG signal is actually dominant over that of the ground gravity for mid-frequency ranges (between ~600m and 5km). This dominance is strictly due to the superior spatial sampling of the AGG survey.

In Chapter 6 the AGG, ground gravity, and upward-continued ground gravity datasets were compared in the context of their final interpretive results. The interpretation completed in this study involved geophysical inversion using software from the University of British Columbia's Geophysical Inversion Facility (UBC-GIF) . Inversion theory and methodology was discussed in terms of the components of the model objective function, the optimization of the inversion solution, and the discretization of the Earth. Examination of these inversion results allow us to make several definitive statements about the quality of interpretation with each gravity dataset. The airborne gravity gradiometry survey contains a much greater amount of information than an airborne gravity survey would at a similar flight height. Although the

ground gravity dataset holds a distinct advantage of being closer to the ground and therefore having much greater signal strength from the geology, the more complete coverage of the AGG survey combined with its significantly more sensitive system produces a final inversion model which is competitive in areas of good ground gravity coverage, and superior in areas of poor ground gravity coverage. In general, and particularly for the purposes of exploring for features 400m or larger, a uniform AGG survey is generally a more reliable method of exploration than a non-uniform and sparse ground gravity survey.

Through the course of this thesis the technique of AGG has been found to be an extremely valuable addition to the exploration toolbox. It not only provides a faster and cheaper method to collect ground gravity data, but in many cases surpasses the resolution commonly found in ground gravity datasets, particularly for features greater than 200-400m. It is apparent that AGG is quickly becoming a mainstay in the exploration community and will prove to be an invaluable tool for important future discoveries.

References

Anstie, J., Aravanis, T., Johnston, P., Mann, A., Longman, M., Sergeant, A., … Winterflood, J. (2010). Preparation for flight testing the VK1 gravity gradiometer. Airborne Gravity 2010: Abstracts from the ASEG-PESA Airborne Gravity 2010 Workshop. *Geoscience Australia Record 2010, 23*, 5-12.

Ash, M.R., Wheeler, M., Miller, H.G., Farquharson, C.G., and Dyck, A.V. (2006). Constrained three-dimensional inversion of potential field data from the Voisey's Bay Ni-Cu-Co deposit, Labrador, Canada*. 76th Annual Meeting of the Society of Exploration Geophysicists* (Vols. 1-6).

Balch, S.. (1999). Geophysical Methods for Nickel Deposits with Examples from Voisey's Bay. GAC-MAC Meeting. St John's, Newfoundland.

Balch, S., Crebs, T.J., King, A., and Verbiski, M. (1998). Geophysics of the Voisey's Bay Ni-Cu-Co deposits. *68th Ann. Internat. Mtg., Soc. Expl. Geophys., Expanded Abstracts*.

Barnes, G. J., and Lumley, J. A.. (2010). Noise analysis and reduction in full tensor gravity gradiometry data. Airborne Gravity 2010 - Abstracts from the ASEG-PESA Airborne Gravity 2010 Workshop. *Geoscience Australia Record 2010*, *23*, 21-27.

Billings, S. D., and Richards, D. (2001) Quality control of gridded aeromagnetic data. *Exploration Geophysics, 31*, 611-616.

Brady, N. (2010). A Turnkey Airborne Gravity System – Concept to Reality, Airborne Gravity 2010 - Abstracts from the ASEG-PESA Airborne Gravity 2010 Workshop, *Geoscience Australia Record 2010*, *23*, 28-36.

Bruton, A.M. (2000). Improving the Accuracy and Resolution of SINS/DGPS Airborne Gravimetry: Ph.D Thesis, The Department of Geomatics Engineering, University of Calgary. *UCGE Report No. 20145*. (http://www.geomatics.ucalgary.ca/Papers/Thesis/KPS/00.20145.AMBruton.pdf)

Crebs, T. J. (1996). Discovery geophysics of the Voisey's Bay Ni-Cu-Co deposit, Labrador, Canada. *66th Ann. Internat. Mtg., Soc. Expl. Geophys., Expanded Abstracts*.

Dampney, C. N. G. (1969). The equivalent source technique. *Geophysics, 34*, 39–53.

Dransfield, M. H., Christensen, A. N., Diorio, P. P., Rose, M. M., and Stone, P. M. (2001). FALCON test results from the Bathurst Mining camp. *Exploration Geophysics, 32,* 243-246.

Dransfield, M. H., and Lee, J. B. (2004). Ed. Lane, R.J.L. The FALCON® airborne gravity gradiometer survey systems. Airborne Gravity 2004 – Abstracts from the ASEG-PESA Airborne Gravity 2004 Workshop. *Geoscience Australian Record, 18*, 15-19.

Dransfield, M. H., Le Roux, T., and Burrows, D. (2010). Airborne gravimetry and gravity gradiometry at Fugro Airborne Surveys. Airborne Gravity 2010 - Abstracts from the ASEG-PESA Airborne Gravity 2010 Workshop. *Geoscience Australia Record, 23*, 49-57.

DiFrancesco, D., Kaputa, D., and Meyer, T. (2008). Gravity gradiometer systems. *Advances and challenges: Preview, 133*, 30-36.

DiFrancesco, D., Grierson, A., Kaputa, D., and Meyer, T. (2009). Gravity gradiometer systems advances and challenges. *Geophysical Prospecting, 57*, 615-623.

DiFrancesco, D. J. (2010). The Gravity Quest. Airborne Gravity 2010 - Abstracts from the ASEG-PESA Airborne Gravity 2010 Workshop. *Geoscience Australia Record, 23*, 44-48

Duff, D., Hurich, C., and Deemer, S. (2012). Seismic properties of the Voisey's Bay massive sulfide deposit: Insights into approaches to seismic imaging. *Geophysics, 77*.

Evans-Lamswood, D., et al. (2000). Physical Controls Associated with the Distribution of Sulfides in the Voisey's Bay Ni-Cu-Co Deposit, Labrador. *Economic Geology, 95*, 749 – 769.

Gabell, A., Tuckett, H., and Olson, D. (2004). Ed. Lane, R.J.L. The GT-1A mobile gravimeter. Airborne Gravity 2004 – Abstracts from the ASEG-PESA Airborne Gravity 2004 Workshop: *Geoscience Australian Record, 18*, 55-61.

Geosoft Inc. (2013). Geosoft Technical Documentation: Preparing Grids for MAGMAP FFT Processing.

Gunn, P. J. (1975). Linear transformations of gravity and magnetic fields. *Geophysical Prospecting, 23*, 300 – 312.

Hatch, D. M., Murphy, C., Mumaw, G., and Brewster, J. (2007). Performance of the Air-FTG System aboard an airship platform. *Preview, 127*, 17 - 22.

Hatch, D., and Pitts, B. (2010). The De Beers Airship Gravity Project, Airborne Gravity 2010 - Abstracts from the ASEG-PESA Airborne Gravity 2010 Workshop, *Geoscience Australia Record, 23*, 97-106.

Hearst, R.B., and Morris, W. A. (2001) Regional gravity setting of the Sudbury Structure. *Geophysics, 66(6)*, 1680 – 1690.

Hinks, D., McIntosh, S., and Lane, R. (2004). A comparison of the Falcon and Air-FTG airborne gravity gradiometer systems at the Kokong Test Block. Airborne Gravity 2004 – Abstracts from the ASEG – PESA Airborne Gravity 2004 Workshop. *Geoscience Australia Record, 18*, 125-134.

Jorgensen, G.J., Kisabeth, J.L., and Routh, P.S., "The role of potential field data and joint inverse modeling in the exploration of the deepwater Gulf of Mexico mini-basin province," Petroleum Frontiers, Vol. 17, No. 4, 2001, pp. 18-35.

Kann, F. (2004). Requirements and general principles of airborne gravity gradiometers for mineral exploration. Airborne Gravity 2004 – Abstracts from the ASEG – PESA Airborne Gravity 2004 Workshop. *Geoscience Australia Record, 18*, 1 – 4.

Kass, M.A., and Li, Y. (2008). Practical aspects of terrain correction in airborne gravity gradiometry surveys. *Exploration Geophysics, 39*, 198-203.

Kerr, A. (2003). Voisey's Bay and the nickel potential of Labrador: A Summary for the Nonspecialist, Current Research, Newfoundland Department of Mines and Energy. *Geological Survey, Report 03-1*, 231-239.

King, A., Fullagar, P.K, and Lamontagne, Y. (1996). Borehole geophysics in exploration, development and production. Short course notes, Prospectors and Developers Association, Toronto.

King, A. (1996). Deep drillhole electromagnetic surveys for nickel-copper sulphides at Sudbury, Canada. *Exploration Geophyics, 27*, 105-118.

King, A. (2007). Ed. Milkereit, B. Review of Geophysical Technology for Ni-Cu-PGE deposits. *Proceedings of Exploration '07: Fifth Dicennial International Conference on Geophysics and Geochemical Exploration for Minerals,* ed. B. Milkereit.

Lane, R. (2004). Ed. Lane, R.J.L. Integrating ground and airborne data into regional gravity compilations. Airborne Gravity 2004 – Abstracts from the ASEG – PESA Airborne Gravity 2004 Workshop. *Geoscience Australia Record, 18*, 81-99

Lane, R. (2010). Introduction. Airborne Gravity 2010 – Abstracts from the ASEG-PESA Airborne Gravity 2010 Workshop, *Geoscience Australia Record, 23*, 1 – 4.

Lee, J. B. (2001). FALCON gravity gradiometer technology. *Exploration Geophysics, 32(4),* 247-250

Li, Y., Kass, M.A., Davis, K., Braga, M., and Martinez, C. (2010). Ed. Lane, R.J.L. Terrain correction and its effect on 3D inversion of airborne gravity gradiometry data. Airborne Gravity 2010 - Abstracts from the ASEG-PESA Airborne Gravity 2010 Workshop. 131 -141.

Li, Y., and Oldenburg, D.W. (1996)/ 3-D inversion of magnetic data. *Geophysics, 61*, 394-408.

Li, Y., and Oldenburg, D.W. (1998). 3D inversion of gravity data. *Geophysics, 63(1*), 109- 119.

Lightfoot, P.C., and Naldrett, A.J. (1999). Geological and geochemical relationships in the Voisey's Bay Intrusion, Nain Plutonic Suite, Labrador, Canada. *Geological Association Canada Short Course Notes, 13*, 1-30.

Lightfoot, P.C. (2007). Advances in Ni-Cu-PGE sulphide deposit models and implications for exploration technologies. Proceedings of Exploration 2007. *Exploration in the New Millenium: Fifth Dicennial Conference on the Geophysics and Geochemistry for*

Mineral Exploration. Toronto.

Murphy, C.A. (2004). Ed. Lane, R.J.L. The Air-FTG™ airborne gravity gradiometer system. Airborne Gravity 2004 – Abstracts from the ASEG-PESA Airborne Gravity 2004 Workshop. *Geoscience Australia Record, 18*, 7-14.

Naldrett, A.J., and Li, C. (2007). The Voisey's Bay deposit, Labrador, Canada, Mineral Deposits of Canada: A Synthesis of Major Deposit-Types, District Metallogeny, the Evolution of Geological Provinces, and Exploration Methods. Geological Association of Canada, Mineral Deposits Division, Special Publication, Volume 5, 387-407.

Olson, D. (2010). GT-1A and GT-2A airborne gravimeters: Improvements in design, operation, and processing from 2003 to 2010. Airborne Gravity 2010 - Abstracts from the ASEG-PESA Airborne Gravity 2010 Workshop *Geoscience Australia Record, 23*, 152 – 171.

Ryan, B. (1996). Commentary on the location of the Nain-Churchill boundary of the Nain area: Geological Survey, Department of Natural Resources, Government of Newfoundland and Labrador, Current Research Report 96(1), 109–129.

Ryan, B., Wardle, R.J., Gower, C.F., and Nunn, G.A.G. (1995). Nickel-copper sulphide mineralization in Labrador: The Voisey's Bay discovery and its exploration implications: Geological Survey, Department of Natural Resources, Government of Newfoundland and Labrador, Current Research Report 95(1), 177–204.

Sander, S., Ferguson, S., Sander, L., and Lavoie, V. (2004). The AIRGrav airborne gravity system. Airborne Gravity 2004 - Abstracts from the ASEG-PESA Airborne Gravity 2004 Workshop. *Geoscience Australia Record, 18*, 49-54.

Sander, L., and Ferguson, S. (2010). Advances in SGL AIRGrav acquisition and progressing. Airborne Gravity 2010 - Abstracts from the ASEG-PESA Airborne Gravity 2010 Workshop. *Geoscience Australia Record, 23*, 172-177.

Spector, A., and Grant, F. S. (1970) Statistical methods for interpreting aeromagnetic data. *Geophysics, 35*, 293–302.

Telford, W. M., Geldart, L. P., and Sheriff, R. E. (1990). Applied Geophysics (Second Edition). Cambridge University Press

UBC Geophysical Inversion Facility. (2005). Inversion Theory Online Tutorial, UBC-GIF website, Department of EOS.

Vajk, R. (1956). Bouguer corrections with varying surface density. *Geophysics, 21*, 1004- 1020.

Veryaskin A. (2000). A novel combined gravity & magnetic gradiometer system for mobile applications. *70th SEG meeting: Expanded Abstracts*. Calgary, Canada.

Williams, N. C. (2006). Applying UBC-GIF potential fields inversions in greenfields or brownfields exploration. *AESC 2006*. Melbourne, Australia.